ABSTRACT

Title of dissertation: STOCHASTIC MAGNETIZATION
DYNAMICS DRIVEN BY A
JUMP-NOISE PROCESS

Andrew Lee, Doctor of Philosophy, 2015

Dissertation directed by: Professor Isaak Mayergoyz
Department of Electrical Engineering

An approach to modeling thermal noise effects in stochastic magnetization dynamics using a jump-noise process is presented. The damping term present in classical Landau-Lifshitz and Landau-Lifshitz-Gilbert equations is shown to result from the average of the jump-noise process in the presented stochastic Landau-Lifshitz equation approach. A numerical technique for solving the Landau-Lifshitz equation driven by a jump-noise process based on the Monte Carlo method is introduced and the results obtained from this method are shown. The drawback of using the Monte Carlo approach is discussed as well as the introduction of an averaging method to model stochastic magnetization dynamics on energy graphs. This averaging technique takes advantage of the difference in time-scale between the precessional motion and thermal effects in the stochastic Landau-Lifshitz model. By averaging over precessional trajectories, a stochastic magnetization dynamics equation on graphs is obtained. This averaging technique is demonstrated to be consistent with Monte Carlo results through numerical simulations. Application of the averag-

ing technique to self-oscillations in magnetization dynamics due to the spin-transfer torque phenomenon is investigated and numerical results are presented. Finally, the power spectral density for magnetization dynamics on energy graphs is calculated. Numerical results for the power spectral density are studied and analyzed.

STOCHASTIC MAGNETIZATION DYNAMICS
DRIVEN BY A JUMP-NOISE PROCESS

by

Andrew Lee

Dissertation submitted to the Faculty of the Graduate School of the
University of Maryland, College Park in partial fulfillment
of the requirements for the degree of
Doctor of Philosophy
2015

Advisory Committee:
Professor Isaak Mayergoyz, Chair/Advisor
Professor Thomas Antonsen
Professor Steven Marcus
Professor Thomas Murphy
Professor Ichiro Takeuchi

Dedication

This dissertation is dedicated to all of my friends, family, and loved ones who have supported me throughout this long journey. In particular, this is dedicated to my grandfather who could not see its completion.

Acknowledgments

I am grateful for all of the people who have helped to make this thesis possible and without whom my graduate experience would have been much bleaker.

First and foremost, I would like to give thanks to my advisor, Professor Isaak Mayergoyz, for giving me the opportunity to work on several interesting and demanding projects over the past five years. He has always been extremely helpful with advice regarding research and personal health and is always equipped with a seemingly endless supply of humorous anecdotes and historical trivia. It has been my honor to work closely with and learn directly from such an exceptional person.

I would also like to thank Dr. Charlie Krafft. For without his tremendous help and support at the Laboratory of Physical Sciences, I would not be where I am now. I would also like to thank Professor Steven Marcus, Professor Thomas Murphy, Professor Thomas Antonsen, and Professor Ichiro Takeuchi for agreeing to serve on my thesis committee and for generously giving their time to review this dissertation.

My colleagues in the magnetics laboratory have also helped to broaden and enrich my graduate life in many ways and deserve a special mention. Dr. David Bowen and Dr. Patrick McAvoy have patiently answered any and all questions I may have and have put up with my antics for many years. Research collaborations with Dr. Ziyu Liu have been extremely fruitful and I have enjoyed many technical discussions with her. Dr. Ling Hung, Dr. Garrett Lang, and Dr. Ryan Suess have also all been extremely helpful in my time here for both moral support and intense

intellectual discussions.

It is impossible to list all of the help and support I have received throughout the years, so I apologize to all of those whom I may have inadvertently left out.

List of Publications

[1] A. Lee, Z. Liu, C. Serpico, G. Bertotti, and I. Mayergoyz, "Monte Carlo Simulations of Landau-Lifshitz Dynamics Driven by a Jump-Noise Process," *J. Appl. Phys.* 111, 07D115 (2012).

[2] Z. Liu, A. Lee, G. Bertotti, C. Serpico, and I. Mayergoyz, "Jump-Noise Process-Driven Magnetization Dynamics and Random Switching of Magnetization," *J. Appl. Phys.* 111, 07D108 (2012).

[3] I. Mayergoyz, G. Bertotti, C. Serpico, Z. Liu, and A. Lee, "Random Magnetization Dynamics at Elevated Temperatures," *J. Appl. Phys.* 111, 07D501 (2012).

[4] D. Bowen, A. Lee, C. Krafft, and I. Mayergoyz, "Analysis of Nested Winding Dielectric-Core Transformers for Ethernet Applications," *IEEE Trans. Magn.* Vol. 48, 4127 (2012).

[5] Z. Liu, A. Lee, P. McAvoy, G. Bertotti, C. Serpico, and I. Mayergoyz, "Monte Carlo Simulations of Random Magnetization Dynamics Driven by a Jump-Noise Process on General Purpose Graphics Processing Units (GPUs)," *IEEE Trans. Magn.* 49, 3133 (2013).

[6] D. Bowen, A. Lee, C. Krafft, I. Mayergoyz, "Design Control of Performance in Nested and Interleaved Winding Printed Circuit Board Transformers for Ethernet Applications," *IEEE Trans. Magn.* Vol. 49, 4013 (2013).

[7] G. Bertotti, C. Serpico, Z. Liu, A. Lee, and I. Mayergoyz, "Spin Torque in the Framework of Random Magnetization Dynamics Driven by a Jump-Noise Process," *Physica B* 435, 8-10 (2014).

[8] A. Lee, Z. Liu, G. Bertotti, C. Serpico, and I. Mayergoyz, "Analysis of Random Magnetization Switching using Monte Carlo Simulations," *Physica B* 435, 100-104 (2014).

[9] D. Bowen, A. Lee, C. Krafft, I. Mayergoyz, "Performance Effects of Device Scale and Core Aspect-Ratio on Dielectric-Core Circuit Board Transformers," *J. Appl. Phys.* 115, 17E717 (2014).

[10] D. Bowen, A. Lee, C. Krafft, I. Mayergoyz, "Zero-Footprint Ethernet Transformers using Circuit-Board Embedded Ferrites," *J. Appl. Phys.* 115, 17E716 (2014).

[11] A. Lee, G. Bertotti, C. Serpico, I. Mayergoyz, "On Random Switching of Magnetization," *IEEE Trans. Magn.* Vol. 50, No. 11, 1300904 (2014)

[12] A. Lee, G. Bertotti, C. Serpico, I. Mayergoyz, "Averaging Technique for Random Magnetization Dynamics Driven by a Jump-Noise Process," *IEEE Trans. Magn.* Vol. 50, No. 11, 1300804 (2014)

[13] D. Bowen, A. Lee, C. Krafft, I. Mayergoyz, "Restoration of Broadband Inductor and Transformer Performance after Ferrite Grinding," *IEEE Mag. Let.* 99, (2015)

[14] I. Mayergoyz, A. Lee, C. Serpico, G. Bertotti, "Numerical Modeling of Random Magnetization Dynamics," *IEEE Trans. Magn.* Vol. 51, No. 3, 7200604 (2015)

Table of Contents

Chapter 1:   Introduction

1.1   Motivation

The study of magnetization dynamics of magnetic materials on the nano-scale has been the focus of extensive research[4,8]. This focus has been largely motivated by the direct application to magnetic recording technologies and other emerging novel phenomena[40]. In the field of magnetic recording technologies, the properties by which the magnetic state of a ferromagnetic material can be manipulated by externally applied fields have been widely explored and exploited. Below the Curie temperature of the ferromagnetic material, spontaneous magnetization of a uniaxial magnetic storage cell will cause the magnetic state to align either parallel or anti-parallel to the easy axis, as defined by the magnetic anisotropy. This allows cells of ferromagnetic material in recording devices to be recorded as either a 0 or a 1 depending on the magnetic orientation. There are several major challenges facing the magnetic recording field. These challenges can be categorized into the following related problems: How can the areal density of magnetic storage be increased? How can the read/write speed be increased? How can thermal stability be improved? These problems can often be framed as an optimization problem as higher areal density due to reduced cell size can lead to increased read/write speeds but also

decreased thermal stability. This is because a simple reduction in size of the storage cells will cause a reduction in the energy barrier between the magnetic states representing 0 and 1. A smaller energy barrier is good for read/write speeds as it will be easier to switch between the two states, but will be detrimental to thermal stability. Thermal fluctuations can cause the magnetic state of the ferromagnet to change and as the energy barrier is reduced, the influence of thermal fluctuations becomes greater. As a result, at smaller energy barriers, the possibility of unwanted magnetic inversions due to decreased thermal stability becomes greater. To better optimize the balance between these competing results, a more thorough understanding of the fundamentals of the magnetization dynamic process is needed under various conditions. This understanding will facilitate improvements in the current process as well as lead to discoveries and advancements with novel techniques such as heat-assisted magnetic recording (HAMR), spin-torque switching, and optical switching. These reasons are the motivation for the research outlined in the following chapters.

1.2 Overview

Theoretical studies and experimental verification often go hand in hand. In the case of magnetization dynamics, theoretical models and numerical analysis complement and often extend and predict results, as experimental techniques can be limited in scope and resolution. At very short time scales and very small spatial dimensions, it is difficult to control magnetic properties and it is often not possible to obtain accurate results. As a result, numerical simulations based on theoretical

models are often used to bridge the gaps and are not limited by size or time or other parameters such as choice in magnetic anisotropy. Therefore, it is of great interest to develop numerical models that can explore the behavior at these extreme conditions to better understand the physics behind magnetization dynamics.

Traditionally, basic magnetization dynamics are described by the Landau-Lifshitz or Landau-Lifshitz-Gilbert equation[13,14,19], which conform to micromagnetic constraints, with modifications or variations to account for more complex behaviors[10]. These basic equations consist of two terms: a term that accounts for precessional motion and a term that accounts for damping. To account for interactions with the thermal bath that introduce thermal fluctuation, these equations were modified to include a white-noise term. In this interpretation of the Landau-Lifshitz equation, there is a precessional term and two noise terms, as damping can be considered as the average effect of thermal noise. This approach can therefore be simplified as these two terms can be combined into a single noise term. This dissertation aims to investigate magnetization dynamics based on this simplified Landau-Lifshitz approach and to develop numerical models that accurately predict ferromagnetic behaviors.

In chapter 2, the traditional Landau-Lifshitz equation for magnetization dynamics is introduced as well as the equivalent Landau-Lifshitz-Gilbert equation. The structure of the equations is discussed as well as the various alternative deterministic forms for modeling magnetization dynamics. The conditions for the use of each form is discussed as well as their application to micromagnetic modeling. The traditional stochastic interpretation of the Landau-Lifshitz equation is also presented

and discussed.

In chapter 3, a new model for magnetization dynamics is presented. In this approach, thermal bath effects typically modeled using the distinct and disjoint damping and white-noise terms that appear in the traditional Stochastic Landau-Lifshitz equation are instead treated using a single jump-noise process term. This is due to the fact that the jump-noise process can have non-zero mean and therefore the expected value of the jump-noise process can be used to account for average thermal bath effects. Using this approach, novel phenomena that arise in magnetization dynamics due to external interactions can be studied.

In chapter 4, a modified approach to studying magnetization dynamics is presented. This approach is based on the concept that for very small damping, magnetization dynamics can be seen to behave on two different time scales with distinct behaviors. The precessional motion at constant magnetic energy occurs on a very fast time scale while damping and other effects occur on a much slower time scale. Thus, using an averaging technique, the behavior at slow time scales can be explored separately as a study of magnetization dynamics on energy graphs. This averaging technique is used to explore the Kramers-Brown approximation[7,17] and to explore magnetization switching behavior at very low temperatures[36,37,38,39].

In chapter 5, the effects of the spin-torque phenomenon on magnetization dynamics is investigated. The spin-transfer torque is the phenomenon by which the orientation of the magnetic state can be altered by injecting a spin-polarized current[1,6,35,41]. The discovery of this effect ushered the advancement of magnetic storage technologies by reducing the applied magnetic field needed for a magnetic

inversion while maintaining thermal stability. It also opened the door for a new field of study in spintronics and has led to novel devices such as spin-torque nano-oscillators (STNOs) where a constant current input can produce an oscillating voltage output. Spin-torque driven magnetization dynamics is traditionally modeled using the Landau-Lifshitz equation with an additional spin-torque term introduced by Slonczewski to form the Landau-Lifshitz-Slonczewski equation. This spin-torque term is an additional term that can also be included in the jump-noise process description as spin-torque can be interpreted as an effect from spin-polarized electron scattering. The spin-torque phenomenon is explored with the help of the averaging technique introduced in chapter 4. This approach is then applied to explore the spin-polarized current injection-induced phenomenon of self-oscillations.

In chapter 6, power spectral density for magnetization dynamics is explored[16]. The study of the power spectral density is important to connect the presented approach to experimental observations. The equations for calculating power spectral density on energy graphs are derived. Numerical simulations are presented and compared with expected experimental results.

Finally, a discussion and summary of the presented research is included in chapter 7. Possible extensions of this research for future study are also presented.

Chapter 2:   Magnetization Dynamics Equations

2.1   Micromagnetic Model

In micromagnetics, the magnetization describes the state of the ferromagnet and is a measure of the magnetic moment per unit volume. The magnetization is therefore a function of the position within the ferromagnet $\mathbf{r}$ and the time t: $\mathbf{M} = \mathbf{M}(\mathbf{r}, t)$. It is an measure of how a magnetic material is affected by magnetic fields, both internally generated as well as those from outside the material. An important property of the magnetization is that for materials far below their Curie temperature, the magnitude of the magnetization is preserved due to strong dominance of local exchange interactions and is equal to the spontaneous magnetization:

$$|\mathbf{M}(\mathbf{r}, t)| = M_s \tag{2.1}$$

This condition is known as the micromagnetic constraint.

The magnetization can be affected by many internal and external sources. In the micromagnetic framework, these sources include externally applied fields, short range exchange interactions, long range magnetostatic interactions, and contributions from the magnetic anisotropy as well as numerous others.

2.1.1 Micromagnetic Parameters

The micromagnetic model and its interactions can also be expressed in terms of the micromagnetic free energy g. The micromagnetic free energy is a function of the magnetization and the applied fields and can be defined by the following volume integral:

$$g(\mathbf{M}, \mathbf{H}_a) = \int_\Omega \left[\frac{A}{M_s^2}((\nabla M_x)^2 + (\nabla M_y)^2 + (\nabla M_z)^2) \right. \tag{2.2}$$

$$\left. + f_{AN}(\mathbf{M}) - \frac{\mu_0}{2}\mathbf{M} \cdot \mathbf{H}_M - \mu_0 \mathbf{M} \cdot \mathbf{H}_a \right] dV.$$

In the above equation, $\mathbf{H}_a$ is the applied magnetic field, Ω is the region of the ferromagnet, A is the exchange stiffness constant, M_s is the spontaneous magnetization, M_x, M_y, and M_z are the x,y, and z components of the magnetization respectively, μ_0 is the free space permeability, and $\mathbf{H}_M$ is the magnetic field from the magnetostatic effect.

The first term in the integral is a term associated with the free energy from exchange interactions. It can be seen from this term that non-uniformities in the magnetization orientation are penalized by increasing the free energy. This is a reflection of the physical manifestation of the exchange interaction wanting to align neighboring spins due to spin-spin interactions.

The second term in the integral, $f_{AN}(\mathbf{M})$, describes the effects from the crystal anisotropy of the ferromagnetic material. In ferromagnetic materials under the Curie temperature there exists a lattice structure that produces an energy landscape of preferred and non-preferred orientations. When all other applied fields are absent,

the magnetization will tend to align with preferred orientations of energy minima, called the easy axes or directions. Maxima of $f_{AN}(\mathbf{M})$ are called the hard axes or directions. There can also exist saddle-points in $f_{AN}(\mathbf{M})$, and these orientations are called intermediate axes.

The third term in the integral represents the free energy contribution from magnetostatic field effects. This contribution depends on the field $\mathbf{H}_M$, which is determined by the following magnetostatic Maxwell equations, subject to interface conditions:

$$\nabla \times \mathbf{H}_M = 0, \nabla \cdot \mathbf{H}_M = -\nabla \cdot \mathbf{M}. \tag{2.3}$$

The last term in the integral is the free energy contribution from interactions with an externally applied magnetic field $\mathbf{H}_a$. This externally applied field is a vector field and can be a function of time. The energy contribution from these externally applied magnetic fields is also known in literature as the Zeeman energy.

These four terms in the micromagnetic free energy integral encompass the major components of interest for this dissertation. There can be additional terms, such as contributions from magnetoelastic effects, but these are beyond the scope of this dissertation.

The four terms of interest in the micromagnetic free energy integral can be combined and interpreted as a single effective field:

$$\mathbf{H}_{eff} = \mathbf{H}_{EX} + \mathbf{H}_{AN} + \mathbf{H}_M + \mathbf{H}_a. \tag{2.4}$$

Here, $\mathbf{H}_M$ and $\mathbf{H}_a$ are the same as previously defined and $\mathbf{H}_{EX}$ and $\mathbf{H}_{AN}$ represent the exchange field and the anisotropy field, respectively. The exchange field, $\mathbf{H}_{EX}$

is defined

$$\mathbf{H}_{EX} = \frac{2A}{\mu_0 M_s^2} \nabla \mathbf{M}, \tag{2.5}$$

while the anisotropy field $\mathbf{H}_{AN}$ is defined

$$\mathbf{H}_{AN} = -\frac{1}{\mu_0} \frac{\partial f_{AN}}{\partial \mathbf{M}}. \tag{2.6}$$

Using these effective fields, the equilibrium magnetization can be found by solving for the micromagnetic energy extrema: $\delta g = 0$. The free energy variation due to magnetization variation $\delta \mathbf{M}$ is defined by

$$\delta g = -\mu_0 \Big[\int_\Omega \mathbf{H}_{eff} \cdot \delta \mathbf{M} dV - \frac{2A}{\mu_0 M_s^2} \oint_\Sigma \frac{\partial \mathbf{M}}{\partial n} \cdot \delta \mathbf{M} dS \Big]. \tag{2.7}$$

The first term is familiar and results from interactions with the effective applied field while the second term is an integration over the surface Σ of the ferromagnet. This second term represents changes in the magnitude of the magnetization as $\partial/\partial n$ is the derivative normal to Σ.

Solving for $\delta g = 0$ results in

$$\mathbf{M} \times \mathbf{H}_{eff} = 0 \tag{2.8}$$

for each point in Ω, and

$$\frac{\partial \mathbf{M}}{\partial n} = 0 \tag{2.9}$$

for each point on Σ. These results are consistent with the micromagnetic constraints as the first result implies that the magnetization will align parallel or antiparallel to the effective applied field and the second result implies that the magnitude of magnetization is preserved. Equation (2.8) is also known as Brown's equation.

2.2 Deterministic Magnetization Dynamics

In the previous section, the equilibrium condition was analyzed and was found to satisfy $\mathbf{M} \times \mathbf{H}_{eff} = 0$ such that the magnetization aligns with the effective applied field. In reality, this condition is very rarely satisfied and the dynamics of the magnetic state when it is not in equilibrium is much more complex and interesting. To study this, Landau and Lifshitz introduced a dynamic equation to model the evolution of the magnetic state[19]. Over the years, there have been many modifications to the basic dynamic equations, including a mathematically equivalent form known as the Landau-Lifshitz-Gilbert equation[13,14].

2.2.1 Landau-Lifshitz equation

The basic Landau-Lifshitz equation and all of its variants are based on the idea that when the magnetic state is not in equilibrium, the effective field $\mathbf{H}_{eff}$ acting on the magnetization will induce a precessional motion. This precessional motion will center around an equilibrium point with a precessional rate γ and will obey

$$\frac{\partial \mathbf{M}}{\partial t} = -\gamma \mathbf{M} \times \mathbf{H}_{eff}. \tag{2.10}$$

The precessional rate γ is the gyromagnetic ratio and is associated with the electron spin.

It can be seen that the free energy in the above equation is conserved and therefore (2.10) cannot be used to describe the thermal relaxations to the equilibrium condition that are expected from physical systems. To account for dissipative

interactions, the Landau-Lifshitz equation took the form

$$\frac{\partial \mathbf{M}}{\partial t} = -\gamma_L \mathbf{M} \times \mathbf{H}_{eff} - \frac{\alpha \gamma_L}{M_s} \mathbf{M} \times (\mathbf{M} \times \mathbf{H}_{eff}), \qquad (2.11)$$

where α is a dimensionless damping factor. From the form of the second term in the equation, it is easy to see that this term acts orthogonal to the magnetization and the precessional motion and drives the magnetization towards regions of lower energy. Therefore, while both terms in the Landau-Lifshitz equation satisfy micromagnetic constraints and preserve the magnitude of magnetization, only the first term preserves free energy.

2.2.2   Landau-Lifshitz-Gilbert Equation

Another common deterministic magnetization dynamics equation was proposed by Gilbert as a modification of the Landau-Lifshitz equation. This Landau-Lifshitz-Gilbert equation has the form:

$$\frac{\partial \mathbf{M}}{\partial t} = -\gamma_G \mathbf{M} \times \mathbf{H}_{eff} + \frac{\alpha}{M_s} \mathbf{M} \times \frac{\partial \mathbf{M}}{\partial t}. \qquad (2.12)$$

As seen from the equation, the first term in the Landau-Lifshitz-Gilbert equation appears to be very similar to the Landau-Lifshitz equation. This first term also represents a precessional term in the magnetization dynamics. The second term is also a damping term with α as a damping component. The difference is that the damping term in the Landau-Lifshitz-Gilbert equation depends on the time derivative of the magnetization. These equations may look different, but with the proper rescaling of γ_G, the Landau-Lifshitz-Gilbert equation can be shown to be mathematically equivalent to the Landau-Lifshitz equation. This can be done by taking

11

the cross product of the magnetization and the time derivative of the magnetization in the Landau-Lifshitz equation to get:

$$\mathbf{M} \times \frac{\partial \mathbf{M}}{\partial t} = \mathbf{M} \times \left[-\gamma_L \mathbf{M} \times \mathbf{H}_{eff} - \frac{\alpha \gamma_L}{M_s} \mathbf{M} \times (\mathbf{M} \times \mathbf{H}_{eff}) \right]. \qquad (2.13)$$

Reorganizing the equations gives:

$$\mathbf{M} \times \frac{\partial \mathbf{M}}{\partial t} = -\gamma_L \mathbf{M} \times (\mathbf{M} \times \mathbf{H}_{eff}) - \frac{\alpha \gamma_L}{M_s} \mathbf{M} \times (\mathbf{M} \times (\mathbf{M} \times \mathbf{H}_{eff})). \qquad (2.14)$$

From the definition of cross product, the second term can be simplified:

$$\frac{\alpha \gamma_L}{M_s} \mathbf{M} \times (\mathbf{M} \times (\mathbf{M} \times \mathbf{H}_{eff})) = \frac{\alpha \gamma_L M_s^2}{M_s} \mathbf{M} \times \mathbf{H}_{eff} = \alpha \gamma_L M_s \mathbf{M} \times \mathbf{H}_{eff}. \qquad (2.15)$$

Therefore, equation (2.14) can be reordered to show:

$$-\gamma_L \mathbf{M} \times (\mathbf{M} \times \mathbf{H}_{eff}) = \mathbf{M} \times \frac{\partial \mathbf{M}}{\partial t} + \alpha \gamma_L M_s \mathbf{M} \times \mathbf{H}_{eff}. \qquad (2.16)$$

Rescaling (2.16) to fit the second term in the Landau-Lifshitz equation gives:

$$-\frac{\alpha \gamma_L}{M_s} \mathbf{M} \times (\mathbf{M} \times \mathbf{H}_{eff}) = \frac{\alpha}{M_s} \mathbf{M} \times \frac{\partial \mathbf{M}}{\partial t} + \alpha^2 \gamma_L \mathbf{M} \times \mathbf{H}_{eff}. \qquad (2.17)$$

Replacing (2.17) in the Landau-Lifshitz equation gives:

$$\frac{\partial \mathbf{M}}{\partial t} = -\gamma_L \mathbf{M} \times \mathbf{H}_{eff} + \frac{\alpha}{M_s} \mathbf{M} \times \frac{\partial \mathbf{M}}{\partial t} + \alpha^2 \gamma_L \mathbf{M} \times \mathbf{H}_{eff}. \qquad (2.18)$$

Regrouping terms gives:

$$\frac{\partial \mathbf{M}}{\partial t} = -(\gamma_L - \alpha^2 \gamma_L)\mathbf{M} \times \mathbf{H}_{eff} + \frac{\alpha}{M_s}\mathbf{M} \times \frac{\partial \mathbf{M}}{\partial t}. \tag{2.19}$$

By defining $\gamma_G = \gamma_L - \alpha^2 \gamma_L$, it is evident that the Landau-Lifshitz-Gilbert equation in (2.12) is recovered, thereby showing the mathematical equivalence of the two magnetization dynamics equation forms.

These two deterministic equations for magnetization dynamics are the most common. While the two equations are mathematically equivalent, one form may be preferred over the other based on the strength of the damping. In the Landau-Lifshitz equation, the equivalent gyromagnetic ratio is dependent on the damping parameter, which better represents ferromagnetic behavior for large damping. On the other hand, the damping in the Landau-Lifshitz-Gilbert equation is proportional to the energy dissipation. In this way, it more accurately predicts slower changes in the magnetization motion as the damping increases. In either case, the equations can be fitted by introducing the appropriate gyromagnetic ratio and damping constants.

2.2.3 Other Deterministic Equations

There are many other forms for deterministic magnetization dynamic equations than the two presented above. One variant is a combination of the Landau-Lifshitz and Landau-Lifshitz-Gilbert equation:

$$\frac{\partial \mathbf{M}}{\partial t} = -\gamma \mathbf{M} \times \mathbf{H}_{eff} + \frac{\alpha_1}{M_s}\mathbf{M} \times \frac{\partial \mathbf{M}}{\partial t} - \frac{\alpha_2 \gamma}{M_s}\mathbf{M} \times (\mathbf{M} \times \mathbf{H}_{eff}). \tag{2.20}$$

Another variant is the Landau-Lifshitz-Bloch equation which is used for magnetization dynamics close to the Curie temperature[40]. This is because the Landau-

Lifshitz-Bloch equation has a term that lies parallel to the applied field such that the magnetization magnitude may no longer be preserved. The Landau-Lifshitz-Bloch equation has the form:

$$\frac{\partial \mathbf{M}}{\partial t} = c_1 \mathbf{H}_{eff} + c_2 \mathbf{H}_{eff} \times \mathbf{M} + c_3 \mathbf{H}_{eff} \times (\mathbf{H}_{eff} \times \mathbf{M}). \tag{2.21}$$

In addition to these equations, there are many other variants but the discussion of their forms and uses are beyond the scope of this dissertation.

This dissertation will focus on the specific case of individual particles with uniform magnetization $\mathbf{M}$. Knowledge and understanding of magnetization dynamics at the level of a single particle can be extended to the general challenge of solving the evolution of complex systems such as for bulk materials, thin films, and other particle ensembles.

2.3   Stochastic Magnetization Dynamics

In the previous section, several deterministic forms of the magnetization dynamic equations were presented. In this section, thermal fluctuations are incorporated into the deterministic magnetization dynamics to model stochastic magnetization dynamics. As magnetic storage cell sizes decrease, the effect of thermal fluctuations plays a larger role. Thermal fluctuations can cause changes to the magnetization state and the aggregate effect may even induce transitions from one stored state to another. In other words, thermal fluctuations may cause an unwanted inversion between stored states in a magnetic storage element from 0 to 1 or vice versa. As this can be a dominant effect in magnetization dynamics, stochastic

magnetization dynamics due to thermal fluctuations will be the focus of the rest of this dissertation.

2.3.1 Ito vs. Stratonovich Calculus

Before any meaningful discussion of stochastic magnetization dynamics can begin, it is important to clarify how the stochastic equations are to be treated. As stochastic magnetization dynamics are described using stochastic differential equations, particularly non-linear stochastic differential equations, it is important to note that these equations cannot be treated using ordinary calculus methods[11,12,15,18].

To treat stochastic differential equations, Ito and Stratonovich defined alternative stochastic calculus methods called Ito and Stratonovich calculus respectively. These two methods both effectively treat stochastic differential equations and differ only in their definition of integration. They are both in common use where Ito calculus is commonly seen in the area of finance for solving the Black-Scholes model for option pricing and Stratonich calculus is frequently used for modeling in physics.

For the case of magnetization dynamics, interpretation in the Stratonovich sense is appropriate and has distinct advantages over the Ito calculus interpretation as will be seen in later chapters.

2.3.2 White Noise

Thermal fluctuations in magnetization dynamics are usually studied by introducing a stochastic term to the deterministic Landau-Lifshitz or Landau-Lifshitz-

Gilbert equation. As the white-noise process has been extensively studied and often appears in mathematical descriptions of other physical systems, the traditional choice is to introduce a white-noise process to the deterministic magnetization dynamics. There is also some debate as to how the white-noise process should be introduced in the equation. One form the stochastic Landau-Lifshitz equation can take is:

$$\frac{d\mathbf{m}}{dt} = -\mathbf{m} \times (\mathbf{h}_{eff} + \nu\mathbf{h}_N(t)) - \alpha\mathbf{m} \times (\mathbf{m} \times \mathbf{h}_{eff}), \qquad (2.22)$$

where $\mathbf{m}$ and $\mathbf{h}_{eff}$ are normalized versions of the magnetization and effective applied field, respectively, and $\mathbf{h}_N$ is a white-noise vector field with parameter ν. ν is a parameter that measure the intensity of thermal perturbations. In this form, the noise term is a perturbation of the precessional term.

An alternative form is:

$$\frac{d\mathbf{m}}{dt} = -\mathbf{m} \times (\mathbf{h}_{eff} + \nu\mathbf{h}_N(t)) - \alpha\mathbf{m} \times [\mathbf{m} \times (\mathbf{h}_{eff} + \nu\mathbf{h}_N(t))] \qquad (2.23)$$

In this form of the stochastic magnetization dynamics, the noise field is a perturbation of the effective field.

In both cases, the noise field is a random field whose components are independent gaussian white-noise processes and both can be shown to be equivalent up to a renormalization of coefficients. Gaussian white-noise processes are defined as the derivative of the isotropic Wiener process $\mathbf{W}(t)$ so

$$\mathbf{h}_N(t) = \frac{d\mathbf{W}(t)}{dt}. \qquad (2.24)$$

By considering the Wiener process, the stochastic Landau-Lifshitz equation (2.22)

16

can be rewritten as:

$$dm = -[\mathbf{m} \times \mathbf{h}_{eff} + \alpha \mathbf{m} \times (\mathbf{m} \times \mathbf{h}_{eff})]dt + \nu \mathbf{m} \times d\mathbf{W}(t). \qquad (2.25)$$

This stochastic differential equation is complex and hard to solve with exact analytical solutions only possible in the simplest cases. To solve more complicated equations of this form, many numerical methods have been developed to evaluate numerical solutions for certain special cases of interest.

Chapter 3:   Jump-Noise Driven Magentization Dynamics

3.1   Stochastic Interpretation

Stochastic magnetization dynamics has traditionally been modeled using a white-noise process in the Landau-Lifshitz or Landau-Lifshitz-Gilbert equations as mentioned in the previous chapter. In their simplest form, these equations contain three terms: a precessional term, a damping term, and a stochastic noise term. In reality, the last two terms can be seen to model the same thermal phenomenon. The reason that these two terms are necessary is that neither term can fully describe the noise effects from the thermal bath on their own. The damping term can model an aggregate effect but does not contain the necessary mathematics to deal with random fluctuations in time. The white-noise term can deal with fluctuations in time but, as white-noise is inherently a zero-mean process, it cannot deal with the aggregate motion of thermal drift. These relations were originally established by using the fluctuation-dissipation theorem such that the Landau-Lifshitz or Landau-Lifshitz-Gilbert equations establish an equilibrium condition that is disturbed by small random fluctuations. This approach works for conditions close to equilibrium such that the damping effect is small, but may not accurately describe the behavior when the magnetization state is far from equilibrium. To develop a better model, the

influence of the thermal bath should be considered as a whole, without restrictions such as applying the fluctuation-dissipation theorem.

One method of accounting for thermal fluctuations without the fluctuation-dissipation theorem is by using a jump, or 'jump-noise' process. In a jump-noise process, the magnetization experiences random, discrete 'jumps' in magnetization that follow a set probability distribution[27,28,31,34]. Since the jump-noise process is not zero-mean, thermal effects can be fully described using a single term. Using this approach, the jump-noise driven magnetization dynamics can also be shown to be equivalent to the traditional stochastic magnetization dynamics under certain cases as the traditional damping term appears as the average of the jump-noise process.

3.1.1   Jump-Process

It is useful to briefly describe the nature of the jump-process and highlight some differences that separate this stochastic process from the Wiener white-noise process.

Under the white-noise stochastic interpretation, random effects will occur as continuous noise that satisfies the Hölder condition, with stationary, independent increments that follow a zero-mean, Gaussian distribution. The stochastic interpretation of the jump process differs in that the jump process has large discrete 'jumps' and can follow a distribution with a non-zero mean. Common usages for the jump process are in the description of particle transport in semiconductor physics or for modeling the movement of prices in financial models.

3.2 Stochastic Magnetization Dynamics using Jump-Noise

As mentioned in the previous section, a jump-noise process can be introduced to account for interactions with the thermal bath. The stochastic magnetization dynamics can therefore be written as

$$\frac{d\mathbf{M}}{dt} = -\gamma(\mathbf{M} \times \mathbf{H}_{eff}) + \mathbf{T}_r(t), \tag{3.1}$$

where $\mathbf{M}$ is the magnetization, γ is the gyromagnetic ratio, and $\mathbf{H}_{eff}$ is the effective magnetic field as described in the previous chapter. In this equation, $\mathbf{T}_r(t)$ is a time-dependent jump-noise process that is introduced to account for thermal bath effects. $\mathbf{T}_r(t)$ is defined by the equation

$$\mathbf{T}_r(t) = \sum_i \mathbf{m}_i \delta(t - t_i), \tag{3.2}$$

where $\mathbf{m}_i$ represent random jumps in the magnetization that occur at random instances of time t_i. This random jump is also known as a 'scattering' event. It is important to note that in this definition of jump-noise, it can be seen that the jump-noise does not directly depend on the magnetization. From the equations presented in (3.1) and (3.2), it is easy to see that the magnetization dynamics consists of the typical precessional motion randomly interrupted by random jumps in magnetization as shown in Figure 3.1.

As the conditions under consideration are far below the Curie temperature, the local exchange interactions prevail and so the magnitude of magnetization must satisfy the micromagnetic constraints:

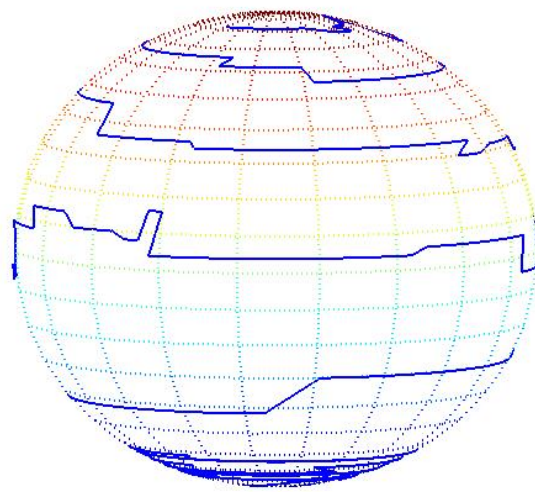$$|\mathbf{M}(t)| = M_s = \text{const}, \tag{3.3}$$

Figure 3.1: Magnetization dynamics consists of precessional motion randomly interrupted by random jumps in magnetization.

where M_s is the spontaneous magnetization. Therefore, the random jumps in magnetization defined by the jump-noise process must remain on the surface of the sphere Σ defined by (3.3).

To solve for the jump-noise process, the statistics for $\mathbf{m}_i$ and t_i must be fully defined. This can be done by introducing the transition probability rate $S(\mathbf{M}_i, \mathbf{M}_{i+1})$, where $\mathbf{M}_i = \mathbf{M}(t_i^-)$ and $\mathbf{M}_{i+1} = \mathbf{M}(t_i^+) = \mathbf{M}_i + \mathbf{m}_i$ are the magnetization immediate prior to and following a random jump at random time t_i, respectively. This transition probability rate represents the rate at which transitions from $\mathbf{M}_i$ to $\mathbf{M}_{i+1}$ are likely to occur. To satisfy (3.3) such that the magnitude of magnetization remains constant, $S(\mathbf{M}_i, \mathbf{M}_{i+1})$ must therefore be defined on the sphere Σ. What this means is that transitions to magnetizations off of the sphere cannot happen, and that $S(\mathbf{M}_i, \mathbf{M}_{i+1}) = 0$ for all $\mathbf{M}_{i+1}$ not on the sphere Σ.

To find the transition probability rate, it is easier to start with a description of the stochastic magnetization dynamics from the point of view of transition probability densities $w(\mathbf{M}, t; \mathbf{M}_0, t_0)$, which describes the probability distribution at time t. This is a Markov approach and for notational simplicity, the 'backward' variables will be omitted from the following chapters. It can be shown that the transition probability density is a solution to

$$\frac{\partial w}{\partial t} = -\gamma \nabla_\Sigma \cdot [(\mathbf{M} \times \nabla_\Sigma g)w] + \hat{C}(w), \tag{3.4}$$

where $\hat{C}(w)$ is a collision integral given by

$$\hat{C}(w) = \oint_\Sigma [S(\mathbf{M}', \mathbf{M})w(\mathbf{M}', t) - S(\mathbf{M}, \mathbf{M}')w(\mathbf{M}, t)]d\Sigma', \tag{3.5}$$

and g is the micromagnetic free energy. g is related to the effective field $\mathbf{H}_{eff}$ by

$$\mathbf{H}_{eff} = -\nabla_\Sigma g. \tag{3.6}$$

By observing (3.4) and (3.5), it is clear that the collision integral does not share the same form of a second-order PDE 'diffusion' term that is expected from a white-noise process. Instead, the collision integral is first-order, which makes (3.4) a linear PDE and considerably easier to solve. Equation (3.4) is therefore convenient for deriving the transition probability rate $S(\mathbf{M}, \mathbf{M}')$.

At thermal equilibrium, the transition probability density follows a global Boltzmann-type distribution and obeys the equations:

$$w(\mathbf{M}, t) = w_0(\mathbf{M}) = Ae^{-\frac{g(\mathbf{M})}{kT}}, \tag{3.7}$$

$$\frac{\partial w_0(\mathbf{M})}{\partial t} = 0, \tag{3.8}$$

and

$$\nabla_\Sigma \cdot [(\mathbf{M} \times \nabla_\Sigma g)w_0] = 0, \tag{3.9}$$

where w_0 is the equilibrium transition probability density and A is a normalization parameter.

This means is that assuming the magnetization is in well R_1, the distribution in that well can be mathematically expressed by the formula

$$w_{o1}(\mathbf{M}) = \frac{1}{Z_1}e^{-\frac{g(\mathbf{M})-g_1}{kT}}, \tag{3.10}$$

where Z_1 is a partition function that is define by

$$Z_1 = \int_{R_1} e^{-\frac{g(\mathbf{M})-g_1}{kT}} dg, \tag{3.11}$$

and g_1 is the energy minimum in R_1.

By using the equation in (3.5), the collision integral at equilibrium becomes

$$\hat{C}(w) = \oint_{\Sigma} [S(\mathbf{M'}, \mathbf{M})w(\mathbf{M'}, t) - S(\mathbf{M}, \mathbf{M'})w(\mathbf{M}, t)]d\Sigma' = 0. \qquad (3.12)$$

Put another way, (3.4) is satisfied at equilibrium if the "detailed balance" condition is satisfied:

$$S(\mathbf{M'}, \mathbf{M})w(\mathbf{M'}, t) = S(\mathbf{M}, \mathbf{M'})w(\mathbf{M}, t). \qquad (3.13)$$

This is a natural result as it expresses that at equilibrium, the probability of scattering from $\mathbf{M}$ to a point $\mathbf{M'}$ on Σ is exactly balanced by the probability of scattering from $\mathbf{M'}$ to $\mathbf{M}$.

From the detailed balance equation and (3.7), it is easy to see that $S(\mathbf{M}, \mathbf{M'})$ can be expressed in the form

$$S(\mathbf{M}, \mathbf{M'}) = \phi(\mathbf{M}, \mathbf{M'})e^{\frac{g(\mathbf{M})-g(\mathbf{M'})}{2kT}}, \qquad (3.14)$$

where $\phi(\mathbf{M}, \mathbf{M'})$ is a symmetric function such that $\phi(\mathbf{M}, \mathbf{M'}) = \phi(\mathbf{M'}, \mathbf{M})$. In general, $\phi(\mathbf{M}, \mathbf{M'})$ should be determined from experimental results, but it is natural to assume that it is narrow peaked at $\mathbf{M} = \mathbf{M'}$ since small jumps in magnetization are much more likely than large jumps. The symmetric function $\phi(\mathbf{M}, \mathbf{M'})$ can therefore be defined as

$$\phi(\mathbf{M}, \mathbf{M'}) = \phi(|\mathbf{M} - \mathbf{M'}|). \qquad (3.15)$$

Using the identity

$$\phi(x) = e^{\ln \phi(x)}, \qquad (3.16)$$

and taking the first three terms of the Taylor expansion for the natural logarithm,

$$\ln \phi(x) \simeq \ln \phi(0) - \frac{|\phi''(0)|}{2\phi(0)} x^2. \tag{3.17}$$

The transition probability rate can therefore be written as

$$S(\mathbf{M}, \mathbf{M}') = A e^{-\frac{|\mathbf{M}-\mathbf{M}'|^2}{2\sigma^2}} e^{\frac{g(\mathbf{M})-g(\mathbf{M}')}{2kT}}, \tag{3.18}$$

where A and σ^2 characterize the thermal bath effects and

$$\sigma^2 = \frac{\phi(0)}{|\phi''(0)|}. \tag{3.19}$$

Now that the transition probability rate is defined, the equation for jump-noise process driven magnetization dynamics can be characterized. From the transition probability rate construct, the timing of the jumps can be characterized by

$$\Pr(t_{i+1} - t_i > \tau) = e^{-\int_{t_i}^{t_{i+1}} \lambda(\mathbf{M}(t))dt}, \tag{3.20}$$

where $\lambda(\mathbf{M}(t))$ is the scattering rate. This scattering rate is defined as

$$\lambda(\mathbf{M}(t)) = \oint_{\Sigma} S(\mathbf{M}(t), \mathbf{M}')d\Sigma', \tag{3.21}$$

where Σ' is the sphere defined by all possible magnetizations of $\mathbf{M}'$.

From equation (3.21) it is easy to see that the scattering rate is the probability of a magnetization scattering event occurring from $\mathbf{M}(t)$ to any point $\mathbf{M}'$ on Σ during a time interval dt. Assuming a scattering event occurs, the conditional probability density of the jump in magnetization $\mathbf{m}_i$ is given by

$$\chi(\mathbf{m}_i | \mathbf{M}_i) = \frac{S(\mathbf{M}_i, \mathbf{M}_i + \mathbf{m}_i)}{\lambda(\mathbf{M}_i)}. \tag{3.22}$$

This conditional probability density satisfies normalization conditions,

$$\oint_{\Sigma} \chi(\mathbf{m}_i|\mathbf{M}_i)d\Sigma_{\mathbf{m}_i} = 1, \tag{3.23}$$

where $\Sigma_{\mathbf{m}_i}$ is the sphere defined by all possible $\mathbf{m}_i$ such that $\mathbf{M}_i + \mathbf{m}_i$ remains on the sphere Σ.

To show that this jump-noise process approach can be interpreted in the same way as the classical stochastic magnetization dynamics, the magnetization damping term can be extracted from the expected value of the jump-noise. The jump noise process defined above can also be written as

$$\mathbf{T}_r(t) = E(\mathbf{T}_r) + \mathbf{T}_r^0(t), \tag{3.24}$$

where the first term is the expected value of the jump-noise process and the second term is the zero-mean fluctuations.

It has been shown[15] that the expected value of the jump-noise process can be written

$$E(\mathbf{T}_r) = \lambda(\mathbf{M}(t))E(\mathbf{m}(t)). \tag{3.25}$$

From a physical viewpoint, it can be safe to assume that only small jumps $\mathbf{m}(t)$ in magnetization have non-negligible probability of occurring. This assumption also follows from (3.22) where large jumps will have a very small transition probability rate. Using this assumption and the fact that jumps in magnetization are constrained to Σ, it can be concluded that

$$\mathbf{M}(t) \cdot E(\mathbf{m}(t)) \simeq 0 \tag{3.26}$$

since the angle of the magnetization does not change significantly.

From equations (3.25) and (3.26) and multiplying through by $\lambda(\mathbf{M}(t))$, it is easy to see that

$$\mathbf{M}(t) \cdot E(\mathbf{T}_r(t)) \simeq 0. \tag{3.27}$$

This implies that the expected value of the jump-noise process is in a direction that is orthogonal to the magnetization $\mathbf{M}(t)$. As a consequence, this means that the magnitude of magnetization is conserved by the jump-noise process. By choosing basis vectors in the plane orthogonal to $\mathbf{M}(t)$, the expected value of the jump-noise process can be written as

$$E(\mathbf{T}_r(t)) \approx -\gamma'(\mathbf{M} \times \mathbf{H}_{eff}) - \alpha\mathbf{M} \times (\mathbf{M} \times \mathbf{H}_{eff}). \tag{3.28}$$

This leads to the expression for the stochastic magnetization dynamics equation:

$$\frac{d\mathbf{M}}{dt} = -(\gamma + \gamma')(\mathbf{M} \times \mathbf{H}_{eff}) - \alpha\mathbf{M} \times (\mathbf{M} \times \mathbf{H}_{eff}) + \mathbf{T}_r^0(t). \tag{3.29}$$

This has the same form as the stochastic Landau-Lifshitz equation. With the appropriate change in basis vectors, it can easily be shown that the stochastic Landau-Lifshitz-Gilbert equation emerges.

3.3   Numerical Modeling

Now that the jump-noise process driven magnetization dynamics has been fully defined, a method of solving the equation is needed. As mentioned at the end of chapter 2, exact analytical solutions of stochastic magnetization dynamics are only possible in certain cases. Therefore, to analyze general stochastic magnetization dynamics, numerical methods are needed.

From (3.1) it is clear that there are two distinct components to the jump-noise driven dynamics. The first component is a deterministic precessional motion and the second component is a random scattering due to the jump-noise process. A natural breakdown for finding a numerical solution is to also have two distinct components – one part to handle the precessional motion and another part to handle the stochastic term.

3.3.1   Precessional Motion

To numerically integrate the precessional motion of the stochastic magnetization dynamics, some extra care is needed. As (3.1) is a stochastic differential equation, ordinary differential equation methods do not necessarily apply. In the case of multiplicative stochastic noise, as with (3.1) where the noise is a function of magnetization, there is a choice in stochastic integration interpretation as mentioned previously. The two different interpretations are known as Itō calculus or Stratonovich calculus. These two interpretations handle random processes differently but have been shown to produce equivalent results after an appropriate transformation. Generally, the use of Itō calculus is more prevalent in fields such as finance theory where the stochastic equation can only depend upon past events. On the other hand, the Stratonovich integral has gained wide acceptance in physics due to its ability to model physical phenomena and the convenient fact that it obeys certain ordinary calculus rules such as the chain rule. To solve (3.1), a numerical strategy based on the Stratonovich interpretation will be used.

Looking at only the precessional component of the magnetization dynamics, the equation is left with:

$$\frac{d\mathbf{M}}{dt} = -\gamma(\mathbf{M} \times \mathbf{H}_{eff}). \tag{3.30}$$

This equation can be solved by using a mid-point finite difference scheme:

$$\frac{\mathbf{M}^{(n+1)} - \mathbf{M}^{(n)}}{\Delta t_n} = -\gamma \frac{\mathbf{M}^{(n+1)} + \mathbf{M}^{(n)}}{2} \times \mathbf{H}_{eff}^{(n+\frac{1}{2})}. \tag{3.31}$$

This scheme is borrowed from finite element analysis techniques where the magnetization is analyzed at discrete time steps $t_1, t_2, ...t_n$ and $\Delta t_n = t_{n+1} - t_n$. In this method, $\mathbf{M}^{(n+1)}$ is the magnetization at t_{n+1}, $\mathbf{M}^{(n)}$ is the magnetization at t_n, and $\mathbf{H}_{eff}^{(n+\frac{1}{2})}$ is the effective magnetic field at $t_{n+\frac{1}{2}} = t_n + \frac{\Delta t_n}{2}$.

An easily seen benefit of this approach is that the micromagnetic constraints are satisfied. This can be proven by dot-multiplying both sides of (3.31) by $\mathbf{M}^{(n+1)} + \mathbf{M}^{(n)}$. Since the right side of (3.31) contains the cross product with respect to $\mathbf{M}^{(n+1)} + \mathbf{M}^{(n)}$ and since the cross product of a vector is orthogonal to itself, the right side of the equation disappears. What remains is:

$$\left[\mathbf{M}^{(n+1)} + \mathbf{M}^{(n)}\right] \cdot \left[\frac{\mathbf{M}^{(n+1)} - \mathbf{M}^{(n)}}{\Delta t_n}\right] = 0. \tag{3.32}$$

Rearranging the terms gives:

$$\left[\mathbf{M}^{(n+1)} + \mathbf{M}^{(n)}\right] \cdot \frac{\mathbf{M}^{(n+1)}}{\Delta t_n} = \left[\mathbf{M}^{(n+1)} + \mathbf{M}^{(n)}\right] \cdot \frac{\mathbf{M}^{(n)}}{\Delta t_n}. \tag{3.33}$$

Multiplying through by Δt_n and distributing gives:

$$\mathbf{M}^{(n+1)} \cdot \mathbf{M}^{(n+1)} + \mathbf{M}^{(n)} \cdot \mathbf{M}^{(n+1)} = \mathbf{M}^{(n+1)} \cdot \mathbf{M}^{(n)} + \mathbf{M}^{(n)} \cdot \mathbf{M}^{(n)}. \tag{3.34}$$

Simplifying this equation gives:

$$|\mathbf{M}^{(n+1)}|^2 = |\mathbf{M}^{(n)}|^2 = M_s^2. \tag{3.35}$$

It is easy to see that this result is independent of $\mathbf{H}_{eff}$ and thus demonstrates that this method will always conserve the magnitude of magnetization and can accurately model precessional magnetization dynamics.

Another method to verify the accuracy of the mid-point finite difference scheme is that as (3.30) only includes the precessional motion, the micromagnetic free energy should remain constant. What this means is that precessional trajectories traced out by the magnetization must form closed trajectories. Figure 3.2 shows that for sufficiently small time steps Δt_n, the numerical scheme does indeed result in closed precessional trajectories. The three trajectories presented together in Figure 3.2 represent closed paths of constant energy under different anisotropy and externally applied field conditions.

3.3.2   Jump-Noise Component

Once the precessional term in (3.1) is solved using the finite midpoint difference scheme, it is necessary to evaluate the second term in the equation. Since the scattering rate $\lambda(\mathbf{M}(t))$ for the jump-noise process is a function of the magnetization, the time-statistics therefore obey a inhomogeneous Poisson distribution. As a result, it is very difficult to determine τ, the time interval between jumps, or scattering events. To handle this random component of the magnetization dynamics,
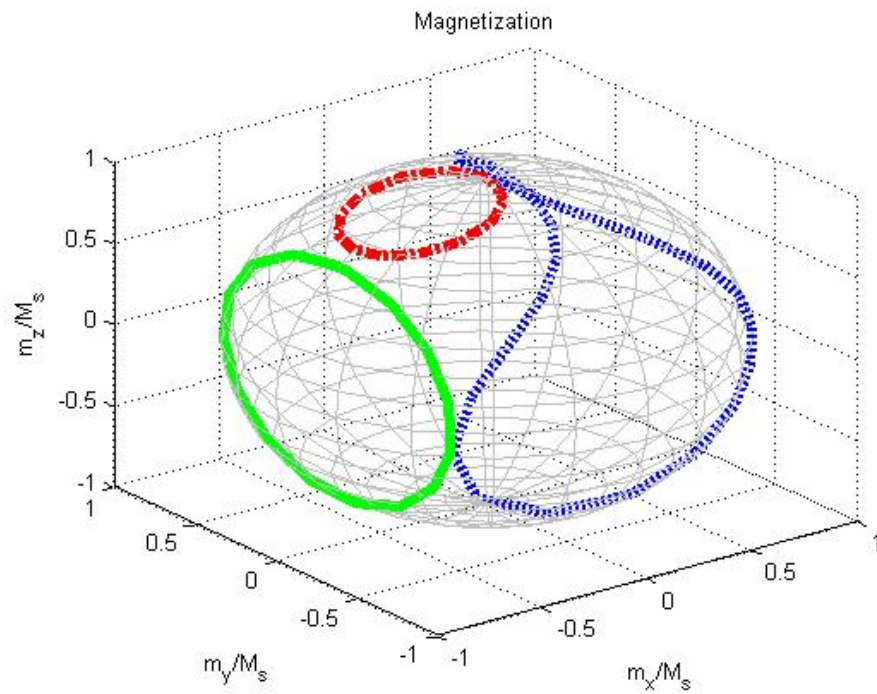
Figure 3.2: Magnetization dynamics with no damping results in closed precessional trajectories. Three separate closed trajectories are shown for different anisotropy and applied field values.

a technique called 'self-scattering' is borrowed from analyzing semiclassical trans-
port of electrons and holes in semiconductor physics[26]. To simplify the problem of
solving jump-noise, a complementary random jump process $\mathbf{T}_r^{(0)}(t)$ that describes
'self-scattering' can be added to (2.1):

$$\frac{d\mathbf{M}}{dt} = -\gamma(\mathbf{M} \times \mathbf{H}_{eff}) + \mathbf{T}_r(t) + \mathbf{T}_r^{(0)}(t). \tag{3.36}$$

While this may seem to make the equation more complex as there are now two
random jump-processes to consider, the way $\mathbf{T}_r^{(0)}(t)$ is defined considerably simplifies
the calculations.

Similar to $\mathbf{T}_r(t)$, $\mathbf{T}_r^{(0)}(t)$ is defined by transition probability rate $S_0(\mathbf{M}_i, \mathbf{M}_{i+1})$.
This transition probability rate is given by

$$S_0(\mathbf{M}_i, \mathbf{M}_{i+1}) = \lambda_0(\mathbf{M}_i)\delta(\mathbf{M}_{i+1} - \mathbf{M}_i). \tag{3.37}$$

The conditional probability density $\chi_0(\mathbf{m}_i|\mathbf{M}_i)$, for this new scattering term is found
to be

$$\chi_0(\mathbf{m}_i|\mathbf{M}_i) = \frac{S_0(\mathbf{M}_i, \mathbf{M}_i + \mathbf{m}_i)}{\lambda_0(\mathbf{M}_i)} = \delta(\mathbf{m}_i). \tag{3.38}$$

What this means is that this additional scattering process will produce jumps in
magnetization that stay exactly in the same place. For this reason, this additional
scattering process is called 'self-scattering.'

Since the addition of a self-scattering process does not actually change the
magnetization dynamics, one can wonder: what is the point of this additional term?
While self-scattering does not affect the stochastic dynamics, the self-scattering rate
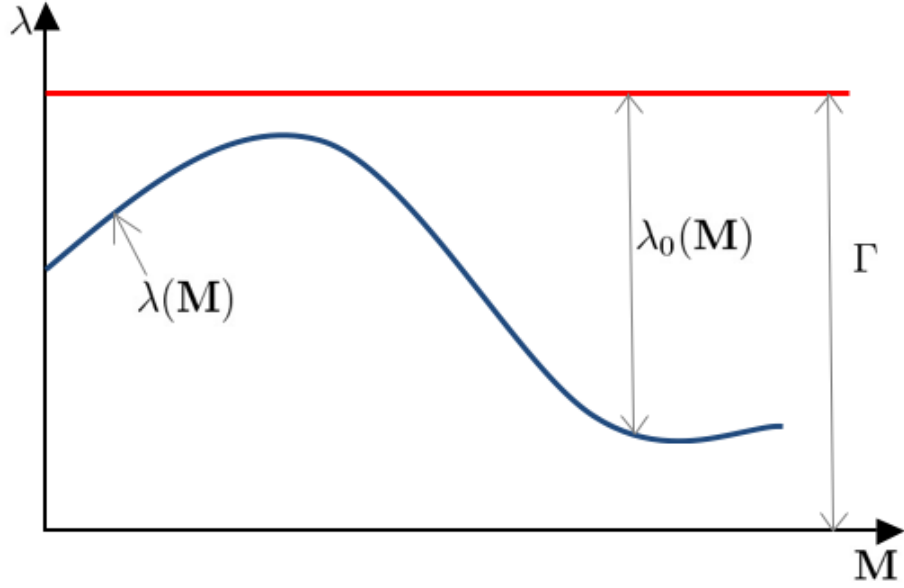can have an impact on the total scattering rate experienced by the magnetization.

Figure 3.3: The self-scattering rate λ_0 is added to the thermal scattering rate λ to create a homogeneous total scattering rate Γ.

By choosing an appropriate self-scattering rate, it is possible to homogenize the total scattering rate in time as seen in Figure 3.3. This greatly simplifies the numerical calculations needed for finding the time between jumps. By choosing $\lambda_0(\mathbf{M}(t))$ such that the total scattering rate Γ is

$$\Gamma = \lambda(\mathbf{M}(t)) + \lambda_0(\mathbf{M}(t)) = \text{const}, \tag{3.39}$$

then the time interval between scattering events becomes much easier to solve.

The statistics for the time between jumps given in (3.4) then becomes

$$\Pr(t_{i+1} - t_i > \tau) = e^{-\Gamma \tau}. \tag{3.40}$$

Since (3.40) gives the probability that scattering occurs after time interval τ, the

complement of this equation gives the probability $P(\tau)$ of scattering during τ:

$$P(t \leq \tau) = 1 - e^{-\Gamma\tau}. \tag{3.41}$$

As seen from (3.40) and (3.41), both of these time statistics are independent of t_i.

To generate the time intervals τ between scattering events for numerical simulations, the inverse of (3.41) can be used:

$$\tau = -\frac{1}{\Gamma} \ln[1 - P(\tau)]. \tag{3.42}$$

Since $P(\tau)$ is a probability distribution with values that lie between 0 and 1, a value for τ can be obtained by randomly generating a value for P that is uniformly distributed between 0 and 1. Thus, if a scattering event occurs at t_i, the next scattering event is calculated to occur at $t_{i+1} = t_i + \tau$.

Once a scattering event has been determined, a determination must be made as to if the scattering event was due to self-scattering or due to thermal fluctuations. Since the total scattering rate is the sum of the individual scattering rates, the probability densities of thermal scattering and self-scattering are proportional to their respective scattering rates, $\lambda(\mathbf{M})$ and $\lambda_0(\mathbf{M})$. Discrimination between the two events can therefore be made by randomly generating a value ν between 0 and Γ whose probability is uniformly distributed. If $0 < \nu < \lambda(\mathbf{M})$, then the scattering is said to be due to thermal fluctuations. The new magnetization is then determined using the conditional probability density in (3.22). If $\lambda(\mathbf{M}) < \nu < \Gamma$, a self-scattering event is determined to have occurred. The new magnetization after the scattering is therefore the same as before the scattering in accordance to the conditional probability density in (3.38). Once these determinations have

been made, the process repeats by generating a new random time interval τ and precessing the magnetization until that time instance is reached.

3.3.3 Monte Carlo Analysis

The evolution of a single instance of a ferromagnetic particle driven by a jump-noise process can be obtained by following the numerical techniques outlined in the previous subsections. Because the jump-noise process is inherently random, the magnetization trajectories resulting from these dynamic evolutions will also be random. As a result, each trajectory will be different and will represent just one of an infinite realm of possible trajectories the magnetization can take. To obtain useful information from these trajectories and to gain a better understanding of the time evolution of the system, a Monte Carlo approach is necessary. By generating hundreds, or thousands, or even more trajectories that differ by their randomly generated time intervals and jumps in magnetization, the Monte Carlo approach can produce a distribution from the aggregate trajectories. Therefore, not only are the possible trajectories obtained, but how likely each realization is will also be known.

Figure 3.4 illustrates the cumulative distribution function for the probability of first switching in a uniaxial particle with energy barrier of $1.74kT$.

Figure 3.5 shows that the cumulative distribution function for the probability of first switching in a uniaxial particle does not change at elevated temperatures as long as the energy barrier remains the same.
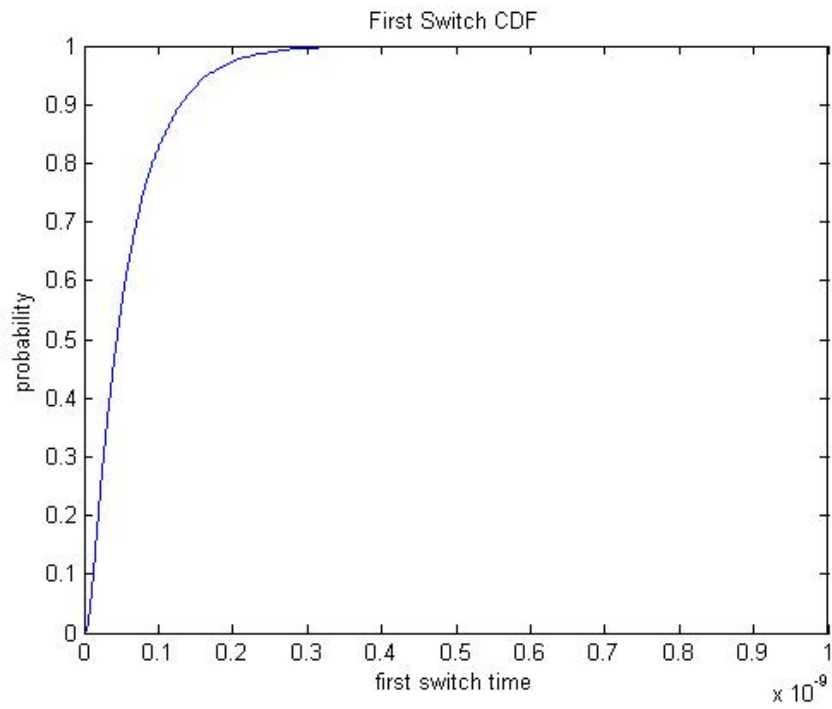
First Switch CDF

probability

first switch time

x 10⁻⁹

Figure 3.4: Cumulative distribution function for $D_x = D_y = 0.1$, $D_z = 0.01$, $H_a = 0$, $T = 300$K, $\sigma^2 = 0.1$, $B = 10^{12}$, normalized $g/kT = 1.7407$.
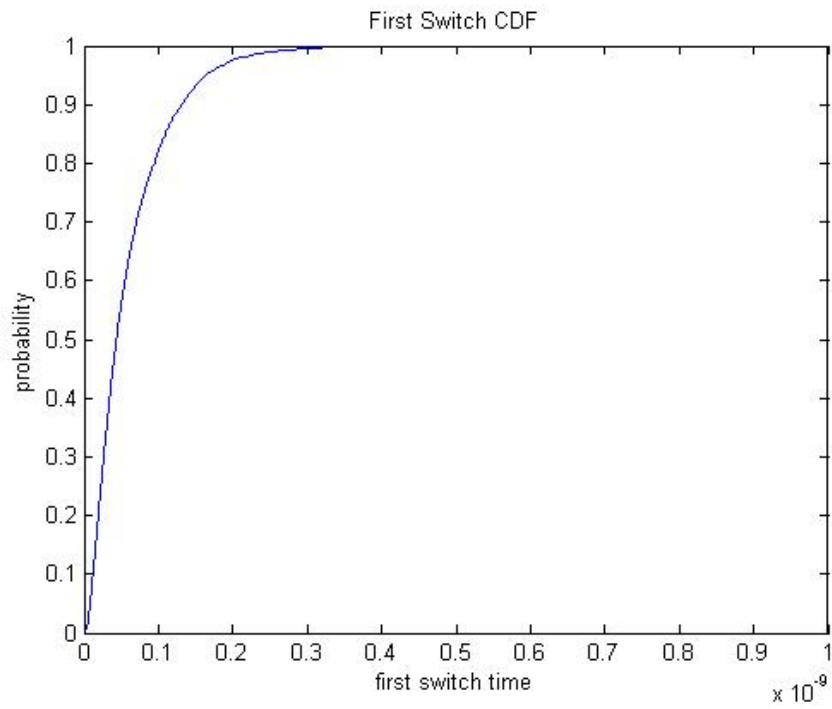
Figure 3.5: Cumulative distribution function for $D_x = D_y = 0.15$, $D_z = 0.01$, $H_a = 0$, $T = 466.7$K, $\sigma^2 = 0.1$, $B = 10^{12}$, normalized $g/kT = 1.7406$.
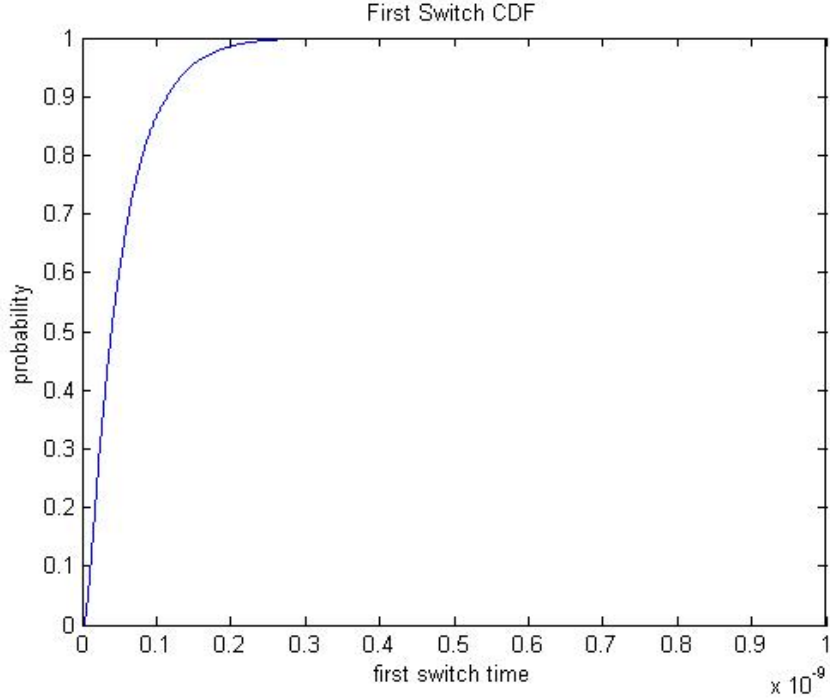
Figure 3.6: Cumulative distribution function for $D_x = D_y = 0.15$, $D_z = 0.01$, $H_a = -0.0277$, $T = 300$K, $\sigma^2 = 0.1$, $B = 10^{12}$, normalized $g/kT = 1.742$.

In figure 3.6, the cumulative distribution function for the probability of first switching in a uniaxial particle can be seen to be the same under applied magnetic fields as long as the energy barrier remains the same.

Because of the random nature of this Monte Carlo approach, simulations results may differ from simulation to simulation, even with the same initial conditions. Therefore, for higher accuracy, a larger number of realizations are necessary. However, even with more realizations, it is not possible to realize every trajectory and so the Monte Carlo approach can only approach the exact solution as the number of trials approach infinity.

3.3.4 Parallel Processing

It should be mentioned that the Monte Carlo approach to modeling magnetization dynamics can be inherently slow since it depends on aggregating large numbers of independent trajectories to create the resulting probability distribution. Using traditional computing resources where calculations are performed on CPUs, this Monte Carlo process can easily become time restrictive.

Using an alternative computational approach, the Monte Carlo method can be designed such that the calculations can be performed in parallel on Graphics Processing Units (GPUs)[25]. Since the trajectories calculated using the Monte Carlo approach are inherently independent from each other, the Monte Carlo simulations are uniquely suited for parallel processing.

Figure 3.7 illustrate the simulated results of the equilibrium distribution for a uniaxial superparamagnetic cobalt nanoparticle. This calculation was performed on GPUs using over 10,000 Monte Carlo simulations and show close agreement with the expected Monte Carlo distribution. Additional details of this GPU approach are beyond the scope of this dissertation and will be omitted.
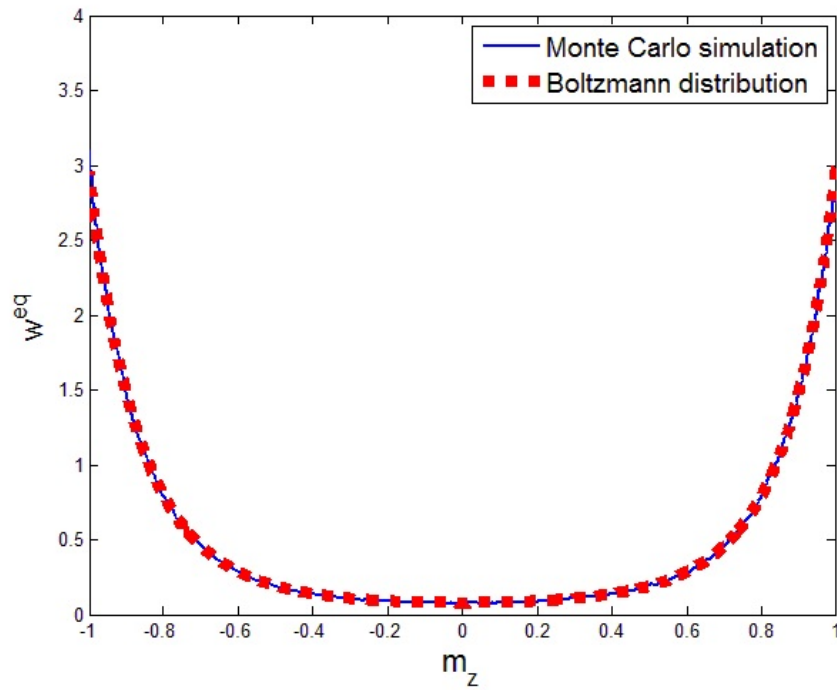
Figure 3.7: Uniaxial cobalt nanoparticle with $D_x = 0.2$ $D_y = 0.2$ $D_z = 0.01$ $M_s = 1.42 \times 10^6$ $\gamma = 1.837$ $T = 300$ $V = 2 \times 10^{-25}$ $\sigma = 0.1$ $B = 10^{12}$.

Chapter 4:   Magnetization Dynamics on Graphs

4.1   Averaging Technique

In the previous chapter, a numerical method of modeling stochastic magnetization dynamics driven by a jump-noise process was discussed. Using the Monte Carlo approach outlined, magnetization dynamics can be accurately analyzed by exploring the many different magnetization trajectories that the magnetization can follow. One distinct disadvantage of this Monte Carlo approach is that many, many magnetization trajectory realizations are needed to form an accurate picture of the magnetization dynamics and even then, the results will not, and in most cases, cannot perfectly reflect all possible instances of the magnetization trajectories. Another disadvantage is that using the Monte Carlo approach can be very time intensive and computationally intensive to obtain an accurate picture of the magnetization dynamics. In this chapter, a different approach to solving stochastic magnetization dynamics is introduced and explored.

Typically, thermal noise effects in the magnetization dynamics equation are small in comparison with the precessional motion. This leads to magnetization damping and thermal fluctuation effects that occur on a much longer time-scale than the precessional motion of the magnetization. As the effects of thermal noise

are the main focus of this research, the stochastic magnetization dynamics on the level of transition probability densities described by equation (3.4) can be averaged over precessional trajectories to isolate the damping and thermal fluctuation components[2,3]. These precessional trajectories are uniquely defined by their micromagnetic free energy g and the implementation of this averaging technique reduces the stochastic magnetization dynamics defined on the sphere Σ, to dynamics defined on specific graphs defined by g. The energy graphs that result from this averaging technique are an accurate and complete reflection of the energy landscapes on Σ and includes all critical nodes such as energy wells (minima), energy peaks (maxima), and saddle points.

As described in chapter 3 in (3.4) and (3.5), the stochastic magnetization dynamics driven by a jump-noise process can be described on the level of transition probability density $w(\mathbf{M}, t)$ using a Kolmogorov-Fokker-Planck equation:

$$
\begin{aligned}
\frac{\partial w}{\partial t} = & -\gamma \nabla_\Sigma \cdot [(\mathbf{M} \times \nabla_\Sigma g_L) w] \\
& + \int_\Sigma [S(\mathbf{M}', \mathbf{M}) w(\mathbf{M}') - S(\mathbf{M}, \mathbf{M}') w(\mathbf{M})] d\Sigma_{\mathbf{M}'}.
\end{aligned} \tag{4.1}
$$

To study (4.1) in the limit of small fluctuations, where $S(\mathbf{M}, \mathbf{M}')$ is small, it is convenient to use a different coordinate system, one in which g plays a role as a coordinate variable. A coordinate system defined by the following unit vectors is considered:

$$
\mathbf{e}_g = \frac{\nabla_\Sigma g}{|\nabla_\Sigma g|}, \quad \mathbf{e}_\psi = \mathbf{M} \times \mathbf{e}_g. \tag{4.2}
$$

These unit vectors are mutually orthogonal and are tangential to the constant energy curves $C_k(g)$, where k denotes an edge of the energy graph. In this coordinate

system, the differential displacements of magnetization (dm_g and dm_ψ) along the unit vectors are given by:

$$dm_g = \mathbf{e}_g \cdot d\mathbf{M} = l_g dg, \quad dm_\psi = \mathbf{e}_\psi \cdot d\mathbf{M} = l_\psi d\psi, \tag{4.3}$$

where l_g and l_ψ are appropriate metric factors. From (4.2), l_g is found to be

$$l_g = \frac{1}{|\nabla_\Sigma g|}. \tag{4.4}$$

Using this new coordinate system, the collision integral $\hat{C}$ can be written as

$$\hat{C} = \sum_n \int_{L_n} \oint_{C_n(g')} [S(\mathbf{M}_n(g', \psi'), \mathbf{M}_k(g, \psi))w_n(g', \psi', t) \tag{4.5}$$

$$- S(\mathbf{M}_k(g, \psi), \mathbf{M}_n(g', \psi'))w_k(g, \psi, t)] dm_{\psi'} dm_{g'},$$

where $\mathbf{M}_k(g, \psi)$ is the magnetization at (g, ψ) on the edge L_n of the energy graph. L_n is an edge of the graph corresponding to the region R_n of the sphere Σ with the property that there exists only one precessional trajectory $C_n(g)$ corresponding to energy g.

In this new coordinate system, one main advantage is that the two axes represent the nature of the separate time-scales in the dynamics of the problem. g represents the slow variable while ψ represents the fast variable. As mentioned previously, the objective is to remove the fast variable from the equation and isolate an approximate diffusion equation that is left in terms of the slow variable g.

To eliminate the fast variable, the assumption is made that the transition probability density $w(\mathbf{M}, t)$ is uniform along each curve $g(\mathbf{M}) = g$. This assumption is valid for fast precessional motions, but breaks down near critical points, called

separatrices, that include boundaries between energy wells where the precessional period goes to infinity. Fortunately, the separatrix has measure zero and so the assumption is generally valid. Because of this, the distribution function of the transition probability density becomes a function of g:

$$w(\mathbf{M}, t) \approx w_k(g(\mathbf{M}), t) \Rightarrow w_k(g, \psi, t) \approx w_k(g, t), \tag{4.6}$$

where k represents the region defined by energy well k that $\mathbf{M}$ belongs to and $\Rightarrow$ indicates a change of variable from a functional dependence on $\mathbf{M}$ to a functional dependence on g.

To facilitate integration with respect to ψ, the probability density distribution function $\rho(g, t)$ is derived in terms of energy and is given by

$$\rho_k(g, t) = \oint_{C_k(g)} \frac{w(\mathbf{M}, t)}{|\nabla_\Sigma g|} dm_\psi \approx w_k(g, t) \tau_k(g), \tag{4.7}$$

where τ_n is a function defining the period such that

$$\tau_n(g) = \oint_{C_n(g)} \frac{dm_\psi}{|\nabla_\Sigma g(\mathbf{M})|} \tag{4.8}$$

and $\rho_k(g, t)$ satisfies the normalization condition imposed by the axioms of probability that the total probability sums to unity:

$$\sum_k \int_{L_k} \rho_k(g, t) dg = 1. \tag{4.9}$$

Since the equations no longer have a ψ dependence, the dm_ψ in the integrals will be replaced with the notation $dl_\mathbf{M}$ in the following equations such that:

$$\tau_n(g) = \oint_{C_n(g)} \frac{dl_\mathbf{M}}{|\nabla_\Sigma g(\mathbf{M})|} \tag{4.10}$$

Returning to (4.1) and integrating both sides over precessional trajectories, the master equation becomes

$$\oint_{C_k(g)} \frac{1}{|\nabla_\Sigma g|} \frac{\partial w}{\partial t} dl_{\mathbf{M}} = -\oint_{C_k(g)} \frac{1}{|\nabla_\Sigma g|} \gamma \nabla_\Sigma \cdot [(\mathbf{M} \times \nabla_\Sigma g_L)w] dl_{\mathbf{M}}$$

$$+ \oint_{C_k(g)} \frac{1}{|\nabla_\Sigma g|} \int_\Sigma [S(\mathbf{M}', \mathbf{M})w(\mathbf{M}') - S(\mathbf{M}, \mathbf{M}')w(\mathbf{M})] d\Sigma_{\mathbf{M}'} dl_{\mathbf{M}}. \qquad (4.11)$$

First, consider the first term on the right side of the equation. This term is integrated along $dl_{\mathbf{M}}$, which is in the e_ψ direction. From the definition of e_ψ in (4.2), it is important to note that $\mathbf{M} \times \nabla_\Sigma g_L$ also lies in the e_ψ direction. But, since the term in the integral is the divergence of $\mathbf{M} \times \nabla_\Sigma g_L$, the integral evaluates to 0:

$$-\oint_{C_k(g)} \frac{1}{|\nabla_\Sigma g|} \gamma \nabla_\Sigma \cdot [(\mathbf{M} \times \nabla_\Sigma g_L)w] dl_{\mathbf{M}} = 0 \qquad (4.12)$$

Therefore, the master equation can be written with only the collision integral:

$$\oint_{C_k(g)} \frac{1}{|\nabla_\Sigma g|} \frac{\partial w}{\partial t} dl_{\mathbf{M}}$$

$$= \oint_{C_k(g)} \frac{1}{|\nabla_\Sigma g|} \int_\Sigma [S(\mathbf{M}', \mathbf{M})w(\mathbf{M}') - S(\mathbf{M}, \mathbf{M}')w(\mathbf{M})] d\Sigma_{\mathbf{M}'} dl_{\mathbf{M}}. \qquad (4.13)$$

Using (4.7) and rearranging, the master equation becomes

$$\frac{\partial \rho(g,t)}{\partial t} = \oint_{C_k(g)} \int_\Sigma \left[\frac{S(\mathbf{M}', \mathbf{M})w(\mathbf{M}')}{|\nabla_\Sigma g(\mathbf{M})|} - \frac{S(\mathbf{M}, \mathbf{M}')w(\mathbf{M})}{|\nabla_\Sigma g(\mathbf{M})|} \right] d\Sigma_{\mathbf{M}'} dl_{\mathbf{M}}. \qquad (4.14)$$

Replacing the $w(\mathbf{M})$ on the right side of the equation with the appropriate approximation on g and taking into account the different energy wells N in Σ:

$$\frac{\partial \rho_k(g,t)}{\partial t} = \sum_n \oint_{C_k(g)} \int_{L_n} \oint_{C_n(g')} \frac{S(\mathbf{M}', \mathbf{M})w_n(g',t)}{|\nabla_\Sigma g(\mathbf{M}')||\nabla_\Sigma g(\mathbf{M})|}$$

$$- \frac{S(\mathbf{M}, \mathbf{M}')w_k(g,t)}{|\nabla_\Sigma g(\mathbf{M}')||\nabla_\Sigma g(\mathbf{M})|} dl_{\mathbf{M}'} dm_{g'} dl_{\mathbf{M}}. \qquad (4.15)$$

Replacing the w and rearranging the integrals gives:

$$\frac{\partial \rho_k(g,t)}{\partial t} = \sum_n \int_{L_n} \oint_{C_k(g)} \oint_{C_n(g')} \frac{S(\mathbf{M'},\mathbf{M})\rho_n(g',t)}{\tau_n(g')|\nabla_\Sigma g(\mathbf{M'})||\nabla_\Sigma g(\mathbf{M})|}$$
$$- \frac{S(\mathbf{M},\mathbf{M'})\rho_k(g,t)}{\tau_k(g)|\nabla_\Sigma g(\mathbf{M'})||\nabla_\Sigma g(\mathbf{M})|} dl_{\mathbf{M'}} dl_{\mathbf{M}} dm_{g'}. \quad (4.16)$$

A new function $K_{n,k}(g',g)$ can be defined related to $S(\mathbf{M'},\mathbf{M})$ by the formula

$$K_{n,k}(g',g) = \frac{1}{\tau_n(g)} \oint_{C_k(g)} \oint_{C_n(g')} \frac{S(\mathbf{M'},\mathbf{M})}{|\nabla_\Sigma g(\mathbf{M'})||\nabla_\Sigma g(\mathbf{M})|} dl_{\mathbf{M'}} dl_{\mathbf{M}}. \quad (4.17)$$

This function $K_{n,k}(g',g)$ can be seen as the equivalent transitions probability rate on energy graphs.

Using this definition, it is easy to see that the stochastic energy dynamics is described by the following continuous master equation

$$\frac{d\rho_k(g,t)}{dt} = \sum_n \int_{L_n} [K_{n,k}(g',g)\rho_n(g',t) - K_{k,n}(g,g')\rho_k(g,t)]dg',$$

$$(k = 1,2,...N), \quad (4.18)$$

where $\rho_n(g,t)$ is the probability density on edge L_n and the summation is performed over all N edges of the graph.

4.2 Alternative Eigenvalue Method

To further study the continuous master equation in (4.18), a more concise form of the equation can be used[29]:

$$\frac{\partial \boldsymbol{\rho}}{\partial t} = \hat{K}\boldsymbol{\rho}, \quad (4.19)$$

where

$$\boldsymbol{\rho}(g) = \begin{pmatrix} \rho_1(g) \\ \rho_2(g) \\ \vdots \\ \rho_N(g) \end{pmatrix}, \tag{4.20}$$

and $\hat{K}$ is an integral matrix operator describing the collision integral defined from the right-hand side of (4.18).

Looking at (4.19), it is clear that there exists an equilibrium distribution $\boldsymbol{\rho}^{(0)}(g) > 0$ that is the solution of the equation

$$\hat{K}\boldsymbol{\rho}^{(0)} = 0. \tag{4.21}$$

From the "detailed balance" equation in (3.13), a similar "detailed balance" can be found for probability distributions on energy graphs.

Starting with the "detailed balance" equation from (3.13),

$$S(\mathbf{M}', \mathbf{M})w^{eq}(\mathbf{M}', t) = S(\mathbf{M}, \mathbf{M}')w^{eq}(\mathbf{M}, t), \tag{4.22}$$

integration along precessional trajectories as shown in (4.11) gives:

$$\oint_{C_k(g)} \oint_{C_n(g')} \frac{S(\mathbf{M}', \mathbf{M})w^{eq}(\mathbf{M}', t)}{|\nabla_\Sigma g(\mathbf{M}')||\nabla_\Sigma g(\mathbf{M})|} dl_{\mathbf{M}'} dl_{\mathbf{M}}$$

$$= \oint_{C_k(g)} \oint_{C_n(g')} \frac{S(\mathbf{M}, \mathbf{M}')w^{eq}(\mathbf{M}, t)}{|\nabla_\Sigma g(\mathbf{M}')||\nabla_\Sigma g(\mathbf{M})|} dl_{\mathbf{M}'} dl_{\mathbf{M}}. \tag{4.23}$$

Since the equilibrium distribution w^{eq} depends on $\mathbf{M}$ or $\mathbf{M}'$, it can be taken out of the inner integral:

$$\oint_{C_n(g')} w^{eq}(\mathbf{M}', t) \oint_{C_k(g)} \frac{S(\mathbf{M}', \mathbf{M})}{|\nabla_\Sigma g(\mathbf{M}')||\nabla_\Sigma g(\mathbf{M})|} dl_{\mathbf{M}} dl_{\mathbf{M}'}$$

$$= \oint_{C_k(g)} w^{eq}(\mathbf{M}, t) \oint_{C_n(g')} \frac{S(\mathbf{M}, \mathbf{M}')}{|\nabla_\Sigma g(\mathbf{M}')||\nabla_\Sigma g(\mathbf{M})|} dl_{\mathbf{M}'} dl_{\mathbf{M}}. \tag{4.24}$$

47

Making the same assumption as in (4.6), the equilibrium distributions can be written:

$$w^{eq}(\mathbf{M}, t) \approx w_k^{eq}(g(\mathbf{M}), t) \approx w_k^{eq}(g, t). \tag{4.25}$$

The equilibrium distribution therefore does not depend on $\mathbf{M}$ or $\mathbf{M}'$ and so can be extracted from the integral. The detailed balance equation can then be written:

$$w_n^{eq}(g', t) \oint_{C_n(g')} \oint_{C_k(g)} \frac{S(\mathbf{M}', \mathbf{M})}{|\nabla_\Sigma g(\mathbf{M}')||\nabla_\Sigma g(\mathbf{M})|} dl_{\mathbf{M}} dl_{\mathbf{M}'}$$
$$= w_k^{eq}(g, t) \oint_{C_k(g)} \oint_{C_n(g')} \frac{S(\mathbf{M}, \mathbf{M}')}{|\nabla_\Sigma g(\mathbf{M}')||\nabla_\Sigma g(\mathbf{M})|} dl_{\mathbf{M}'} dl_{\mathbf{M}}. \tag{4.26}$$

From (4.7), the equilibrium distribution can be written as an equilibrium distribution on energy graphs:

$$\rho_k^{(0)}(g, t) \approx w_k^{eq}(g, t) \tau_k(g), \tag{4.27}$$

and

$$\rho_n^{(0)}(g', t) \approx w_n^{eq}(g', t) \tau_n(g'). \tag{4.28}$$

Replacing $w_k^{eq}(g, t)$ and $w_n^{eq}(g', t)$ with their appropriate equilibrium distributions on energy graphs in the detailed balance equation gives:

$$\frac{\rho_n^{(0)}(g', t)}{\tau_n(g')} \oint_{C_n(g')} \oint_{C_k(g)} \frac{S(\mathbf{M}', \mathbf{M})}{|\nabla_\Sigma g(\mathbf{M}')||\nabla_\Sigma g(\mathbf{M})|} dl_{\mathbf{M}} dl_{\mathbf{M}'}$$
$$= \frac{\rho_k^{(0)}(g, t)}{\tau_k(g)} \oint_{C_k(g)} \oint_{C_n(g')} \frac{S(\mathbf{M}, \mathbf{M}')}{|\nabla_\Sigma g(\mathbf{M}')||\nabla_\Sigma g(\mathbf{M})|} dl_{\mathbf{M}'} dl_{\mathbf{M}}. \tag{4.29}$$

From the definition in (4.17), it is easy to see that $\boldsymbol{\rho}_0 = \rho^{(0)}$ satisfies the "detailed balance" condition

$$K_{h,k}(g', g) \rho_h^{(0)}(g') = K'_{k,h}(g, g') \rho_k^{(0)}(g). \tag{4.30}$$

This "detailed balance" condition is necessary to prove that the operator $\hat{K}$ is self-adjoint in the Hilbert space using an inner product defined by

$$\langle \boldsymbol{\rho}, \boldsymbol{\rho}' \rangle_{\rho_0} = \sum_k \int_{L_k} \frac{\rho_k(g)\rho_k'(g)}{\rho^{(0)}(g)} dg. \tag{4.31}$$

By definition, if operator $\hat{K}$ is self-adjoint, then

$$\langle \hat{K}\boldsymbol{\rho}, \boldsymbol{\rho}' \rangle_{\rho_0} = \langle \boldsymbol{\rho}, \hat{K}\boldsymbol{\rho}' \rangle_{\rho_0} \tag{4.32}$$

and the converse is also true.

Next, an eigenvalue approach to solving (4.19) by solving the eigenvalue problem is considered:

$$\hat{K}\boldsymbol{\rho}^{(\nu)} = \lambda_\nu \boldsymbol{\rho}^{(\nu)}. \tag{4.33}$$

Since $\hat{K}$ is self-adjoint, all of its eigenvalues λ_ν must be real. Furthermore, by using the detailed-balance condition (4.30), it can be shown that

$$\langle \hat{K}\boldsymbol{\rho}^{(\nu)}, \boldsymbol{\rho}^{(\nu)} \rangle_{\rho_0} < 0. \tag{4.34}$$

From the master equation, the inner product can be written:

$$\langle \hat{K}\boldsymbol{\rho}^{(\nu)}, \boldsymbol{\rho}^{(\nu)} \rangle_{\rho_0} = \int_{L_k} \frac{1}{\rho_0(g)} \left[\int_{L_n} \left[K(g', g)\rho^{(\nu)}(g') \right. \right.$$
$$\left. \left. - K(g, g')\rho^{(\nu)}(g) \right] dg' \right] \rho^{(\nu)}(g) dg \tag{4.35}$$

Rearranging the order of the integrals gives:

$$\langle \hat{K}\boldsymbol{\rho}^{(\nu)}, \boldsymbol{\rho}^{(\nu)} \rangle_{\rho_0}$$
$$= \int_{L_k} \int_{L_n} \frac{1}{\rho_0(g)} \left[K(g', g)\rho^{(\nu)}(g') - K(g, g')\rho^{(\nu)}(g) \right] \rho^{(\nu)}(g) dg' dg \tag{4.36}$$

Using the detailed balance equation,

$$K(g', g)\rho_0(g') = K(g, g')\rho_0(g), \tag{4.37}$$

it can be seen that $K(g', g)$ is symmetric in the $1/\rho_0$ space:

$$\frac{K(g', g)}{\rho_0(g)} = \frac{K(g, g')}{\rho_0(g')}. \tag{4.38}$$

Using (4.38), (4.36) can be rewritten as

$$\langle \hat{K}\boldsymbol{\rho}^{(\nu)}, \boldsymbol{\rho}^{(\nu)} \rangle_{\rho_0}$$
$$= \int_{L_k} \int_{L_n} \frac{K(g', g)}{\rho_0(g)} \left[\rho^{(\nu)}(g')\rho^{(\nu)}(g) - \frac{\rho_0(g')}{\rho_0(g)} \left(\rho^{(\nu)}(g) \right)^2 \right] dg'dg. \tag{4.39}$$

But, the indices used in the integrals are arbitrary so can be switched:

$$\langle \hat{K}\boldsymbol{\rho}^{(\nu)}, \boldsymbol{\rho}^{(\nu)} \rangle_{\rho_0}$$
$$= \int_{L_k} \int_{L_n} \frac{K(g, g')}{\rho_0(g')} \left[\rho^{(\nu)}(g)\rho^{(\nu)}(g') - \frac{\rho_0(g)}{\rho_0(g')} \left(\rho^{(\nu)}(g') \right)^2 \right] dgdg'. \tag{4.40}$$

Using (4.38), the first term in the integral can be replaced such that:

$$\langle \hat{K}\boldsymbol{\rho}^{(\nu)}, \boldsymbol{\rho}^{(\nu)} \rangle_{\rho_0}$$
$$= \int_{L_k} \int_{L_n} \frac{K(g', g)}{\rho_0(g)} \left[\rho^{(\nu)}(g)\rho^{(\nu)}(g') - \frac{\rho_0(g)}{\rho_0(g')} \left(\rho^{(\nu)}(g') \right)^2 \right] dgdg'. \tag{4.41}$$

Since they share common terms, (4.39) and (4.41) can be combined to give

$$\langle \hat{K}\boldsymbol{\rho}^{(\nu)}, \boldsymbol{\rho}^{(\nu)} \rangle_{\rho_0}$$
$$= \frac{1}{2} \int_{L_k} \int_{L_n} \frac{K(g', g)}{\rho_0(g)} \left[\rho^{(\nu)}(g')\rho^{(\nu)}(g) - \frac{\rho_0(g')}{\rho_0(g)} \left(\rho^{(\nu)}(g) \right)^2 \right.$$
$$\left. + \rho^{(\nu)}(g)\rho^{(\nu)}(g') - \frac{\rho_0(g)}{\rho_0(g')} \left(\rho^{(\nu)}(g') \right)^2 \right] dgdg'. \tag{4.42}$$

Rearranging the terms gives:

$$\langle \hat{K} \boldsymbol{\rho}^{(\nu)}, \boldsymbol{\rho}^{(\nu)} \rangle_{\rho_0}$$

$$= -\frac{1}{2} \int_{L_k} \int_{L_n} \frac{K(g',g)}{\rho_0(g)} \left[\frac{\rho_0(g')}{\rho_0(g)} \left(\rho^{(\nu)}(g) \right)^2 \right.$$

$$\left. + \frac{\rho_0(g)}{\rho_0(g')} \left(\rho^{(\nu)}(g') \right)^2 - 2\rho^{(\nu)}(g)\rho^{(\nu)}(g') \right] dg dg'. \qquad (4.43)$$

The terms within the bracket can be simplified by completing the square to give:

$$\langle \hat{K} \boldsymbol{\rho}^{(\nu)}, \boldsymbol{\rho}^{(\nu)} \rangle_{\rho_0}$$

$$= -\frac{1}{2} \int_{L_k} \int_{L_n} \frac{K(g',g)}{\rho_0(g)} \left[\sqrt{\frac{\rho_0(g')}{\rho_0(g)}} \rho^{(\nu)}(g) - \sqrt{\frac{\rho_0(g)}{\rho_0(g')}} \rho^{(\nu)}(g') \right]^2 dg dg'. \qquad (4.44)$$

Evaluating each term in the integral it can be seen that

$$\frac{K(g',g)}{\rho_0(g)} > 0, \qquad (4.45)$$

since $K(g',g)$ and ρ_0 are both strictly positive and

$$\left[\sqrt{\frac{\rho_0(g')}{\rho_0(g)}} \rho^{(\nu)}(g) - \sqrt{\frac{\rho_0(g)}{\rho_0(g')}} \rho^{(\nu)}(g') \right]^2 > 0, \qquad (4.46)$$

since the value in the bracket is squared. Therefore it is easy to see that

$$\langle \hat{K} \boldsymbol{\rho}^{(\nu)}, \boldsymbol{\rho}^{(\nu)} \rangle_{\rho_0} < 0. \qquad (4.47)$$

This inequality implies that all eigenvalues of $\hat{K}$ are negative:

$$\lambda_\nu < 0. \qquad (4.48)$$

This can be seen from the definition of the eigenfunction:

$$\hat{K} \rho^{(\nu)} = \lambda_\nu \rho^{(\nu)}. \qquad (4.49)$$

51

Taking the inner product with the eigenvector gives:

$$\langle \hat{K}\rho^{(\nu)}, \rho^{(\nu)} \rangle = \langle \lambda_\nu \rho^{(\nu)}, \rho^{(\nu)} \rangle = \lambda_\nu \langle \rho^{(\nu)}, \rho^{(\nu)} \rangle. \tag{4.50}$$

Therefore the eigenvalues can be found by

$$\lambda_\nu = \frac{\langle \hat{K}\rho^{(\nu)}, \rho^{(\nu)} \rangle}{\langle \rho^{(\nu)}, \rho^{(\nu)} \rangle}. \tag{4.51}$$

Since the inner product of a vector with itself is strictly positive,

$$\langle \rho^{(\nu)}, \rho^{(\nu)} \rangle > 0, \tag{4.52}$$

and using (4.47), it is evident that all eigenvalues of $\hat{K}$ are negative.

Futhermore, since $\hat{K}$ is self-adjoint, its eigenfunction vectors $\boldsymbol{\rho}^{(\nu)}(g)$ are orthonormal:

$$\langle \boldsymbol{\rho}^{(\nu)}(g), \boldsymbol{\rho}^{(\nu')}(g) \rangle_{\rho_0} = \delta_{\nu\nu'}, \tag{4.53}$$

where $\delta_{\nu\nu'}$ is the Kronecker delta function.

Now that the eigenvalue problem has been explored, (4.19) can be solved using eigenfunction expansions. This means that assuming the eigenvalue problem is solved and the solution consists of eigenvalues λ_ν and eigenfunctions $\boldsymbol{\rho}^{(\nu)}(g)$ has been found, a solution for (4.19) can easily be expressed.

It is easy to check that the vector functions $\boldsymbol{\rho}^{(\nu)} e^{\lambda_\nu t}$ are solutions of equation (4.19). Using this, a general solution of equation (4.19) can be written as

$$\boldsymbol{\rho}(g, t) = \sum_\nu a_\nu \boldsymbol{\rho}^{(\nu)}(g) e^{\lambda_\nu t}, \tag{4.54}$$

where the unknown coefficients a_ν are determined using the initial condition $\boldsymbol{\rho}(g, 0)$, which is assumed to be normalized

$$\sum_k \int_{L_k} \rho_k(g, 0) dg = 1. \tag{4.55}$$

From (4.54) it is easy to see that at $t = 0$,

$$\boldsymbol{\rho}(g, 0) = \sum_{\nu} a_{\nu} \boldsymbol{\rho}^{(\nu)}(g). \tag{4.56}$$

Using the orthonormality relations from (4.53) and the equation (4.56), the coefficient a_{ν} can be found to be

$$a_{\nu} = \langle \boldsymbol{\rho}(g, 0), \boldsymbol{\rho}^{(\nu)}(g) \rangle_{\rho_0}. \tag{4.57}$$

Substituting the coefficient expression into formula (4.54), the probability density can be expressed as

$$\boldsymbol{\rho}(g, t) = \sum_{\nu} \langle \boldsymbol{\rho}(g, 0), \boldsymbol{\rho}^{(\nu)}(g) \rangle_{\rho_0} \boldsymbol{\rho}^{(\nu)}(g) e^{\lambda_{\nu} t}. \tag{4.58}$$

This solution to the master equation in (4.18) can be used for any initial condition and it gives an analytical representation of the time-dynamics of $\boldsymbol{\rho}(g, t)$ provided that the eigenvalue problem in (4.19) has been solved. It is important to mention that the summation in (4.54) includes a term with $\boldsymbol{\rho}^{(0)}(g)$ that corresponds to an eigenvalue of zero. As a result of this and using the inequality in (4.47) in the limit of $t \to \infty$, formula (4.54) is reduced to

$$\boldsymbol{\rho}(g, \infty) = \langle \boldsymbol{\rho}(g, 0), \boldsymbol{\rho}^{(0)}(g) \rangle_{\rho_0} \boldsymbol{\rho}^{(0)}(g). \tag{4.59}$$

From the definition of inner product (4.31) and the normalization condition for $\boldsymbol{\rho}(g, 0)$ in (4.55), the first part of the term in (4.59) is seen to be

$$\langle \boldsymbol{\rho}(g, 0), \boldsymbol{\rho}^{(0)}(g) \rangle_{\rho_0} = 1, \tag{4.60}$$

and so

$$\boldsymbol{\rho}(g, \infty) = \boldsymbol{\rho}^{(0)}(g). \tag{4.61}$$

Figure 4.1: Uniaxial particles have an energy graph with two edges connecting the minimum energy wells at the energy maximum.

This means that the dynamic probability distribution will tend towards the equilibrium probability distribution as $t \to \infty$, as expected.

4.3 Numerical Method Comparison

The techniques described in the previous sections have been numerically implemented and their accuracy have been tested in the case of uniaxial magnetic particles with various energy barrier heights. The energy graph for this particle consists of two edges corresponding to two energy wells. These edges are connected at the point corresponding to the energy maximum, while the 'free' unconnected ends of these edges correspond to the two energy minima as shown in Figure 4.1.

The equilibrium distribution $\rho^{(0)}(g)$ is first computed by using a discretized version of equation (4.21) and the normalization condition (4.55). This equilibrium distribution has been compared with the Boltzmann equilibrium distribution

$$w_0(g(\mathbf{m})) = \frac{1}{Z}e^{-\frac{g(\mathbf{m})}{kT}} \tag{4.62}$$

that has been properly averaged along precessional trajectories of constant energy.
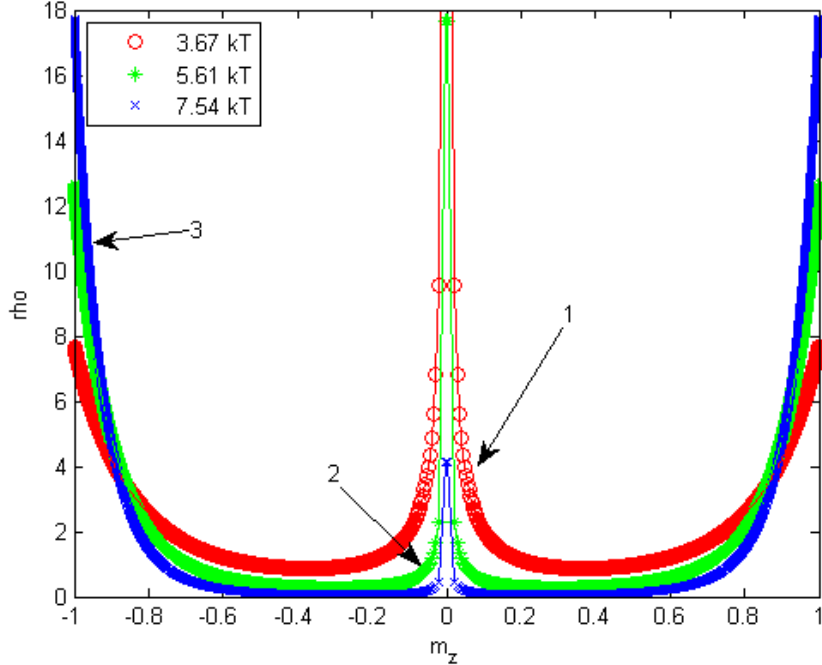
Figure 4.2: Computational results for equilibrium distributions, marked with symbols, closely match the predicted analytical results, marked with lines, for various energy barriers.

In this equation, Z is a partition function.

Figure 4.2 represents the results from these comparisons for three different values of energy barrier heights. It can be seen from this figure that the averaged Boltzmann distributions are sharply peaked at $M_z = 0$, which corresponds to $g = g_{max}$. This occurs because the averaged Boltzmann distributions $\rho^{av}(g)$ are given by the formula

$$\rho^{av}(g) = w_0(g)\tau_n(g), \tag{4.63}$$

where $\tau_n(g)$ is defined by equation (4.8). From (4.8) it can be seen that as $\tau_n(g)$ approaches $g = g_{max}$, its value goes to ∞ as expected from the precessional period approaching infinity at a separatrix. It is evident from Figure 4.7 that the equilib-
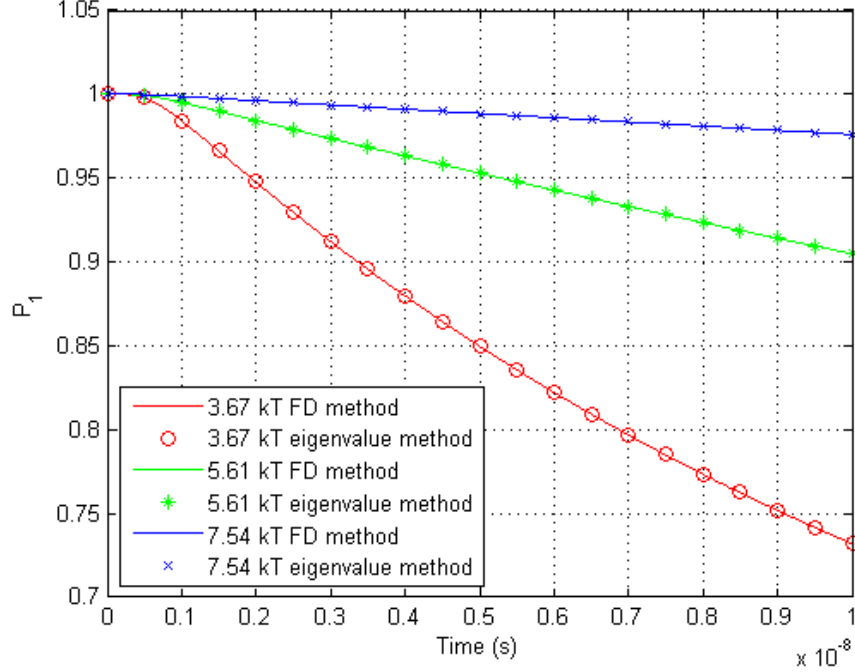
Figure 4.3: Results comparing the probability distribution of magneti-
zation dynamics obtained from using the finite difference method versus
using the eigenvalue method show very close agreement for various en-
ergy barriers.

rium distributions $\rho^{(0)}(g)$ computed using (4.14) accurately resolve the center peaks

of $\rho^{av}(g)$ as expected.

Figure 4.3 shows the results of the time dynamics of the probability density

function, $\rho(g, t)$. This study was carried out for the case of a uniaxial magnetic

particle with initial condition

$$\rho(g, 0) = \delta(g - g_{min}), \tag{4.64}$$

which corresponds to the initial localization of magnetization to the energy minima

of energy well 1. The numerical analysis was performed by solving a discretized

version of (4.18) by using the finite difference technique presented in chapter 3 as

well as by using the eigenvalue method discussed in section 4.3. In both cases, a finite energy mesh was introduced to the energy graph and was used to create a finite matrix to replace the integral operator $\hat{K}$. Meshes of up to 5000 points were used in the computations for increased accuracy. The comparison of these two techniques is illustrated in Figure 4.3, where the vertical axis corresponds to the probability $P_1(t)$ that the magnetization still lies within energy well 1, where it was initialized. This probability is computed as

$$P_1(t) = \int_{L_1} \rho(g,t)dg = \int_{g_{min}}^{g_{max}} \rho(g,t)dg. \tag{4.65}$$

From the figure, it is easy to see that there is very good agreement between these two techniques. The difference between these two approaches is that the eigenvalue technique has been shown to be much more computationally efficient when the simulations are carried out over longer time intervals. These simulations can therefore be extremely helpful in studying the time dynamics of $\rho(g,t)$ as it approaches equilibrium or to study the random switching at high energy barriers as these simulations are typically very computationally intensive.

Figure 4.4, 4.5, 4.6, and 4.7 illustrate the time dynamics of $\rho(g,t)$ for the case of an energy barrier of 3.67 kT. From these figures, it is easy to see its gradual approach to the equilibrium distribution $\rho^{(0)}(g)$ from the starting initial condition (4.64). In these figures, the results of the eigenvalue analysis based on formula (4.58) are compared with results from the Monte-Carlo simulations of random magnetization dynamics described in (3.1) and (3.2). These Monte-Carlo simulations were conducted by using over 10^4 realizations and the computations were performed with
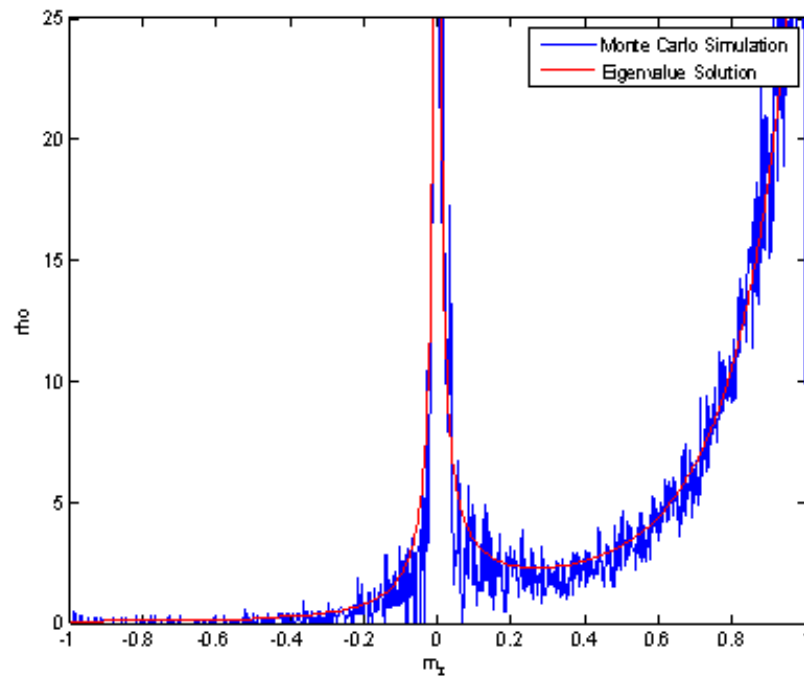
Figure 4.4: A comparison of the probability density distribution at $t = 10^{-9}$ s shows good agreement between the Monte-Carlo method and the averaging technique.
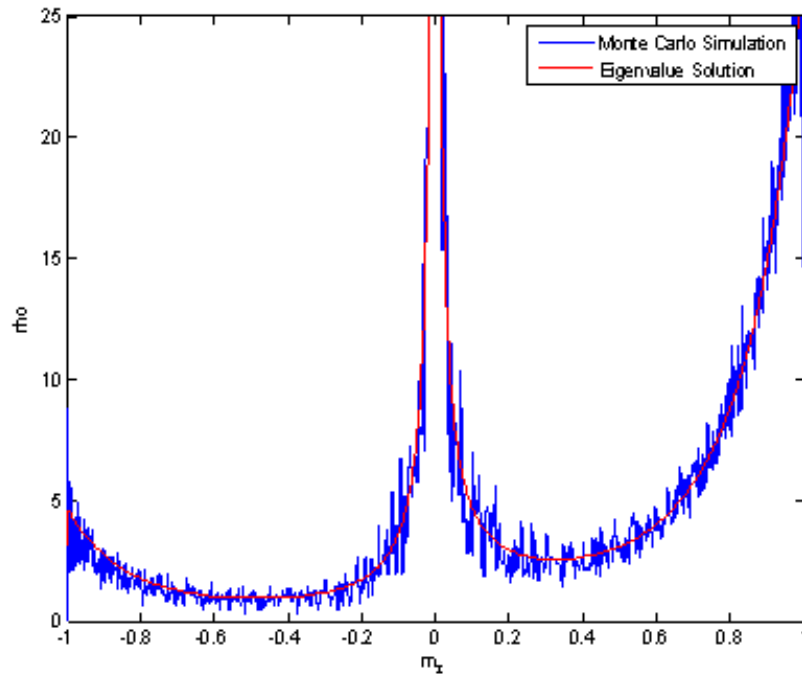
Figure 4.5: A comparison of the probability density distribution at $t = 5 \times 10^{-9}$ s shows good agreement between the Monte-Carlo method and the averaging technique.
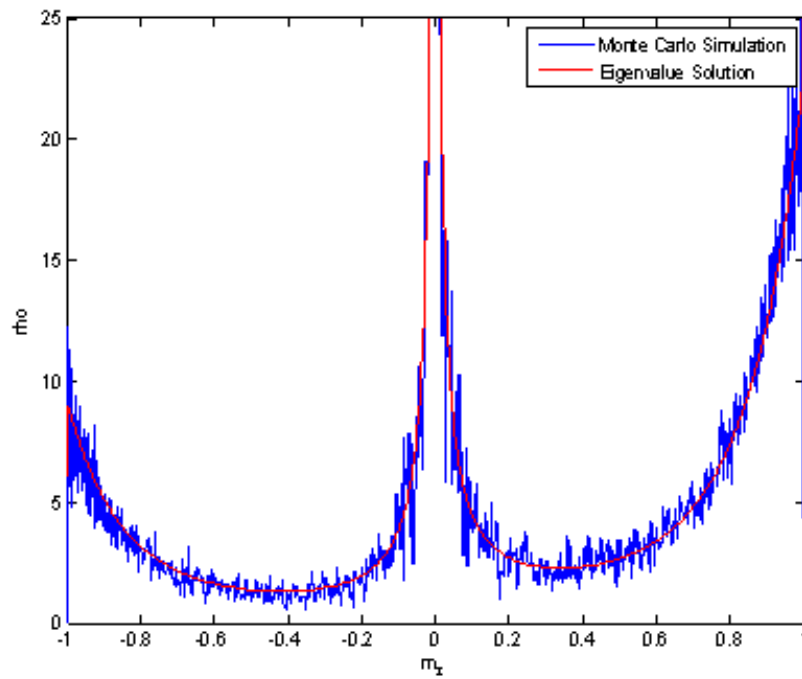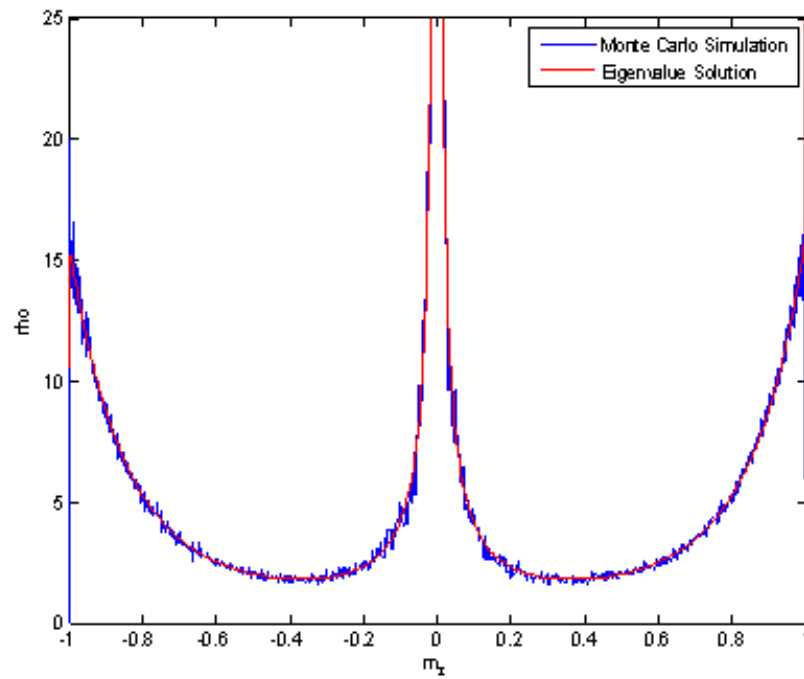
Figure 4.6: A comparison of the probability density distribution at $t = 10^{-8}$ s shows good agreement between the Monte-Carlo method and the averaging technique.

Figure 4.7: A comparison of the probability density distribution at $t = 10^{-7}$ s shows good agreement between the Monte-Carlo method and the averaging technique.

the help of GPUs. As expected, the figures show that the Monte-Carlo simulations exhibit some sample noise but otherwise agree quite well with the numerical simulations based on formula (4.58). This agreement remains true over time and is observed at various time instances of $\rho(g,t)$-dynamics.

4.3.1 Verifying the Kramers-Brown Approximation

The Kramers-Brown approximation is an approximation that has been extensively applied in the theoretical study of random magnetization switching, specifically in the case of two-well uniaxial magnetic particles. The essence of this approximation is that a "truncated" Boltzmann distribution is established in an energy well long before random switching from one well to the other well is likely to occur.

It is interesting to clarify the meaning of a "sufficiently high" energy barrier and how the necessary ratio can depend on the time-scale at which the "truncated" Boltzmann distribution is formed to determine when this approximation can be held as valid. Figures 4.8, 4.9, 4.10, and 4.11 show the time-evolution of the formation of the truncated Boltzmann distribution and how they are formed for different energy barriers. The height of the energy barrier is measured in terms of the relation to kT. In these figures, the truncated Boltzmann distributions averaged over precessional trajectories $\rho^{(0)}(g)$ are shown as dotted lines and the distributions of $\rho_1(g,t)$ are shown at various time instances. The distribution functions $\rho_1(g,t)$ were computed using a δ-function as the initial condition corresponding to the localization of magnetization at the energy minimum g_1. By comparing the figures, the formation time
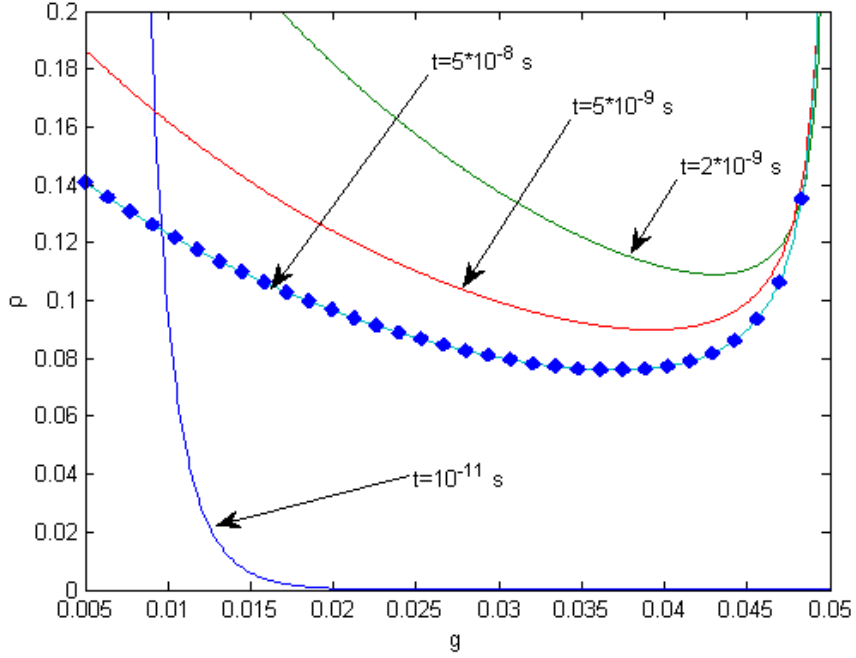
Figure 4.8: For a 1.74kT energy barrier, $\rho_1(g,t)$ quickly escapes the initial energy well and approaches the truncated Boltzmann distribution.

of $\rho^{(0)}(g)$) is clearly seen to increase as the height of the energy barrier increases.

Additionally, the formation time of truncated Boltzmann distributions were compared with the average switching (exit) time between wells. This time was also computed from the solution of equation (4.18). For the sake of numerical simulations, the formation time for $\rho^{(0)}(g)$ was defined as the time $\tilde{t}$ by which the difference between $\rho^{(0)}(g)$ and $\rho_1(g,t)$ was found to be less than 1%.

The average time of switching from well R_1 to the other well R_2 was also computed. These computations were computed through the use of the continuous master equation (4.18). The average switching times were compared with the for-
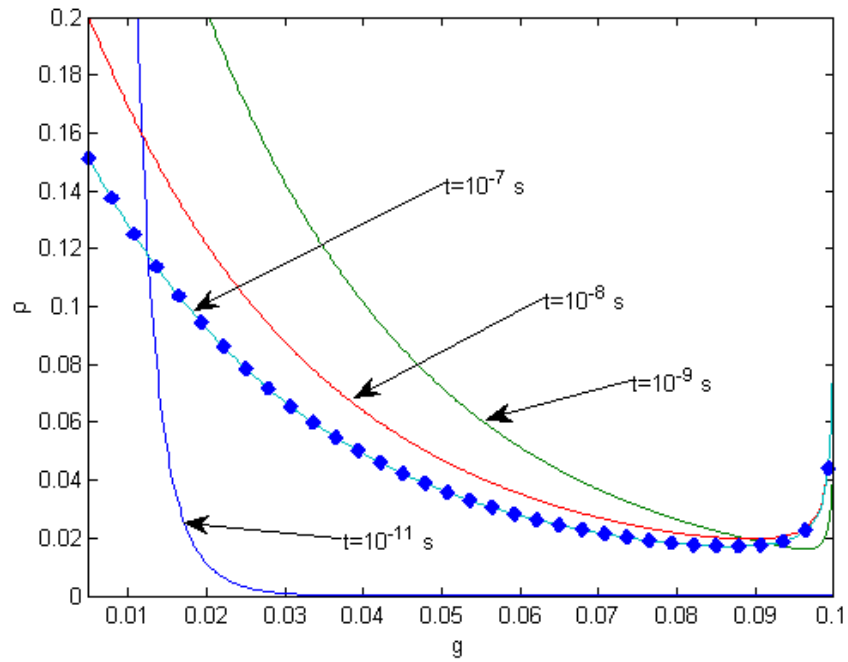
Figure 4.9: For a 3.67kT energy barrier, $\rho_1(g, t)$ quickly escapes the initial energy well and approaches the truncated Boltzmann distribution.
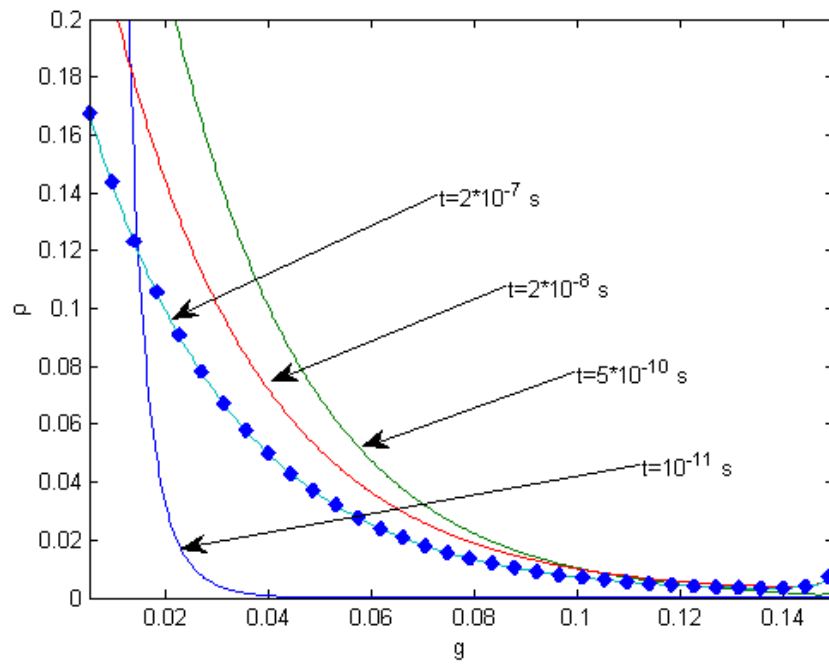
Figure 4.10: For a 5.61kT energy barrier, $\rho_1(g,t)$ quickly escapes the initial energy well and approaches the truncated Boltzmann distribution.
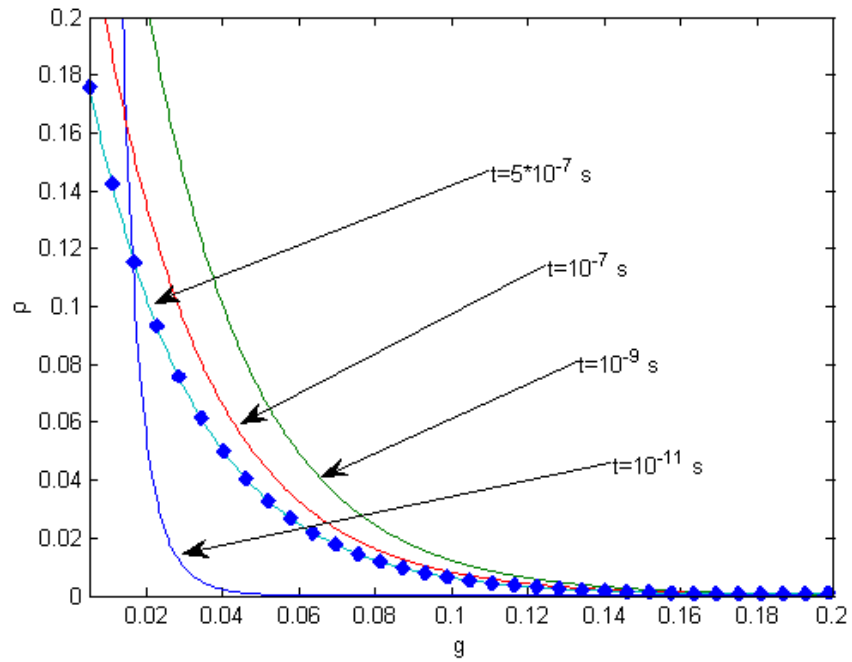
Figure 4.11: For a 7.54kT energy barrier, $\rho_1(g, t)$ quickly escapes the initial energy well and approaches the truncated Boltzmann distribution.
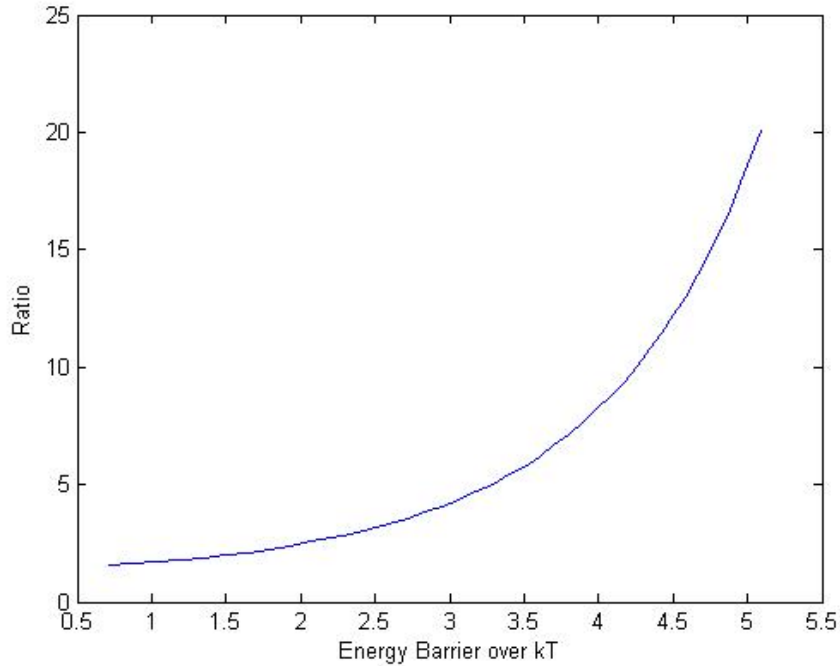
Figure 4.12: The ratio between average switching time to the time needed to establish a truncated Boltzmann distribution is shown as a function of the height of the energy barrier. At energy barrier values of about 4kT, the Boltzmann distribution is formed an order of magnitude faster than thermal switching.

mation times $\tilde{t}$ of the truncated Boltzmann distributions and is illustrated in Figure 4.12. In this figure, the ratio of the average switching time to the time it takes to establish the Boltzmann distribution is shown for various energy barriers heights. It is apparent that this ratio is close to 20 when the energy barrier is about 5 kT. Thus, at energy barriers over 5kT, the Boltzmann distribution is established over an order of magnitude faster than the switching occurs and so the Kramers-Brown approximation can be regarded as sufficiently accurate.

4.3.2 Low Temperature Magnetization Switching

Low temperature magnetization switching was also studied using the continuous master equation in (4.18). The purpose of studying low temperature magnetization switching is to analyze deviations of the switching rate from the classical Arrhenius Law. In other words, deviations from the predictions from thermally activated switching theory. It has been found that at very low temperatures, the magnetization switching rate appreciably deviates from the Arrhenius Law and exhibits some features that have been experimentally observed and are usually attributed to the physical phenomenon of "macroscopic quantum tunneling" of magnetization[36−39]. It is worthwhile to stress that in our theoretical study, this phenomenon emerges solely from the use of a jump-noise process for the description of thermal bath effects. That is, the "macroscopic quantum tunneling" phenomenon appears without the use of any quantum mechanical considerations. However, it is conceivable that the jump-noise process in (3.1) may reflect discontinuous magnetization transitions occurring at the microscopic quantum mechanical level.

The abrupt deviation from thermal activation theory that occurs at crossover temperature T_c and the dependence of this crossover temperature on the height of the energy barrier has been studied. The results are shown in Figure 4.13. The units on the y-axis are chosen to reflect experimental results. It is plotted as the negative inverse of the natural logarithm of the initial switching rate. The initial switching rate at very low temperatures in the presence of applied DC magnetic fields of opposite orientations, both parallel and anti-parallel to the easy axis, has been
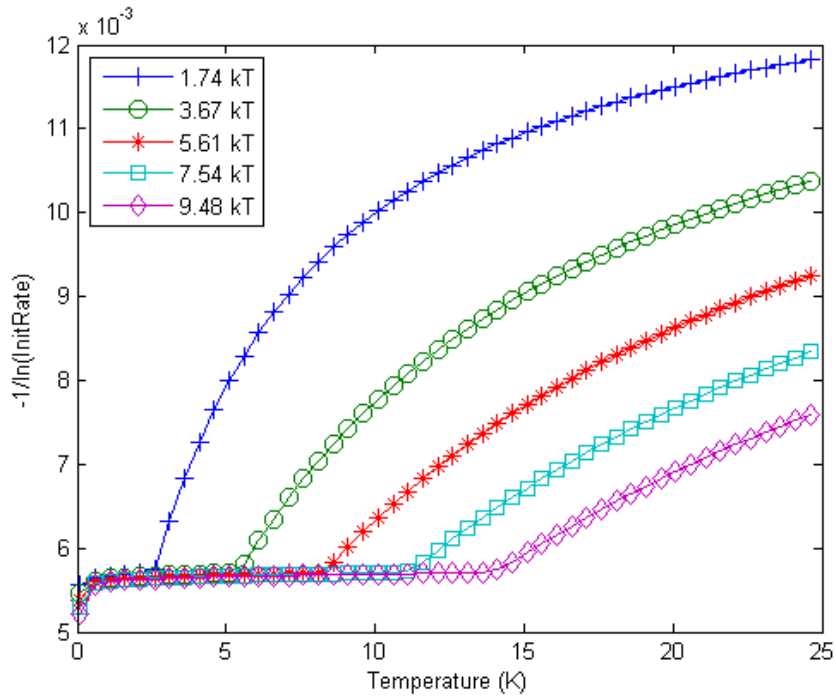
Figure 4.13: At very low temperatures, 'crossover' is experienced. The crossover temperature T_c depends on the energy barrier height.

numerically simulated and studied. The results are displayed in Figure 4.14. These numerical results are in qualitative agreement with previously reported experimental results.
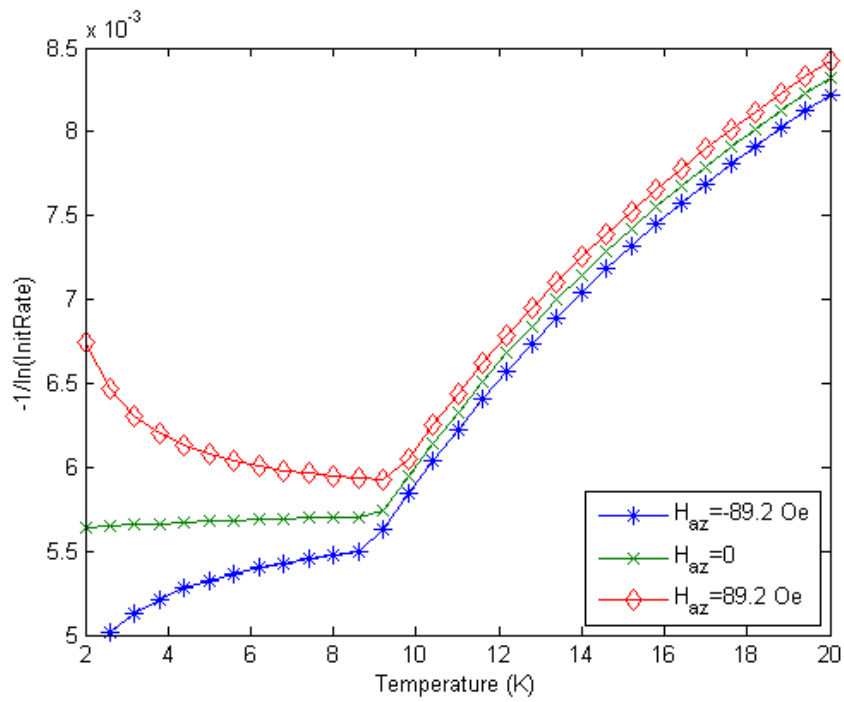
Figure 4.14: The behavior at temperatures below crossover is highly dependent on the applied magnetic field. Applied fields of opposite polarities show splitting of the switching rate.

Chapter 5:   Spin-Torque Effect in Magnetization Dynamics

5.1   Spin-Transfer Torque

When electrons flow across a ferromagnetic element, they exert a quantum-mechanical torque to the element known as a spin-transfer torque. When the current density is large enough, this spin-transfer torque phenomenon appears and can play a large role in the magnetization dynamics of the ferromagnet[1,6,41]. The discovery of this spin-transfer torque phenomenon has opened the field of spintronics and has led to novel devices and discoveries such as Spin-Torque Nano-Oscillators (STNOs).

5.2   Magnetization Dynamics with Spin-Transfer Torque

Traditionally, spin-transfer torque is introduced to the Landau-Lifshitz-Gilbert equation as an additional spin-torque term. This new equation was derived by Slonczewski and forms the Landau-Lifshitz-Slonczewski equation[35]. The normalized, dimensionless magnetization dynamics described by the Landau-Lifshitz-Slonczewski equation is given as

$$\frac{d\mathbf{m}}{dt} = -\mathbf{m} \times \mathbf{h}_{eff} + \alpha \mathbf{m} \times \frac{d\mathbf{m}}{dt} + \beta \frac{\mathbf{m} \times (\mathbf{m} \times \mathbf{e}_p)}{1 + c_p \mathbf{m} \cdot \mathbf{e}_p}, \qquad (5.1)$$

where β is a normalized injected spin-polarized current, c_p is a constant that is dependent on the spin-polarizing factor of the injected current, and $\mathbf{e}_p$ is the unit vector specifying the direction of spin polarization. The physical basis for this term is a 'damping-like' effect that brings the magnetization in line with the spin-polarized current direction from the term $\mathbf{m} \times (\mathbf{m} \times \mathbf{e}_p)$.

5.3 Jump-Noise Driven Spin-Transfer Torque

When jump-noise driven magnetization dynamics is considered, how the transition probability rate $S(\mathbf{M}, \mathbf{M}')$ is modified in the presence of spin-polarized current injection must be determined. When $S(\mathbf{M}, \mathbf{M}')$ was determined in chapter 3, the assumption of an equilibrium state was made, but this spin-polarized injection is a non-equilibrium process whose steady state may be quite different from the thermodynamic equilibrium. This non-equilibrium condition leads to the breaking of the symmetry of the function $\phi(\mathbf{M}, \mathbf{M}')$.

To determine the form of the asymmetric function $\phi(\mathbf{M}, \mathbf{M}')$, the way that spin-polarized current injection changes the random scattering to favor the reduction of the exchange energy between the "free-layer" magnetization $\mathbf{M}$ and the magnetic moment carried by the injected polarized electrons must be considered. The natural question is why does the spin-polarized current injection modify the random scattering such that it only favors the reduction of the exchange energy rather than the reduction of the total magnetic energy related to the effective field. First, the favoring of the reduction of exchange energy is consistent with the semiclassi-

cal (WKB) quantum-mechanical approach used for the derivation in the expression for spin-torque. Second, the strong exchange interaction prevails in ferromagnets over all other interactions at small spatial scales compatible with the continuum hypothesis. For these two reasons, it is natural to conclude that the spin transfer is mostly driven by the exchange interaction. It is worthwhile to point out that a somewhat similar situation occurs in micromagnetics, where the exchange interaction constraint $|\mathbf{M}(t)| = M_s(T) = \text{const}$ is taken into account before all other interactions that favor the reduction of the total magnetic energy are accounted for.

The injected spin-polarized electrons have spin orientation parallel or antiparallel to $\mathbf{e}_p$, where $\mathbf{e}_p$ is the magnetization orientation in the fixed layer. The strength of the spin-polarized electrons is also proportional to the injected current density J. Therefore, the exchange energy is proportional to $J\mathbf{M} \cdot \mathbf{e}_p$ and is minimized by random spin-transfer scattering. As a result, this spin-transfer scattering favors a magnetization state for which $\mathbf{M} \cdot \mathbf{e}_p = M_s$ when electrons flow from the fixed layer to the free layer ($J < 0$) and $\mathbf{M} \cdot \mathbf{e}_p = -M_s$ for the opposite flow ($J > 0$) of electrons.

In addition to the exchange interaction, there exist interface phenomena which affect the polarization and scattering of the injected electrons and modify the portion of spin-polarized electrons that play a role in the injected current. For this reason, the energy of interaction $J\mathbf{M}\cdot\mathbf{e}_p$ must be scaled by a function that takes into account the interface processes. This function depends on the orientations of $\mathbf{M}$ and $\mathbf{e}_p$ and can therefore be written as a function $\eta(\mathbf{M} \cdot \mathbf{e}_p)$. As a result, the effective energy of interaction between injected electrons and free layer magnetization can be written

as $J\eta(\mathbf{M} \cdot \mathbf{e}_p)\mathbf{M} \cdot \mathbf{e}_p$ or simply as $\Psi(\mathbf{M} \cdot \mathbf{e}_p)$ where $\Psi(u) = J\eta(u)u$. Putting this in a similar form as the transition probability rate in (3.14) which describes thermal scattering, the function $\phi(\mathbf{M}, \mathbf{M}')$ can naturally be written in the following form which reflects the nature of spin-transfer and interface scattering:

$$\phi(\mathbf{M}, \mathbf{M}') = A \exp\left(-\frac{|\mathbf{m}|^2}{2\sigma^2}\right) \exp\left\{\frac{\Psi(\mathbf{M} \cdot \mathbf{e}_p) - \Psi(\mathbf{M}' \cdot \mathbf{e}_p)}{2kT}\right\}. \tag{5.2}$$

By substituting (5.2) into (3.14), the transition probability rate becomes

$$S(\mathbf{M}, \mathbf{M}') = A \exp\left\{-\frac{|\mathbf{m}|^2}{2\sigma^2} + \frac{\Phi(\mathbf{M}) - \Phi(\mathbf{M}')}{2kT}\right\}, \tag{5.3}$$

where

$$\Phi(\mathbf{M}) = g(\mathbf{M}) + \Psi(\mathbf{M} \cdot \mathbf{e}_p). \tag{5.4}$$

In the case of small jump-noise processes where jumps in magnetization $\mathbf{m}$ of small magnitude are the most probable, the following approximation can be used:

$$\Phi(\mathbf{M}) - \Phi(\mathbf{M}') \simeq -\mathbf{m} \cdot \nabla_\Sigma \Phi. \tag{5.5}$$

This leads to the following expression for the transition probability rate:

$$S(\mathbf{M}, \mathbf{M}') \simeq A \exp\left\{-\frac{|\mathbf{m}|^2}{2\sigma^2} - \frac{\mathbf{m} \cdot \nabla_\Sigma \Phi}{2kT}\right\}. \tag{5.6}$$

From (3.21) and (3.25), the expected value of the jump-noise process can be written as

$$E[\mathbf{T}_r(t)] = \oint_\Sigma \mathbf{m} S(\mathbf{M}, \mathbf{M}')d\mathbf{m}. \tag{5.7}$$

By substituting (5.6) into equation (5.7), the expected value of the jump-noise process is found to be

$$E[\mathbf{T}_r(t)] \simeq A \int \mathbf{m} \cdot \exp\left\{-\frac{|\mathbf{m}|^2}{2\sigma^2} - \frac{\mathbf{m} \cdot \nabla_\Sigma \Phi}{2kT}\right\} d\mathbf{m}. \tag{5.8}$$

By completing the square in the power of the exponent in (5.8), the integral can be reduced to a Gaussian integral which is easier to analyze. Solving this integral leads to the following result:

$$E[\mathbf{T}_r(t)] = -\frac{\pi A \sigma^4}{kT} \exp\left\{\frac{1}{2}\left(\frac{\sigma |\nabla_\Sigma \Phi|}{2kT}\right)^2\right\} \nabla_\Sigma \Phi, \tag{5.9}$$

where

$$\nabla_\Sigma \Phi = \nabla_\Sigma g + \nabla_\Sigma \Psi(\mathbf{M} \cdot \mathbf{e}_p). \tag{5.10}$$

The first term in the right-hand side of (5.10) can be written in the form

$$\nabla_\Sigma g = \frac{\mu_0 V}{M_s^2} \mathbf{M} \times (\mathbf{M} \times \mathbf{H}_{\text{eff}}), \tag{5.11}$$

where V is the volume of the free layer.

The second term in (5.10) can be transformed:

$$\nabla_\Sigma \Psi(\mathbf{M} \cdot \mathbf{e}_p) = -\frac{\Psi'(\mathbf{M} \cdot \mathbf{e}_p)}{M_s^2} \mathbf{M} \times (\mathbf{M} \times \mathbf{e}_p), \tag{5.12}$$

where Ψ' is the derivative of Ψ.

By introducing the the damping coefficient

$$\alpha = \frac{\pi \mu_0 V A \sigma^4}{\gamma M_s^2 kT} \exp\left\{\frac{1}{2}\left(\frac{\sigma |\nabla_\Sigma \Phi|}{2kT}\right)^2\right\}, \tag{5.13}$$

and using formulas (5.9)-(5.13), the expected value of the jump-noise process becomes

$$E[\mathbf{T}_r(t)] = -\alpha\gamma \mathbf{M} \times (\mathbf{M} \times \mathbf{H}_{\text{eff}})$$
$$+ \frac{\alpha\gamma}{\mu_0 V} \Psi'(\mathbf{M} \cdot \mathbf{e}_p)\mathbf{M} \times (\mathbf{M} \times \mathbf{e}_p). \tag{5.14}$$

The equation for the average stochastic magnetization dynamics equation in (3.1) can now be considered:

$$\frac{d\mathbf{M}}{dt} = -\gamma(\mathbf{M} \times \mathbf{H}_{eff}) + E[\mathbf{T}_r(t)]. \tag{5.15}$$

Substituting (5.14) into (5.15), the equation becomes

$$\frac{d\mathbf{M}}{dt} = -\gamma(\mathbf{M} \times \mathbf{H}_{\text{eff}}) - \alpha\gamma\mathbf{M} \times (\mathbf{M} \times \mathbf{H}_{\text{eff}})$$
$$+ \frac{\alpha\gamma}{\mu_0 V}\Psi'(\mathbf{M} \cdot \mathbf{e}_p)\mathbf{M} \times (\mathbf{M} \times \mathbf{e}_p). \tag{5.16}$$

This magnetization dynamics equation has a form which is mathematically similar to the Slonczewski equation. The magnetization dynamics equation matches the Landau-Lifshitz-Slonczewski equation in the case of the particular choice of function Ψ:

$$\Psi(\mathbf{M} \cdot \mathbf{e}_p) = \frac{b\mu_0 V}{\tilde{c}_p}\ln(1 + \tilde{c}_p\mathbf{M} \cdot \mathbf{e}_p), \tag{5.17}$$

where b is a parameter proportional to the spin-polarized current density, $\tilde{c}_p = c_p/M_s$ and c_p depends only on polarizing factor P. Indeed, in this case

$$\Psi'(\mathbf{M} \cdot \mathbf{e}_p) = \frac{b\mu_0 V}{1 + \tilde{c}_p\mathbf{M} \cdot \mathbf{e}_p} \tag{5.18}$$

and the dynamics equation (5.16) is reduced to

$$\frac{d\mathbf{M}}{dt} = -\gamma(\mathbf{M} \times \mathbf{H}_{\text{eff}}) - \alpha\gamma\mathbf{M} \times (\mathbf{M} \times \mathbf{H}_{\text{eff}})$$
$$+ \alpha\gamma b\frac{\mathbf{M} \times (\mathbf{M} \times \mathbf{e}_p)}{1 + \tilde{c}_p\mathbf{M} \cdot \mathbf{e}_p}. \tag{5.19}$$

In general, the factor $\Psi'(\mathbf{M} \cdot \mathbf{e}_p)$ in (5.16) accounts for interface effects and should be identified from experimental results.

Next, an expression for the damping coefficient α in terms of the scattering rate $\lambda(\mathbf{M}(t))$ can be found. To do this, (5.6) is substituted into (3.21) to find

$$\lambda(\mathbf{M}(t)) \simeq A \int \exp \left\{ -\frac{|\mathbf{m}|^2}{2\sigma^2} - \frac{\mathbf{m} \cdot \nabla_\Sigma \Phi}{2kT} \right\} d\mathbf{m}. \tag{5.20}$$

Evaluating the integral in (5.20) by completing the square, the scattering rate is obtained:

$$\lambda(\mathbf{M}) = 2\pi A\sigma^2 \exp \left\{ \frac{1}{2} \left(\frac{\sigma |\nabla_\Sigma \Phi|}{2kT} \right)^2 \right\}. \tag{5.21}$$

Using this formula in (5.13), the damping coefficient is found to be

$$\alpha = \lambda(\mathbf{M}) \frac{\mu_0 V \sigma^2}{2\gamma kT M_s^2}. \tag{5.22}$$

Equations (5.21) and (5.22) clearly reveal the dependence of the damping coefficient α on $\mathbf{M}$ and other properties of the jump-noise process. Equations (5.4), (5.21) and (5.22) also suggest that the damping coefficient α is affected by the presence of spin-polarized current injection. This is as expected based on physical intuition because the spin-polarized current injection affects overall random thermal scattering which is the mechanism that is ultimately responsible for damping.

Finally, the magnetization dynamics in (5.16) can be represented in the following equivalent form:

$$\frac{d\mathbf{M}}{dt} = -\gamma \mathbf{M} \times \mathbf{H}_{\text{eff}} - \lambda(\mathbf{M}) \frac{\sigma^2}{2kT} \nabla_\Sigma \Phi. \tag{5.23}$$

This equation describes the magnetization dynamics on the sphere Σ. According to the Helmholtz decomposition theorem, any dynamics on a sphere can be fully described in terms of two potentials:

$$\frac{d\mathbf{M}}{dt} = \mathbf{M} \times \nabla_\Sigma \Gamma - \nabla_\Sigma \Omega. \tag{5.24}$$

From (5.22) and (5.23) it can be seen that if the scattering rate λ is constant, and thus independent of magnetization, the potentials Γ and Ω are merely scaled versions of g and Φ, respectively. In the case when the scattering rate is dependent on magnetization, the identification of potentials Γ and Ω is much harder.

It is interesting to note that in the specific case of uniaxial symmetry, the magnetization-dependent scattering rate $\lambda(\mathbf{M})$ does not affect the analysis of magnetization oscillations caused by spin-polarized current injection. According to (5.23), these microwave magnetization oscillations, called self-oscillations, will occur along precessional trajectories with the property that at each point in these trajectories

$$\nabla_\Sigma \Phi = 0. \tag{5.25}$$

Using (5.25), the analysis of magnetization oscillations in uniaxial systems can be performed in much the same way as described in literature and an analytical solution can be obtained. For non-uniaxial systems, the analysis of magnetization oscillations is based on the use of Melnikov functions and the frequency of oscillation may be affected by the magnetization dependence of the scattering rate.

5.3.1 Magnetization Dynamics with Spin-Torque

The magnetization dynamics in (3.4) can be modified in a similar manner to reflect the effects of the spin-transfer torque.

Starting from a generalized magnetization dynamics equation with jump-noise and spin torque:

$$\frac{d\mathbf{M}}{dt} = -\gamma(\mathbf{M} \times \mathbf{H}_{\text{eff}}) + \mathbf{T}_r(t) + \beta \frac{\mathbf{M} \times (\mathbf{M} \times \mathbf{e}_p)}{1 + \tilde{c}_p \mathbf{M} \cdot \mathbf{e}_p}. \tag{5.26}$$

78

This equation can be seen on the level of transition probability densities by finding

$$\frac{\partial w(\mathbf{M}, t)}{\partial t} = \nabla_\Sigma \cdot \left(\frac{d\mathbf{M}}{dt}\right) w. \tag{5.27}$$

Inserting (5.26) into (5.27), this equation becomes

$$\frac{\partial w(\mathbf{M}, t)}{\partial t} = \nabla_\Sigma \cdot \left(-\gamma(\mathbf{M} \times \mathbf{H}_{\text{eff}}) + \mathbf{T}_r(t) + \beta \frac{\mathbf{M} \times (\mathbf{M} \times \mathbf{e}_p)}{1 + \tilde{c}_p \mathbf{M} \cdot \mathbf{e}_p}\right) w. \tag{5.28}$$

It is easy to see that there are three distinct components to this master equation:

$$\begin{aligned}
\frac{\partial w(\mathbf{M}, t)}{\partial t} =& \nabla_\Sigma \cdot (-\gamma(\mathbf{M} \times \mathbf{H}_{\text{eff}})w) \\
&+ \nabla_\Sigma \cdot (\mathbf{T}_r(t)w) + \nabla_\Sigma \cdot \left(\beta \frac{\mathbf{M} \times (\mathbf{M} \times \mathbf{e}_p)}{1 + \tilde{c}_p \mathbf{M} \cdot \mathbf{e}_p} w\right).
\end{aligned} \tag{5.29}$$

The first term corresponds to the precessional term, the second to the jump-noise, and the last term corresponds to the spin-torque term.

In (4.1), the master equation was shown with just the precessional and jump-noise terms to be

$$\begin{aligned}
\frac{\partial w}{\partial t} =& -\gamma \nabla_\Sigma \cdot [(\mathbf{M} \times \nabla_\Sigma g_L)w] \\
&+ \int_\Sigma [S(\mathbf{M}', \mathbf{M})w(\mathbf{M}') - S(\mathbf{M}, \mathbf{M}')w(\mathbf{M})]d\Sigma_{\mathbf{M}'}.
\end{aligned} \tag{5.30}$$

Therefore, taking the divergence of the spin-torque term, it is shown to be:

$$\nabla_\Sigma \cdot \left(\beta \frac{\mathbf{M} \times (\mathbf{M} \times \mathbf{e}_p)}{1 + \tilde{c}_p \mathbf{M} \cdot \mathbf{e}_p} w\right) = \nabla_\Sigma \left[\left(\frac{\beta}{\tilde{c}_p} \nabla_\Sigma \ln(1 + \tilde{c}_p \mathbf{M} \cdot \mathbf{e}_p)\right) w\right]. \tag{5.31}$$

Adding this to (5.30) gives the master equation with spin-torque:

$$\begin{aligned}
\frac{\partial w}{\partial t} =& -\gamma \nabla_\Sigma \cdot [(\mathbf{M} \times \nabla_\Sigma g_L)w] \\
&+ \int_\Sigma [S(\mathbf{M}', \mathbf{M})w(\mathbf{M}') - S(\mathbf{M}, \mathbf{M}')w(\mathbf{M})]d\Sigma_{\mathbf{M}'} \\
&+ \nabla_\Sigma \left[\left(\frac{\beta}{\tilde{c}_p} \nabla_\Sigma \ln(1 + \tilde{c}_p \mathbf{M} \cdot \mathbf{e}_p)\right) w\right].
\end{aligned} \tag{5.32}$$

5.4 Spin-Transfer Torque on Energy Graphs

In chapter 4, an averaging technique was used to efficiently model stochastic magnetization dynamics driven by a jump-noise process under small thermal noise conditions. This method can be generalized to the case when the magnetization dynamics are also driven by spin-polarized current injection. This generalized equation has the same form as (4.18) but with an additional term to account for spin-transfer torque.

To derive the equation with spin-transfer torque on energy graphs, the magnetization dynamics equation with spin-transfer torque in (5.32) is used:

$$
\begin{aligned}
\frac{\partial w}{\partial t} = & - \gamma \nabla_\Sigma \cdot [(\mathbf{M} \times \nabla_\Sigma g_L) w] \\
& + \int_\Sigma [S(\mathbf{M}', \mathbf{M}) w(\mathbf{M}') - S(\mathbf{M}, \mathbf{M}') w(\mathbf{M})] d\Sigma_{\mathbf{M}'} \\
& - \nabla_\Sigma \left[\left(\frac{\beta}{\tilde{c}_p} \nabla_\Sigma \ln(1 + \tilde{c}_p \mathbf{M} \cdot \mathbf{e}_p) \right) w \right].
\end{aligned}
\tag{5.33}
$$

Integrating this equation along precessional trajectories gives:

$$
\begin{aligned}
\oint_{C_k(g)} \frac{1}{|\nabla_\Sigma g_L|} \frac{\partial w}{\partial t} dm_\psi = & \oint_{C_k(g)} \frac{1}{|\nabla_\Sigma g_L|} \bigg[- \gamma \nabla_\Sigma \cdot [(\mathbf{M} \times \nabla_\Sigma g_L) w] \\
& + \int_\Sigma [S(\mathbf{M}', \mathbf{M}) w(\mathbf{M}') - S(\mathbf{M}, \mathbf{M}') w(\mathbf{M})] d\Sigma_{\mathbf{M}'} \\
& + \nabla_\Sigma \left[\left(\frac{\beta}{\tilde{c}_p} \nabla_\Sigma \ln(1 + \tilde{c}_p \mathbf{M} \cdot \mathbf{e}_p) \right) w \right] \bigg] dm_\psi.
\end{aligned}
\tag{5.34}
$$

Following the steps in chapter 4,

$$
\oint_{C_k(g)} \frac{1}{|\nabla_\Sigma g_L|} \frac{\partial w}{\partial t} dm_\psi = \frac{\partial \rho_k(g,t)}{\partial t},
\tag{5.35}
$$

The first term in the integral evaluates to 0,

$$-\oint_{C_k(g)} \frac{1}{|\nabla_\Sigma g|} \gamma \nabla_\Sigma \cdot [(\mathbf{M} \times \nabla_\Sigma g_L) w] dl_{\mathbf{M}} = 0, \tag{5.36}$$

and the second term becomes a collision integral on energy graphs.

Therefore, the equation becomes:

$$\frac{d\rho_k(g,t)}{dt} = \sum_n \int_{L_n} [K_{n,k}(g',g)\rho_n(g',t) - K_{k,n}(g,g')\rho_k(g,t)] dg'$$

$$+ \oint_{C_k(g)} \frac{1}{|\nabla_\Sigma g_L|} \left[\nabla_\Sigma \left[\left(\frac{\beta}{\tilde{c}_p} \nabla_\Sigma \ln(1 + \tilde{c}_p \mathbf{M} \cdot \mathbf{e}_p) \right) w \right] \right] dm_\psi,$$

$$(k = 1, 2, ...N). \tag{5.37}$$

Looking at only the second term, specifically the term inside the gradient:

$$A(\mathbf{M}, t) = (\nabla_\Sigma \ln(1 + \tilde{c}_p \mathbf{M} \cdot \mathbf{e}_p)) w(\mathbf{M}, t). \tag{5.38}$$

Writing this term as a function of energy gives

$$A(g, \psi, t) = (\nabla_\Sigma \ln(1 + \tilde{c}_p \mathbf{M}(g, \psi) \cdot \mathbf{e}_p)) w_k(g, \psi, t). \tag{5.39}$$

Since the coordinate system of interest is $\mathbf{e}_g$ and $\mathbf{e}_\psi$, the term in (5.39) can be decomposed:

$$A(g, \psi, t) = [(\nabla_\Sigma \ln(1 + \tilde{c}_p \mathbf{M}(g, \psi) \cdot \mathbf{e}_p)) w_k(g, \psi, t)] \cdot \mathbf{e}_g$$

$$+ [(\nabla_\Sigma \ln(1 + \tilde{c}_p \mathbf{M}(g, \psi) \cdot \mathbf{e}_p)) w_k(g, \psi, t)] \cdot \mathbf{e}_\psi. \tag{5.40}$$

Using the definitions in (4.2) and (4.7), this term becomes:

$$A(g, \psi, t) = \left[(\nabla_\Sigma \ln(1 + \tilde{c}_p \mathbf{M}(g, \psi) \cdot \mathbf{e}_p)) \frac{\rho_k(g,t)}{\tau_k(g)} \right] \cdot \left(\frac{\nabla_\Sigma g_L}{|\nabla_\Sigma g_L|} \right)$$

$$+ \left[(\nabla_\Sigma \ln(1 + \tilde{c}_p \mathbf{M}(g, \psi) \cdot \mathbf{e}_p)) \frac{\rho_k(g,t)}{\tau_k(g)} \right] \cdot \left(\mathbf{M}(g, \psi) \times \frac{\nabla_\Sigma g_L}{|\nabla_\Sigma g_L|} \right). \tag{5.41}$$

For temporary notational simplicity, let

$$B(g, \psi, t) = (\nabla_\Sigma \ln(1 + \tilde{c}_p \mathbf{M}(g, \psi) \cdot \mathbf{e}_p)) \frac{\rho_k(g, t)}{\tau_k(g)}. \tag{5.42}$$

Thus,

$$A(g, \psi, t) = B(g, \psi, t) \cdot \left(\frac{\nabla_\Sigma g_L}{|\nabla_\Sigma g_L|} \right) + B(g, \psi, t) \cdot \left(\mathbf{M}(g, \psi) \times \frac{\nabla_\Sigma g_L}{|\nabla_\Sigma g_L|} \right). \tag{5.43}$$

Applying the gradient from the master equation in (5.37) gives

$$\nabla_\Sigma A(g, \psi, t) = \nabla_\Sigma \left[B(g, \psi, t) \cdot \left(\frac{\nabla_\Sigma g_L}{|\nabla_\Sigma g_L|} \right) \right.$$
$$\left. + B(g, \psi, t) \cdot \left(\mathbf{M}(g, \psi) \times \frac{\nabla_\Sigma g_L}{|\nabla_\Sigma g_L|} \right) \right]. \tag{5.44}$$

This in turn can be expanded in terms of m_g and m_ψ:

$$\nabla_\Sigma A(g, \psi, t) =$$
$$\frac{d}{dm_g} \left[B(g, \psi, t) \cdot \left(\frac{\nabla_\Sigma g_L}{|\nabla_\Sigma g_L|} \right) + B(g, \psi, t) \cdot \left(\mathbf{M}(g, \psi) \times \frac{\nabla_\Sigma g_L}{|\nabla_\Sigma g_L|} \right) \right]$$
$$+ \frac{d}{dm_\psi} \left[B(g, \psi, t) \cdot \left(\frac{\nabla_\Sigma g_L}{|\nabla_\Sigma g_L|} \right) + B(g, \psi, t) \cdot \left(\mathbf{M}(g, \psi) \times \frac{\nabla_\Sigma g_L}{|\nabla_\Sigma g_L|} \right) \right]. \tag{5.45}$$

It is evident that the second term in the first derivative lies solely along the e_ψ direction and first term in the second derivative lies solely along the e_g direction. Therefore, those derivatives both evaluate to 0 leaving:

$$\nabla_\Sigma A(g, \psi, t) = \frac{d}{dm_g} \left[B(g, \psi, t) \cdot \left(\frac{\nabla_\Sigma g_L}{|\nabla_\Sigma g_L|} \right) \right]$$
$$+ \frac{d}{dm_\psi} \left[B(g, \psi, t) \cdot \left(\mathbf{M}(g, \psi) \times \frac{\nabla_\Sigma g_L}{|\nabla_\Sigma g_L|} \right) \right]. \tag{5.46}$$

Changing the variables from dm_g to dg and dm_ψ to $d\psi$ using (4.3) gives:

$$\nabla_\Sigma A(g, \psi, t) = \frac{d}{dg} \left[B(g, \psi, t) \cdot \nabla_\Sigma g_L \right]$$
$$+ \frac{d}{d\psi} \left[B(g, \psi, t) \cdot (\mathbf{M}(g, \psi) \times \nabla_\Sigma g_L) \right]. \tag{5.47}$$

Returning to the equation in (5.37), the gradient in (5.47) is integrated along precessional trajectories. But, since the second term in (5.47) lies perpendicular to the path of integration, the term evaluates to 0. Thus,

$$\oint_{C_k(g)} \frac{1}{|\nabla_\Sigma g_L|} \left[\frac{\beta}{\tilde{c}_p} \nabla_\Sigma \left[A(g, \psi, t) \right] \right] dm_\psi$$
$$= \oint_{C_k(g)} \frac{1}{|\nabla_\Sigma g_L|} \left[\frac{\beta}{\tilde{c}_p} \frac{d}{dg} \left[B(g, \psi, t) \cdot \nabla_\Sigma g_L \right] \right] dm_\psi. \qquad (5.48)$$

Changing the order of integration and differentiation,

$$\oint_{C_k(g)} \frac{1}{|\nabla_\Sigma g_L|} \left[\frac{\beta}{\tilde{c}_p} \nabla_\Sigma \left[A(g, \psi, t) \right] \right] dm_\psi$$
$$= \frac{d}{dg} \oint_{C_k(g)} \frac{1}{|\nabla_\Sigma g_L|} \left[\frac{\beta}{\tilde{c}_p} \left[B(g, \psi, t) \cdot \nabla_\Sigma g_L \right] \right] dm_\psi. \qquad (5.49)$$

Replacing $B(g, \psi, t)$ gives:

$$\oint_{C_k(g)} \frac{1}{|\nabla_\Sigma g_L|} \left[\frac{\beta}{\tilde{c}_p} \nabla_\Sigma \left[A(g, \psi, t) \right] \right] dm_\psi$$
$$= \frac{d}{dg} \oint_{C_k(g)} \left[\frac{\beta}{\tilde{c}_p} \left[(\nabla_\Sigma \ln(1 + \tilde{c}_p \mathbf{M}(g, \psi) \cdot \mathbf{e}_p)) \frac{\rho_k(g, t)}{\tau_k(g)} \cdot \frac{\nabla_\Sigma g_L}{|\nabla_\Sigma g_L|} \right] \right] dm_\psi. \qquad (5.50)$$

Defining a function

$$\Phi_k(g) = \frac{\beta}{\tilde{c}_p \tau_k(g)} \oint_{C_k(g)} \frac{\nabla_\Sigma \ln[1 + c_p \mathbf{M} \cdot \mathbf{e}_p] \cdot \nabla_\Sigma g_L}{|\nabla_\Sigma g_L|} dm_\psi, \qquad (5.51)$$

the modified magnetization dynamics equation from (5.37) can be written as

$$\frac{\partial}{\partial t} \rho_k(g, t) = \frac{\partial}{\partial g} [\Phi_k(g) \rho_k(g, t)] \qquad (5.52)$$
$$+ \sum_n \int_{L_n} [K_{n,k}(g', g) \rho_n(g', t) - K_{k,n}(g, g') \rho_k(g, t)] dg',$$

$$(k = 1, 2, ...N).$$

It is interesting to point out that the stochastic differential equation for micromagnetic energy g corresponding to equation (5.52) can be written in a form similar

to the jump-noise driven magnetization dynamics equation (3.1). If the effects of thermal fluctuations are small enough that they can be neglected, then (5.52) results in the following deterministic equation for energy

$$\frac{dg_k}{dt} = -\Phi_k(g_k) + E(T_r^{(k)}(g)),\tag{5.53}$$

where $E(T_r^{(k)}(g))$ is the expected value of a jump-noise process $T_r^{(k)}(g)$ for energy on graphs.

Similar to in (3.25), the expected value of the jump-noise process on graphs can be given as

$$E[T_r(g)] = \lambda(g)E(\Delta g)\tag{5.54}$$

where $\lambda(g)$ is the scattering rate of graphs given by

$$\lambda(g) = \int_{L_n} K(g, g')dg'.\tag{5.55}$$

$E(\Delta g)$ is the expected value of the jump in energy Δg and is defined by

$$E(\Delta g) = \int_{L_n} (\Delta g)\chi(\Delta g, g)d(\Delta g),\tag{5.56}$$

where $\chi(\Delta g, g)$ is the conditional probability density on graphs given by

$$\chi(\Delta g, g) = \frac{K(g, g + \Delta g)}{\lambda(g)}.\tag{5.57}$$

As can be seen, this jump-noise process is fully defined by the transition probability rate $K_{k,n}(g, g') = K_{k,n}(g, g + \Delta g)$. In this way, the semi-analytical averaging approach first introduced in chapter 4 can be used to quickly and accurately analyze the complex dynamics of spin-torque driven magnetization dynamics.

5.5 Self-Oscillations

With the addition of the spin-transfer torque, it is possible to have periodic so-lutions of the magnetization dynamics[32,33]. These solutions are known as limit cycles or "self-oscillations" of the magnetization. The formation of these self-oscillations is due to the balance of competing forces when thermal effects are perfectly balanced against the effects of spin-transfer torque. As the spin torque term in the magne-tization dynamics equation is dependent on the magnetization, the balance points where self-oscillations appear are also magnetization-dependent.

By solving the spin-torque driven magnetization dynamics equation, the self-oscillations are seen to be located at the extrema of the micromagnetic energy g, like energy wells or peaks. Like other energy artifacts, these self-oscillations can be stable or unstable. This means that for stable self-oscillations, the limit cycles act as energy wells and will attract precessional magnetization trajectories to their own stable periodic trajectory.

The approach outlined in section 5.2 was used to numerically study stable self-oscillations in uniaxial magnetic nanosystems caused by the injection of spin-polarized currents. Using the spin-torque driven magnetization dynamics equa-tions on graphs, the self-oscillation phenomenon was studied in two ways. The first method was to observe stationary equilibrium distributions that occur when

$$\frac{\partial}{\partial t}\rho_k(g,t) = 0. \tag{5.58}$$

From (5.53), this equilibrium condition produces the equality

$$\frac{\partial}{\partial t}[\Phi_k(g)\rho_k^{(0)}(g)] = \sum_n \int_{L_n} [K_{k,n}(g,g')\rho_k^{(0)}(g) - K_{n,k}(g',g)\rho_n^{(0)}(g')]dg'. \quad (5.59)$$

Solving for $\rho_k^{(0)}(g)$ for $k = 1, 2, ...N$ produces the stationary equilibrium distribution under spin-polarized current injection.

The second method to study the self-oscillation phenomenon solves for extrema in the micromagnetic energy equation. As stable self-oscillations behave as energy wells, they satisfy the equation

$$\frac{dg_k}{dt} = 0. \quad (5.60)$$

Using (5.28), this condition is seen to be satisfied when

$$\Phi_k(g_k) = E(T_r^{(k)}(g)), \quad (5.61)$$

which is when the jump-noise process is balanced by the spin-torque effect.

The numerical results of these two studies are shown in Figures 5.1, 5.2, and 5.3. These figures represent the stationary distributions of $\rho(g)$ (dashed lines) for various values of spin-polarized current injection as well as graphs of the function

$$F(g) = -\Phi(g) + E(T_r(g)) \quad (5.62)$$

represented by continuous lines.

It is apparent from these figures that the location of the maximum $\rho(g)$ practically coincides with the zero of $F(g)$. In other words, this maximum of $\rho(g)$ and self-oscillations occur along specific precessional trajectories that are defined by the zeros of function $F(g)$.
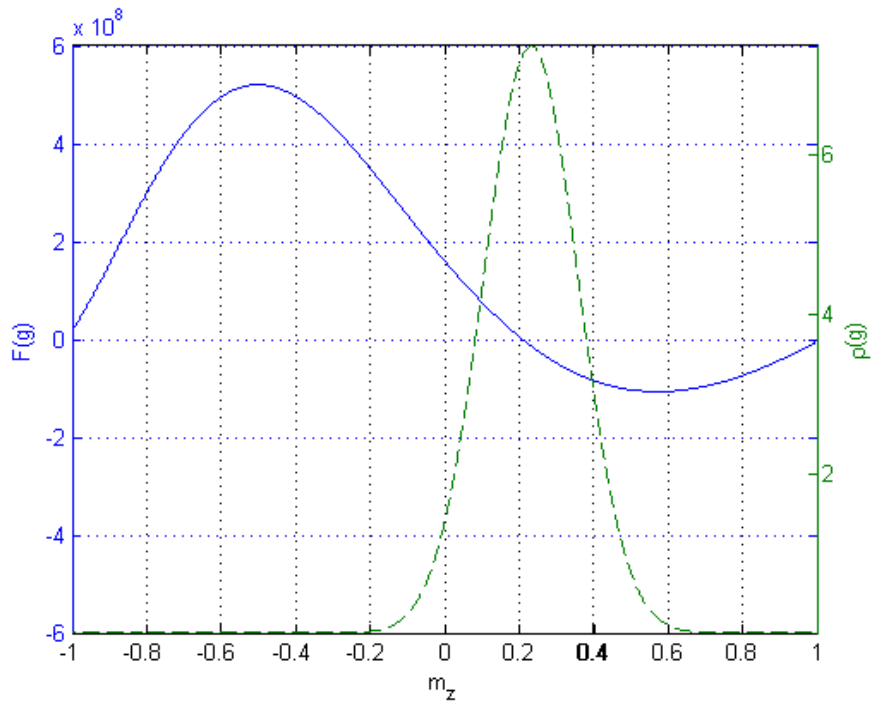
Figure 5.1: $F(g)$ and $\rho(g)$ for $D_x = D_y = 0$, $D_z = 1$, $H_{az} = 1.6$, $e_{pz} = -1$, $c_p = 0.5$, $\beta = 2 \times 10^8$.
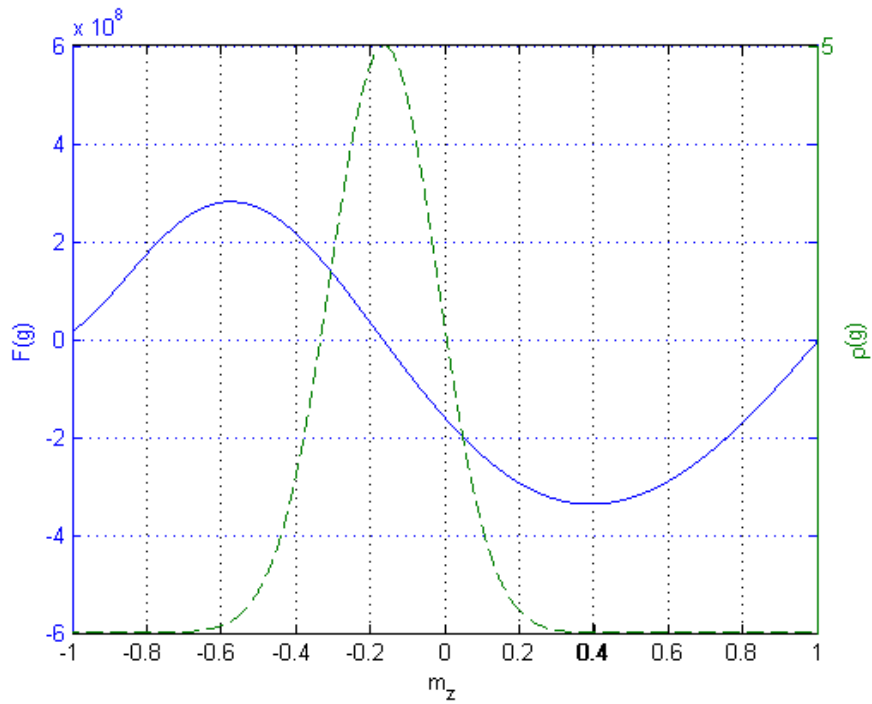
Figure 5.2: $F(g)$ and $\rho(g)$ for $D_x = D_y = 0$, $D_z = 1$, $H_{az} = 1.6$, $e_{pz} = -1$, $c_p = 0.5$, $\beta = 4 \times 10^8$.
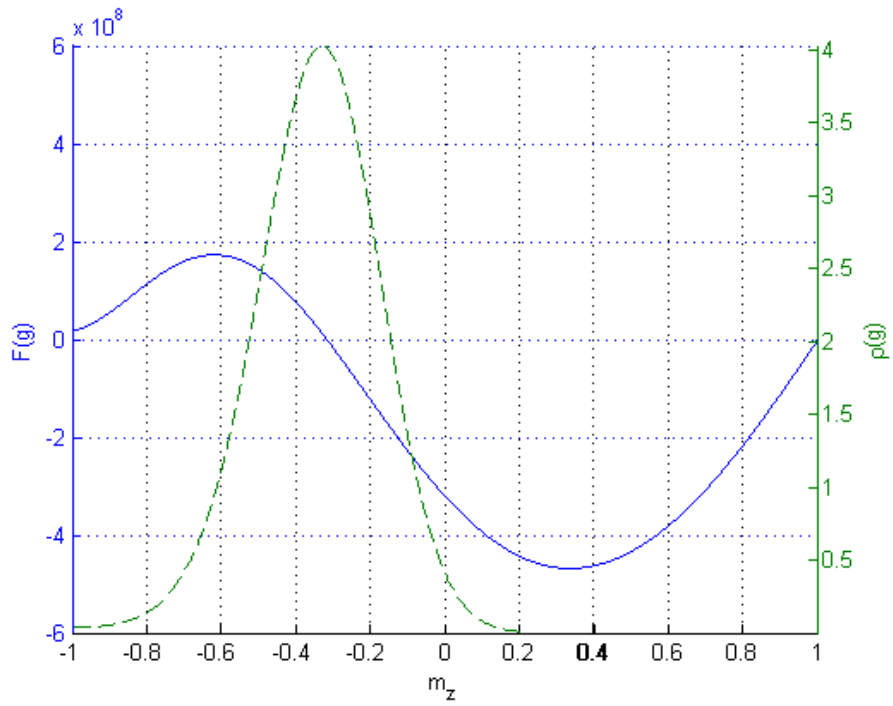
Figure 5.3: $F(g)$ and $\rho(g)$ for $D_x = D_y = 0$, $D_z = 1$, $H_{az} = 1.6$, $e_{pz} = -1$, $c_p = 0.5$, $\beta = 5 \times 10^8$.

Chapter 6: Power Spectral Density of Magnetization Dynamics

6.1 Power Spectral Density

The previously outlined analytical approach and numerical simulations in this dissertation provide a good theoretical basis for the jump-noise process driven magnetization dynamics. Yet, most of the numerical simulations are hard to quantitatively verify with experimental setups. A quantity that can more easily be measured in laboratories is the power spectral density of a magnetic particle[4,16]. Therefore, an analytical derivation for power spectral density would provide a good connection between the theoretical analytical approach outlined in this dissertation and any experimentally obtained results obtained in the future.

6.1.1 Calculating Power Spectral Density

One thing to point out is that the power spectral density can only be calculated for linear, time-invariant stochastic processes that are square-integrable. Since the Landau-Lifshitz equation driven by a jump-noise process in equation (3.1) is not linear, the magnetization dynamics on the level of transition probability densities given in (3.4) can be used. Furthermore, a steady-state solution is assumed such

that the process is stationary. From these assumptions, the power spectral density can be calculated.

The first step for calculating the power spectral density is to find the autocorrelation function. The autocorrelation function for an arbitrary function f defined on the magnetization sphere is given by:

$$\hat{C}_f(\tau) = \langle [f(\mathbf{m}(t_0 - \tau)) - \langle f(\mathbf{m}) \rangle][f(\mathbf{m}(t_0)) - \langle f(\mathbf{m}) \rangle] \rangle. \tag{6.1}$$

Once the autocorrelation function is found, the power spectral density can be found as the Fourier transform of the autocorrelation function:

$$\hat{S}_f(\omega) = \int_{-\infty}^{\infty} \hat{C}_f(\tau) e^{-j\omega\tau} d\tau. \tag{6.2}$$

6.1.2 Power Spectral Density on Energy Graphs

The power spectral density as defined on energy graphs can be found using a similar line of reasoning. The autocorrelation function on energy graphs for a function f is given by

$$\hat{C}_f(\tau) = \langle [f(g(t_0 - \tau)) - \langle f(g) \rangle][f(g(t_0)) - \langle f(g) \rangle] \rangle. \tag{6.3}$$

This autocorrelation function can be expanded to:

$$\hat{C}_f(\tau) = \langle f(g(t_0 - \tau))f(g(t_0)) - f(g(t_0 - \tau))\langle f(g) \rangle \\ - \langle f(g) \rangle f(g(t_0)) + \langle f(g) \rangle \langle f(g) \rangle \rangle. \tag{6.4}$$

Taking the expected value of the expression gives:

$$\hat{C}_f(\tau) = \langle f(g(t_0 - \tau))f(g(t_0)) \rangle - \langle f(g(t_0 - \tau))\langle f(g) \rangle \rangle \\ - \langle \langle f(g) \rangle f(g(t_0)) \rangle + \langle \langle f(g) \rangle \langle f(g) \rangle \rangle. \tag{6.5}$$

91

Simplifying the expression gives:

$$\hat{C}_f(\tau) = \langle f(g(t_0 - \tau))f(g(t_0))\rangle - \langle f(g)\rangle\langle f(g)\rangle - \langle f(g)\rangle\langle f(g)\rangle + \langle f(g)\rangle\langle f(g)\rangle. \quad (6.6)$$

Canceling the terms gives the expression:

$$\hat{C}_f(\tau) = \langle f(g(t_0 - \tau))f(g(t_0))\rangle - \langle f(g)\rangle\langle f(g)\rangle. \quad (6.7)$$

The expected value operator used in the previous expressions is defined by

$$\langle f(g)\rangle = \int_L f(g)\rho^{eq}(g)dg. \quad (6.8)$$

The expression can be simplified by defining $g = g(t_0)$ and $g' = g(t_0 - \tau)$. Using the definition for expected value and the new notation gives:

$$\hat{C}_f(\tau) = \int_L \int_L f(g)f(g')\rho(g, t_0; g', t_0 - \tau)dg'dg$$
$$- \int_L \int_L f(g)f(g')\rho^{eq}(g)\rho^{eq}(g')dg'dg. \quad (6.9)$$

The probability distribution function is a stationary function so it can be written as a conditional probability:

$$\rho(g, t_0; g', t_0 - \tau) = \rho(g, \tau|g', 0)\rho^{eq}(g'). \quad (6.10)$$

Using this definition for probability distribution, the autocorrelation function can be written:

$$\hat{C}_f(\tau) = \int_L \int_L f(g)f(g')\rho(g, \tau|g', 0)\rho^{eq}(g')dg'dg$$
$$- \int_L \int_L f(g)f(g')\rho^{eq}(g)\rho^{eq}(g')dg'dg. \quad (6.11)$$

Combining the two integrals gives:

$$\hat{C}_f(\tau) = \int_L \int_L f(g)f(g')[\rho(g,\tau|g',0) - \rho^{eq}(g)]\rho^{eq}(g')dg'dg. \tag{6.12}$$

This integral can be rewritten as:

$$\hat{C}_f(\tau) = \int_L f(g)\left[\int_L f(g')[\rho(g,\tau|g',0) - \rho^{eq}(g)]\rho^{eq}(g')dg'\right]dg \tag{6.13}$$

The equation within the brackets can be redefined as a separate equation:

$$\psi_f(g,\tau) = \int_L f(g')[\rho(g,\tau|g',0) - \rho^{eq}(g)]\rho^{eq}(g')dg'. \tag{6.14}$$

Therefore, the autocorrelation function is:

$$\hat{C}_f(\tau) = \int_L f(g)\psi_f(g,\tau)dg. \tag{6.15}$$

The power spectral density is then the Fourier transform of the autocorrelation function:

$$\hat{S}_f(\omega) = \int_{-\infty}^{\infty} \hat{C}_f(\tau)e^{-j\omega\tau}d\tau \tag{6.16}$$

Since the autocorrelation function is an even function, the power spectral density can be written:

$$\hat{S}_f(\omega) = 2\mathbb{R}\left\{\int_0^{\infty} \hat{C}_f(\tau)e^{-j\omega\tau}d\tau\right\} \tag{6.17}$$

Inserting the definition of the autocorrelation function from (6.15), the power spectral density is:

$$\hat{S}_f(\omega) = 2\mathbb{R}\left\{\int_0^{\infty}\left[\int_L f(g)\psi_f(g,\tau)dg\right]e^{-j\omega\tau}d\tau\right\}. \tag{6.18}$$

The order of the two integrals can be interchanged

$$\hat{S}_f(\omega) = 2\mathbb{R}\left\{\int_L f(g)\left[\int_0^{\infty}\psi_f(g,\tau)e^{-j\omega\tau}d\tau\right]dg\right\} \tag{6.19}$$

The function in the inner bracket can be defined as the Fourier Transform of the previously defined function $\psi(g, \tau)$:

$$\Psi_f(g, \omega) = \int_0^\infty \psi_f(g, \tau) e^{-j\omega\tau} d\tau. \tag{6.20}$$

Therefore, the power spectral density can be found by solving the equation:

$$\hat{S}_f(\omega) = 2\mathbb{R} \left\{ \int_L f(g) \Psi_f(g, \omega) dg \right\}. \tag{6.21}$$

6.2 Analytical Approach

The previously outlined approach solves for the power spectral density in the case of an arbitrary function $f(g)$. To analyze the power spectral density for free energy, the function to consider is for $f(g) = g$.

6.2.1 Deriving the Free Energy Power Spectral Density

Considering the function $f(g) = g$, the initial autocorrelation function becomes:

$$\hat{C}_g(\tau) = \langle [g - \langle g \rangle][g' - \langle g \rangle] \rangle. \tag{6.22}$$

This autocorrelation function can be equivalently written as:

$$\hat{C}_g(\tau) = \langle gg' \rangle - \langle g \rangle \langle g \rangle. \tag{6.23}$$

Using the definition for expected value to be:

$$\langle g \rangle = \int_L g \rho^{eq}(g) dg, \tag{6.24}$$

the autocorrelation function can be written as

$$\hat{C}_g(\tau) = \int_L \int_L gg' \rho(g, t_0; g', t_0 - \tau) dg' dg - \int_L \int_L gg' \rho^{eq}(g) \rho^{eq}(g') dg' dg. \qquad (6.25)$$

Again, using the fact that the probability distribution function is a stationary function, the probability distribution function can be written

$$\rho(g, t_0; g', t_0 - \tau) = \rho(g, \tau | g', 0) \rho^{eq}(g'). \qquad (6.26)$$

The autocorrelation function becomes

$$\hat{C}_g(\tau) = \int_L \int_L gg' \rho(g, \tau | g', 0) \rho^{eq}(g') dg' dg - \int_L \int_L gg' \rho^{eq}(g) \rho^{eq}(g') dg' dg. \qquad (6.27)$$

These integrals can be combined to become

$$\hat{C}_g(\tau) = \int_L \int_L gg' [\rho(g, \tau | g', 0) - \rho^{eq}(g)] \rho^{eq}(g') dg' dg. \qquad (6.28)$$

Rearranging the integrals gives:

$$\hat{C}_g(\tau) = \int_L g \left[\int_L g' [\rho(g, \tau | g', 0) - \rho^{eq}(g)] \rho^{eq}(g') dg' \right] dg. \qquad (6.29)$$

Defining the function inside the brackets as ψ, the autocorrelation function becomes

$$\hat{C}_g(\tau) = \int_L g \psi_g(g, \tau) dg, \qquad (6.30)$$

where

$$\psi_g(g, \tau) = \int_L g' [\rho(g, \tau | g', 0) - \rho^{eq}(g)] \rho^{eq}(g') dg'. \qquad (6.31)$$

Using this definition for the autocorrelation function, the power spectral density is given as the Fourier transform:

$$\hat{S}_g(\omega) = \int_{-\infty}^{\infty} \hat{C}_g(\tau) e^{-j\omega\tau} d\tau. \qquad (6.32)$$

95

The autocorrelation function is an even function so the power spectral density can be written as:

$$\hat{S}_g(\omega) = 2\mathbb{R}\left\{\int_0^\infty \hat{C}_g(\tau)e^{-j\omega\tau}d\tau\right\}. \tag{6.33}$$

Plugging in the equation for the autocorrelation function gives:

$$\hat{S}_g(\omega) = 2\mathbb{R}\left\{\int_0^\infty \left[\int_L g\psi_g(g,\tau)dg\right]e^{-j\omega\tau}d\tau\right\}. \tag{6.34}$$

Rearranging the integrals, the power spectral density can be defined as

$$\hat{S}_g(\omega) = 2\mathbb{R}\left\{\int_L g\Psi_g(g,\omega)dg\right\}, \tag{6.35}$$

where

$$\Psi_g(g,\omega) = \int_0^\infty \psi_g(g,\tau)e^{-j\omega\tau}d\tau. \tag{6.36}$$

6.2.2 Solving for Free Energy Power Spectral Density

Now that there is an equation to describe the power spectral density on energy graphs, it is clear from (6.35), (6.36) and (6.31) that the power spectral density can be found from the probability distribution function. To find an analytical solution to the power spectral density, the equation for magnetization dynamics on grpah can be manipulated to find solutions to $\Psi(g,\omega)$. Starting from the general form of the equation for magnetization dynamics on graphs that includes the spin-torque term:

$$\frac{\partial}{\partial t}\rho_k(g,t) = \frac{\partial}{\partial g}[\Phi_k(g)\rho_k(g,t)]$$
$$+ \sum_n \int_{L_n} [K_{n,k}(g',g)\rho_n(g',t) - K_{k,n}(g,g')\rho_k(g,t)]dg'. \tag{6.37}$$

In this equation, $\rho(g, t)$ was notationally simplified to only include the last magnetization state in the Markov process. The full expression is $\rho(g_0, t_0; g, t_0 + \tau)$, which describes the initial state g_0 at time t_0 and the current state g at later time $t_0 + \tau$.

$$\frac{\partial}{\partial t}\rho_k(g_0, t_0; g, t_0 + \tau) = \frac{\partial}{\partial g}[\Phi_k(g)\rho_k(g_0, t_0; g, t_0 + \tau)]$$
$$+ \sum_n \int_{L_n} [K_{n,k}(g', g)\rho_n(g_0, t_0; g', t_0 + \tau)$$
$$- K_{k,n}(g, g')\rho_k(g_0, t_0; g, t_0 + \tau)]dg' \quad (6.38)$$

Since the probability distribution is a stationary process, it can be viewed as a probability distribution starting at time t and ending at time τ:

$$\rho(g_0, t_0; g, t_0 + \tau) = \rho(g_0, 0; g, \tau) \quad (6.39)$$

Using this probability distribution, the equation becomes:

$$\frac{\partial}{\partial t}\rho_k(g_0, 0; g, \tau) = \frac{\partial}{\partial g}[\Phi_k(g)\rho_k(g_0, 0; g, \tau)]$$
$$+ \sum_n \int_{L_n} [K_{n,k}(g', g)\rho_n(g_0, 0; g', \tau) - K_{k,n}(g, g')\rho_k(g_0, 0; g, \tau)]dg' \quad (6.40)$$

It in important to look at the behavior at time $t = 0$. At that time, the initial boundary condition can be described as the magnetization starting at $g = g_0$:

$$\rho(g_0, 0; g, \tau)|_{\tau=0} = \delta(g - g_0) \quad (6.41)$$

This initial boundary condition implies that the probability distribution can be defined as a conditional probability dependent on the starting magnetization:

$$\rho(g, \tau|g_0, 0) \equiv \rho(g_0, 0; g, \tau) \quad (6.42)$$

The equation then becomes:

$$\frac{\partial}{\partial t}\rho_k(g,\tau|g_0,0) = \frac{\partial}{\partial g}[\Phi_k(g)\rho_k(g,\tau|g_0,0)]$$

$$+\sum_n \int_{L_n}[K_{n,k}(g',g)\rho_n(g',\tau|g_0,0) - K_{k,n}(g,g')\rho_k(g,\tau|g_0,0)]dg' \qquad (6.43)$$

At equilibrium the probability distribution ρ^{eq} is stationary and satisfies:

$$\frac{\partial}{\partial g}[\Phi_k(g)\rho_k^{eq}(g)] + \sum_n \int_{L_n}[K_{n,k}(g',g)\rho_n^{eq}(g') - K_{k,n}(g,g')\rho_k^{eq}(g)]dg'$$

$$= \frac{\partial}{\partial t}\rho_k^{eq} = 0 \qquad (6.44)$$

(6.44) can be subtracted from (6.43) to obtain:

$$\frac{\partial}{\partial t}\rho_k(g,\tau|g_0,0) - \frac{\partial}{\partial t}\rho_k^{eq} = \frac{\partial}{\partial g}[\Phi_k(g)\rho_k(g,\tau|g_0,0)] - \frac{\partial}{\partial g}[\Phi_k(g)\rho_k^{eq}(g)]$$

$$+\sum_n \int_{L_n}[K_{n,k}(g',g)\rho_n(g',\tau|g_0,0) - K_{k,n}(g,g')\rho_k(g,\tau|g_0,0)]dg'$$

$$-\sum_n \int_{L_n}[K_{n,k}(g',g)\rho_n^{eq}(g') - K_{k,n}(g,g')\rho_k^{eq}(g)]dg' \qquad (6.45)$$

This expression can be simplified to:

$$\frac{\partial}{\partial t}[\rho_k(g,\tau|g_0,0) - \rho_k^{eq}(g)] = \frac{\partial}{\partial g}[\Phi_k(g)[\rho_k(g,\tau|g_0,0) - \rho_k^{eq}(g)]]$$

$$+\sum_n \int_{L_n}[K_{n,k}(g',g)[\rho_n(g,\tau|g_0,0)$$

$$- \rho_n^{eq}(g)] - K_{k,n}(g,g')[\rho_k(g,\tau|g_0,0) - \rho_k^{eq}(g)]]dg' \qquad (6.46)$$

The difference between the probability distribution and the equilibrium distribution can be defined as:

$$\zeta_k(g,\tau|g_0,0) \equiv \rho_k(g,\tau|g_0,0) - \rho_k^{eq}(g) \qquad (6.47)$$

The initial boundary condition for this new function is:

$$\zeta_k(g,\tau|g_0,0)|_{\tau=0} = \rho_k(g,\tau|g_0,0)|_{\tau=0} - \rho_k^{eq}(g) = \delta(g-g_0) - \rho_k^{eq}(g) \qquad (6.48)$$

Using this function ζ, the equation is shown to satisfy:

$$\frac{\partial}{\partial t}\zeta_k(g,\tau|g_0,0) = \frac{\partial}{\partial g}[\Phi_k(g)\zeta_k(g,\tau|g_0,0)]$$

$$+ \sum_n \int_{L_n} [K_{n,k}(g',g)\zeta_n(g',\tau|g_0,0) - K_{k,n}(g,g')\zeta_k(g,\tau|g_0,0)]dg' \quad (6.49)$$

From ζ, the function ψ_g defined in (6.31) can be obtained. To do this, a new function

is defined:

$$\psi_k(g,\tau) \equiv \int_L g' \rho_k^{eq}(g')\zeta_k(g,\tau|g',0)dg' \quad (6.50)$$

Applying the same integration to the equation (6.49) gives:

$$\int_L g'' \rho_k^{eq}(g'')[\frac{\partial}{\partial t}\zeta_k(g,\tau|g'',0)]dg'' =$$

$$\int_L g'' \rho_k^{eq}(g'')[\frac{\partial}{\partial g}[\Phi_k(g)\zeta_k(g,\tau|g'',0)]]dg''$$

$$+ \int_L g'' \rho_k^{eq}(g'')[\sum_n \int_{L_n} [K_{n,k}(g',g)\zeta_n(g',\tau|g'',0)$$

$$- K_{k,n}(g,g')\zeta_k(g,\tau|g'',0)]dg']dg'' \quad (6.51)$$

Using the definition of ψ from (6.50), the equation can be written:

$$\frac{\partial}{\partial t}\psi_k(g,\tau|g_0,0) = \frac{\partial}{\partial g}[\Phi_k(g)\psi_k(g,\tau|g_0,0)]$$

$$+ \sum_n \int_{L_n} [K_{n,k}(g',g)\psi_n(g',\tau|g_0,0) - K_{k,n}(g,g')\psi_k(g,\tau|g_0,0)]dg' \quad (6.52)$$

Using (6.50), the initial boundary condition for ψ_k is seen to satisfy:

$$\psi_k(g,\tau|g_0,0)|_{\tau=0} = \int_L g'' \rho_k^{eq}[\delta(g-g_0) - \rho_k^{eq}(g)]dg'' \quad (6.53)$$

This simplifies to the expression:

$$\psi_k(g,\tau|g_0,0)|_{\tau=0} = \rho_k^{eq}[g - \langle g \rangle] \quad (6.54)$$

From (6.36), the next step in finding the power spectral density is to take the Fourier transform of ψ_k to find Ψ_k by using the equation:

$$\Psi_k(g,\omega|g_0) = \int_0^\infty \psi_k(g,\tau|g_0,0)e^{-j\omega\tau}d\tau \tag{6.55}$$

Applying this same Fourier transform to equation (6.52) gives:

$$\int_0^\infty \frac{\partial}{\partial t}\psi_k(g,\tau|g_0,0)e^{-j\omega\tau}d\tau = \int_0^\infty \frac{\partial}{\partial g}[\Phi_k(g)\psi_k(g,\tau|g_0,0)]e^{-j\omega\tau}d\tau$$

$$+ \int_0^\infty \sum_n \int_{L_n} [K_{n,k}(g',g)\psi_n(g',\tau|g_0,0)$$

$$- K_{k,n}(g,g')\psi_k(g,\tau|g_0,0)]dg'e^{-j\omega\tau}d\tau \tag{6.56}$$

Performing this one-sided integration gives:

$$j\omega\Psi_k(g,\omega|g_0) - \psi(g,\tau|g_0,0)|_{\tau=0} = \frac{\partial}{\partial g}[\Phi_k(g)\Psi_k(g,\omega|g_0)]$$

$$+ \sum_n \int_{L_n} [K_{n,k}(g',g)\Psi_n(g',\omega|g_0) - K_{k,n}(g,g')\Psi_k(g,\omega|g_0)]dg' \tag{6.57}$$

This final equation can now be used to solve for Ψ_k. The power spectral density can then be found from Ψ_k by integrating:

$$\hat{S}(\omega) = 2\mathbb{R}\left\{\int_L g\Psi(g,\omega)dg\right\} \tag{6.58}$$

6.2.3 Alternative Eigenvalue approach

In the case of no applied spin-torque where the spin-torque term can be neglected, the equation for the power spectral density in (6.57) can be simplified to:

$$j\omega\Psi_k(g,\omega|g_0) - \psi_k(g,\tau|g_0,0)|_{\tau=0}$$

$$= \sum_n \int_{L_n} [K_{n,k}(g',g)\Psi_n(g',\omega|g_0) - K_{k,n}(g,g')\Psi_k(g,\omega|g_0)]dg' \tag{6.59}$$

The right side of the equation takes the same form as the collision integral in (4.18) and so can be solved using the same eigenvalue approach.

Writing the right side of the equation in matrix form $\hat{K}$, the eigenvalue solutions will take the form:

$$\hat{K}\phi_i = \lambda_i\phi_i \qquad (6.60)$$

for some eigenvector ϕ_i.

Using the eigenvectors from $\hat{K}$, $\Psi_k(g,\omega)$ can be decomposed to take the form:

$$\Psi_k(g,\omega) = \sum_i \lambda_i a_i(\omega)\phi_i(g) \qquad (6.61)$$

On the left side of equation (6.59), the second term can be expressed as an orthogonal mapping of the initial boundary condition onto the eigenvectors such that:

$$\psi_k(g,\tau|g_0,0)|_{\tau=0} = \rho_k^{eq}[g - \langle g \rangle] = \sum_i b_i\phi_i(g), \qquad (6.62)$$

where

$$b_i = \langle \rho_k^{eq}[g - \langle g \rangle], \phi_i(g) \rangle. \qquad (6.63)$$

Using this decomposition method, the master equation can be expressed in terms of eigenvectors such that:

$$j\omega a_i(\omega)\phi_i(g) - b_i\phi_i(g) = \lambda_i a_i(\omega)\phi_i(g) \qquad (6.64)$$

Solving for this expression, a_i is found to be:

$$a_i = \frac{b_i}{j\omega - \lambda_i} \qquad (6.65)$$

Therefore, $\Psi_k(g,\omega)$ can be found to satisfy:

$$\Psi(g,\omega) = \sum_i \frac{\lambda_i \langle \rho_k^{eq}[g - \langle g \rangle], \phi_i(g) \rangle}{j\omega - \lambda_i}\phi_i(g) \qquad (6.66)$$

101

This eigenvalue approach allows for a very fast calculation of power spectral density. Rather than having to solve for each value of ω in (6.57) or (6.59), Ψ can be expressed as a function of ω in (6.66). In fact, the power spectral density can be expressed:

$$\hat{S}(\omega) = 2\mathbb{R}\left\{\int_L g \sum_i \frac{\lambda_i \langle \rho_k^{eq}[g - \langle g \rangle], \phi_i(g)\rangle}{j\omega - \lambda_i} \phi_i(g)dg\right\}. \qquad (6.67)$$

This equation can be rearranged to give a succinct expression for PSD:

$$\hat{S}(\omega) = 2\mathbb{R}\left\{\sum_i \frac{\lambda_i}{j\omega - \lambda_i} \int_L g\langle \rho_k^{eq}[g - \langle g \rangle], \phi_i(g)\rangle \phi_i(g)dg\right\}. \qquad (6.68)$$

6.3   Numerical Results and Discussion

The techniques described in the previous sections have been numerically implemented for the case of uniaxial particles with and without the spin-torque effect. Since the probability distribution function on energy graphs is a stationary distribution, the power spectral density is expected to only reflect the stochastic noise that appears in the magnetization dynamics without peaks due to precessional trajectories.

As seen in Figures 6.1, 6.2, and 6.3, the power spectral density starts with a flat intensity response at lower frequencies then achieves a 'knee' and decreases on the log-scale as the frequency increases. The placement of the 'knee' illustrates the effect of thermal noise and shows how the nature of the thermal noise can influence the placement of the 'knee'. The roll-off in intensity appears to follow a $1/f^2$ dependence and is the same in each of the figures.

From comparing figures 6.1 and 6.2 where the intensity of the noise is in-
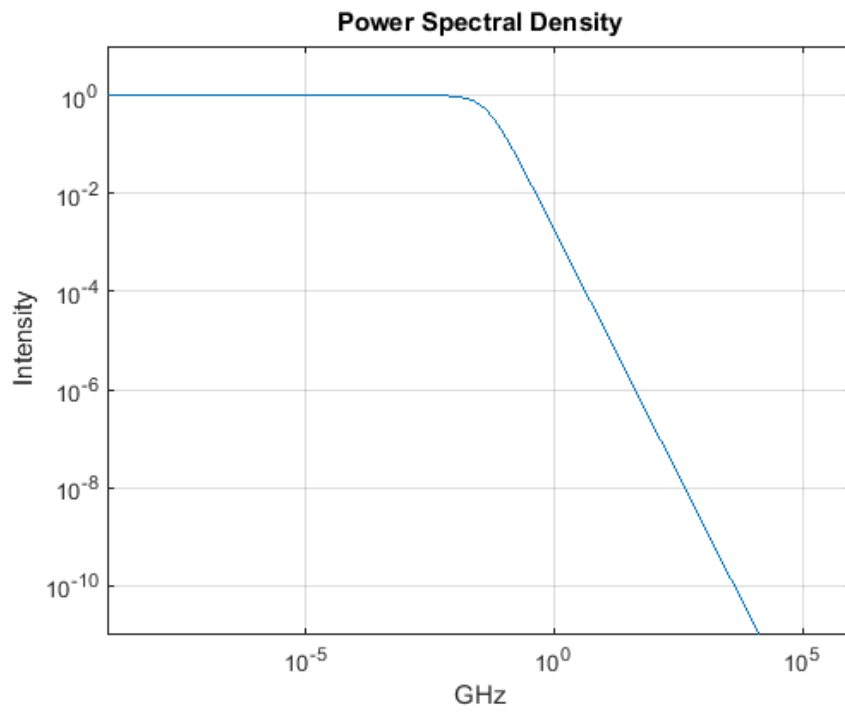
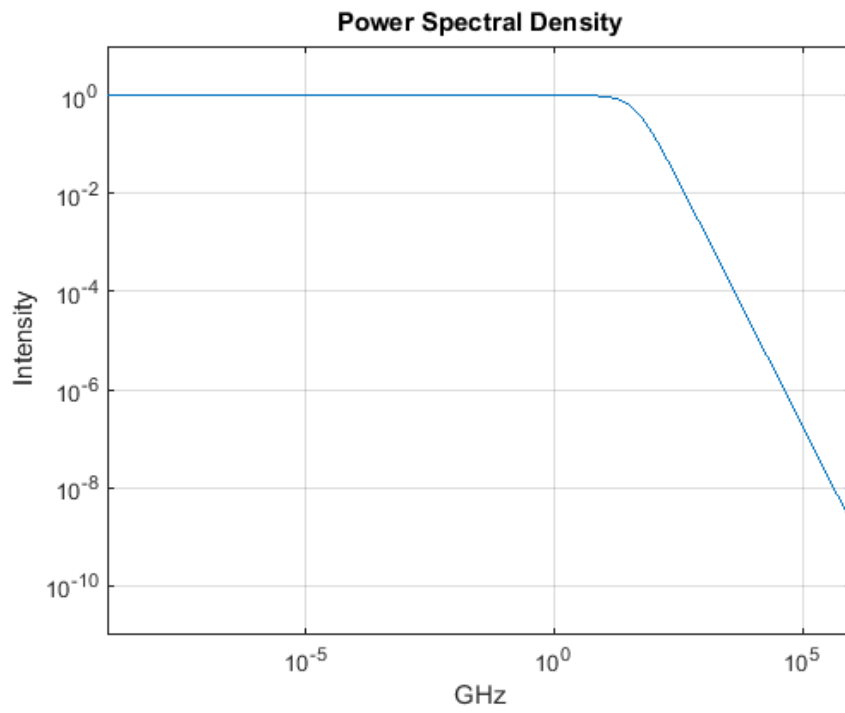Figure 6.1: Uniaxial particle with $K_{eff} = 0.5, H_{az} = -0.7, \sigma^2 = 0.001, B = 10^{12}$.

Figure 6.2: Uniaxial particle with $K_{eff} = 0.5, H_{az} = -0.7, \sigma^2 = 0.001, B = 10^{15}$.
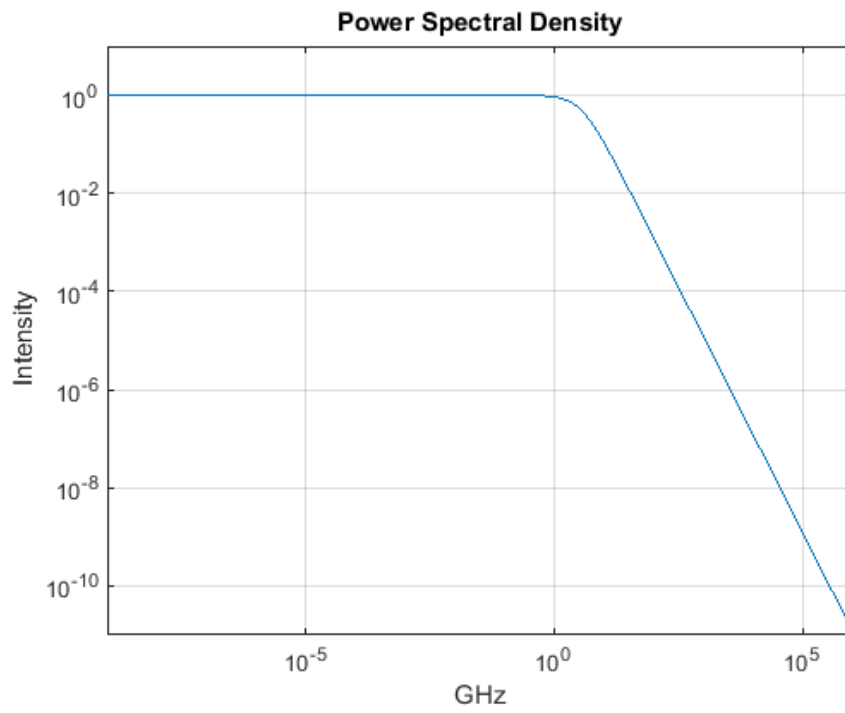
Figure 6.3: Uniaxial particle with $K_{eff} = 0.5, H_{az} = -0.7, \sigma^2 = 0.01, B = 10^{12}$.

creased from $B = 10^{12}$ to $B = 10^{15}$, the placement of the knee is shifted to higher frequencies. This makes some physical sense as thermal noise with higher intensity correlates with more frequent jumps and therefore the noise is present in more frequencies. Likewise, from comparing figures 6.1 and 6.3 where the distribution of the noise is increased from $\sigma^2 = 0.001$ to $\sigma^2 = 0.01$, the placement of the knee is also shifted to higher frequencies. This also makes physical sense as larger σ^2 allows for larger jumps in magnetization and therefore an overall larger transition probability rate and scattering rate. This again leads to more thermal noise present at higher frequencies. This phenomenon can be analytically seen in (3.18) and (4.17) as an increase in the noise parameters leads to an increase in the transition probability rate.

Figures 6.4, 6.5, and 6.6 represent the same power spectral densities as in Figures 6.1, 6.2, and 6.3 but calculated using the eigenvalue approach described in section 6.2.3. As seen from these figures, the power spectral densities exactly match their respective plots in Figures 6.1, 6.2, and 6.3.

Figures 6.7, 6.8, and 6.9 show the effect of spin-torque on the power spectral density. Since the addition of spin-torque changes the nature of the eigenvalue equation and the operator may no longer be self-adjoint, the eigenvalue approach cannot be used to solve for the spin-torque case. Therefore, the results shown here are from numerically solving (6.57) and (6.58). As seen from these figures, the addition of spin-torque modifies the power spectral density. Discounting the asymptotic dip that results from numerical errors, the power spectral density is seen to have two separate knees. By comparing figure 6.7 with figures 6.2 and 6.5, the
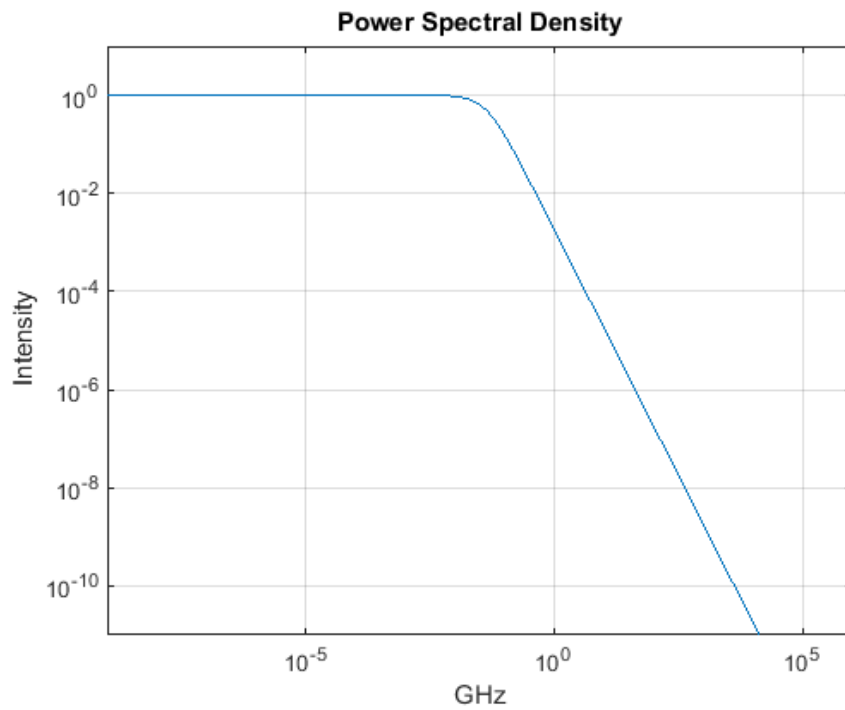
106

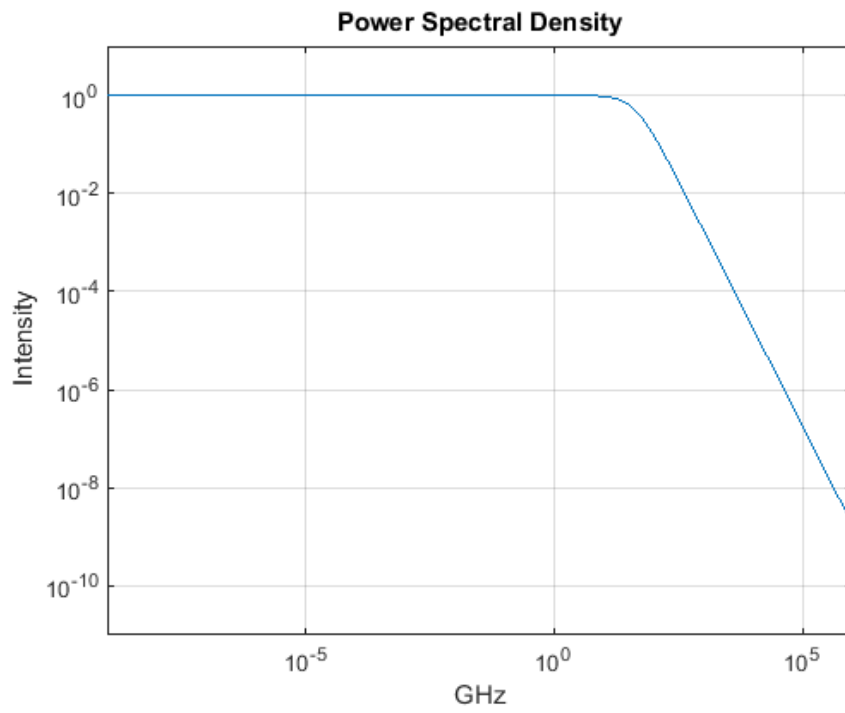Figure 6.4: Uniaxial particle with $K_{eff} = 0.5, H_{az} = -0.7, \sigma^2 = 0.001, B = 10^{12}$.

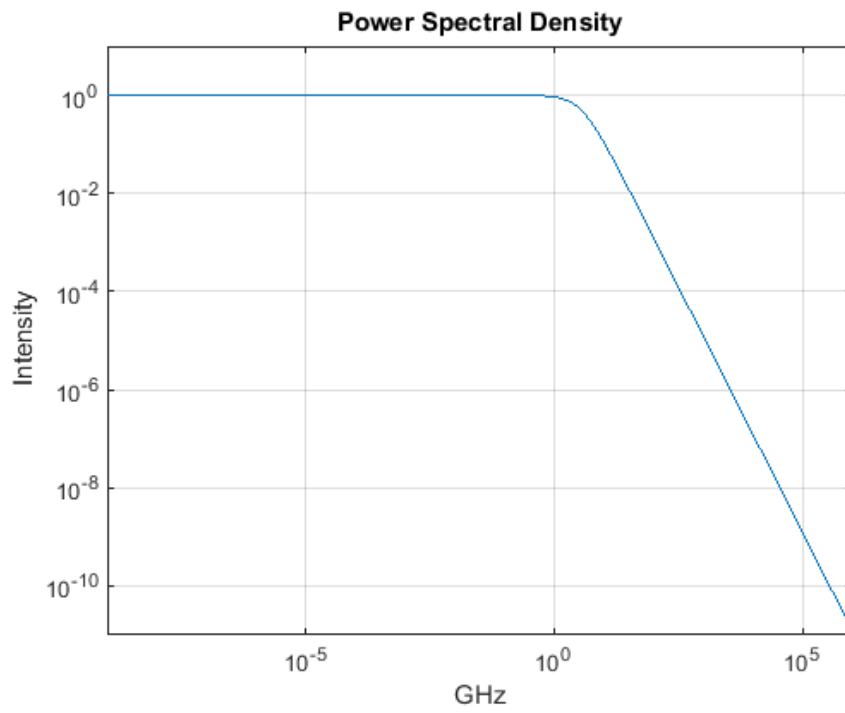Figure 6.5: Uniaxial particle with $K_{eff} = 0.5, H_{az} = -0.7, \sigma^2 = 0.001, B = 10^{15}$.

Figure 6.6: Uniaxial particle with $K_{eff} = 0.5, H_{az} = -0.7, \sigma^2 = 0.01, B = 10^{12}$.
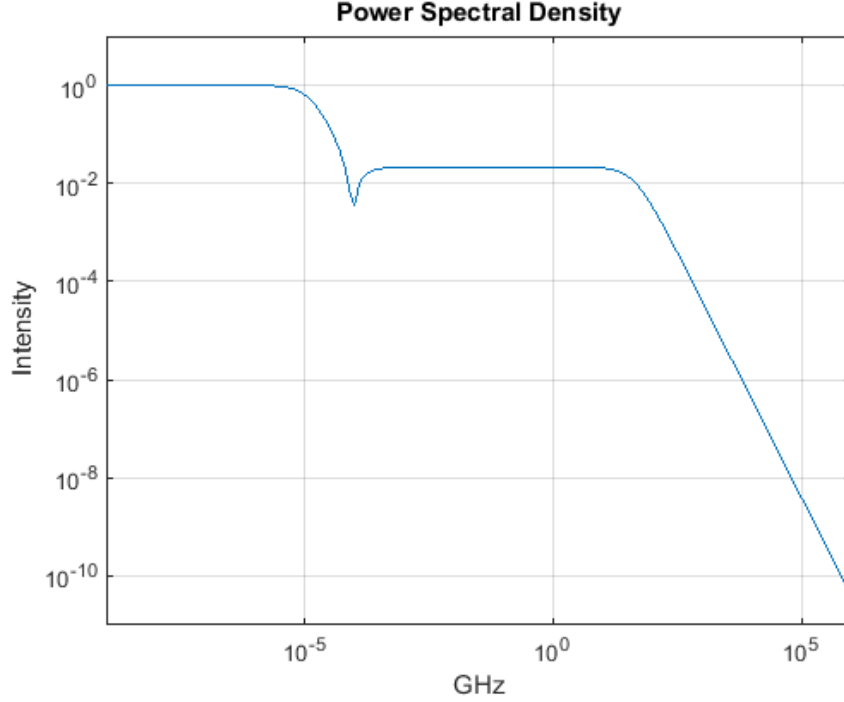
Power Spectral Density

Figure 6.7: Uniaxial particle with $K_{eff} = 0.5, H_{az} = -0.7, \sigma^2 = 0.001, B = 10^{15}$ and spin-torque characterized by $e_{pz} = -1, c_p = 0.5, \beta = 10^7$.

second knee is seen to correspond with the knee due to thermal noise, whereas the first knee is a result of the spin-torque effect. This is also illustrated by comparing figures 6.7, 6.8, and 6.9 where the strength of the spin torque (β) is increased from $\beta = 10^7$ to $\beta = 10^9$ and $\beta = 10^{12}$. This increase in the spin-torque shifts the location of the first knee to higher frequencies and in the case of $\beta = 10^{12}$, the first and second knees are almost equivalent.

This change in the power spectral density due to spin-torque can be viewed as an increase in the noise from a noise source separate from that of the thermal bath. The appearance of the second 'knee' can be seen as a direct result of equations (5.3),
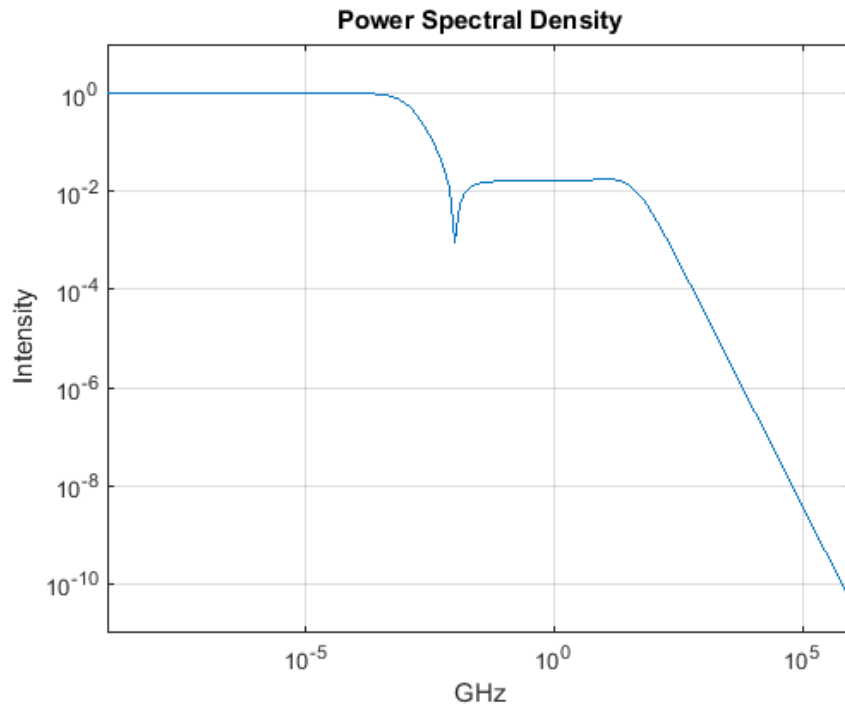
Figure 6.8: Uniaxial particle with $K_{eff} = 0.5, H_{az} = -0.7, \sigma^2 = 0.001, B = 10^{15}$ and spin-torque characterized by $e_{pz} = -1, c_p = 0.5, \beta = 10^9$.
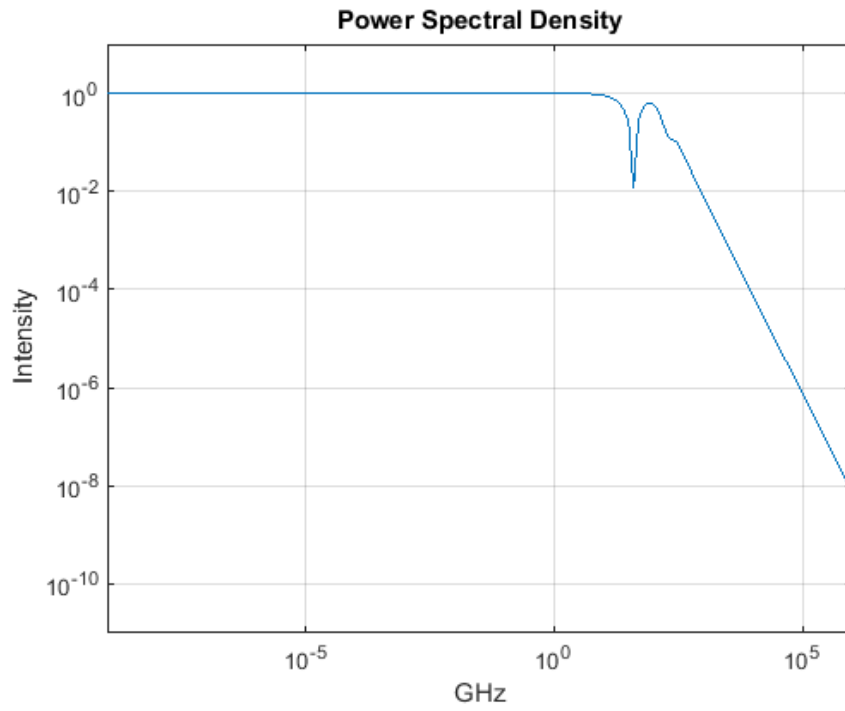
Figure 6.9: Uniaxial particle with $K_{eff} = 0.5, H_{az} = -0.7, \sigma^2 = 0.001, B = 10^{15}$ and spin-torque characterized by $e_{pz} = -1, c_p = 0.5, \beta = 10^{1}2$.

(5.4), and (5.17) where the transition probability rate has an additional exponential dependence on the spin-torque term.

Chapter 7: Discussion and Future Directions

7.1 Discussion

In this dissertation, a stochastic model to describe thermal fluctuation effects for jump-noise driven magnetization dynamics is developed. The motivation behind this new approach is to simplify the dynamic equations and combine the separate noise-induced terms in the traditional approach to a single jump-noise process. It has been shown in this dissertation that this jump-noise approach is qualitatively consistent with experimentally observed physical phenomena and has been shown to be mathematically equivalent to the traditional approach as both the damping and fluctuation effects emerge from elements of the jump-noise process. Details of a Monte Carlo numerical simulation method of modeling this jump-noise driven magnetization dynamics is presented in this dissertation as well as the benefits and drawbacks of this approach.

To overcome the drawbacks of using a Monte-Carlo approach, an averaging technique is introduced that reduces magnetization dynamics on a sphere to magnetization dynamics on a coordinate system defined by the free energy. Additionally, an eigenvalue-based method of solving magnetization dynamics on graphs that drastically reduces the needed computational usage is presented. Verification of the

114

accuracy of these approaches is obtained by comparing the Monte Carlo approach and the presented techniques in the study of magnetization switching at very low temperatures as well an exploration of the necessary conditions required for the Kramers-Brown approximation.

Another area of interest that is studied in this dissertation is the phenomenon of spin-transfer torque induced by spin-polarized current injection. An approach for magnetization dynamics driven by a jump-noise process that accounts for spin-torque is derived as well as an equivalent approach on energy graphs. These equations are used to analyze the spin-transfer torque effect and in particular, self-oscillations resulting from a balance between spin torque and damping are examined.

Additionally, the power spectral density for magnetization dynamics driven by a jump-noise process is derived and explored. The study of the power spectral density provides a link between the theoretical research outlined in this dissertation with potential experimental results obtainable in the laboratory setting. This link can potentially provide a substantive argument for the use of the jump-noise driven magnetization dynamics model. If this jump-noise driven magnetization dynamics model is supplemented by experimental results, it may open a new chapter of understanding the behavior of magnetization dynamics.

Finally, there are several more areas where this jump-noise driven magnetization dynamics and jump-noise driven magnetization dynamics on graphs can be applied. The following topics are a few possible directions for the future application of the techniques described in this dissertation.

7.2   Energy Graphs with Multiple Branches

In chapter 4, an averaging technique was introduced and used to explore the simple case of magnetization switching between the two energy wells of a uniaxial particle. In chapter 5, this problem was complicated slightly with the addition of a spin-transfer torque term and an externally applied magnetic field, but both of these fields were applied either parallel or anti-parallel to the easy axis. This led to a problem that has at most two energy wells and an associated energy graph that also has at most two branches. The situation of a uniaxial particle with fields applied parallel or anti-parallel to the easy axis is a very limiting case as it is easy to see that energy graphs with multiple branches can result from the change in many separate factors. One easy way to create a system with multiple branches is to remove the constraint of a uniaxial particle. Systems with a bi-axial structure can exhibit three energy branches by applying an effective field parallel to an easy axis. This creates a situation where there are three energy minima with their own associated energy wells. Therefore, to further explore stochastic magnetization dynamics on graphs, the techniques advanced in this dissertation, specifically the averaging technique, can be applied to more complicated micromagnetic scenarios such as energy graphs with multiple branches.

7.3 Magnetization Bifurcation

Extending the concepts discussed in the previous section regarding multiple branches, there can be interesting and complex behaviors in magnetization dynamics that arise under various conditions. As seen in chapter 5 and discussed in the introduction, magnetization dynamics is subject to damping and applied fields and is influenced by other phenomena such as the spin-transfer torque and magneto-optical effects. Under these different applied conditions, magnetization dynamics can exhibit a wide range of interesting effects such as self-oscillations, node-splitting, and the formation and dissolution of saddle-points. In the interest of exploring these effects, bifurcation diagrams that map the changes in magnetization dynamics behaviors as a function of various parameters can be quickly and accurately created and analyzed using the averaging techniques presented in chapter 4. These bifurcation diagrams can be used for many applications, such as to pinpoint the parameters necessary for node splitting between 2-branch energy graphs and 3-branch energy graphs. These diagrams may also be able to shed light on new and interesting phenomena that have yet to be discovered.

Bibliography

[1] D.V. Berkov and J. Miltat, "Spin-Torque Driven Magnetization Dynamics: Micromagnetic Modeling," *J. Magn. Magn. Mater.* 320, 1238 (2008)

[2] G. Bertotti, I. Mayergoyz, and C. Serpico, "Averaging Technique for the Analysis of Magnetization Relaxations," *J. Appl. Phys.* 95, 6598 (2004).

[3] G. Bertotti, I. Mayergoyz, and C. Serpico, "Analysis of Random Landau-Lifshitz Dynamics by Using Stochastic Processes on Graphs," *J. Appl. Phys.* 99, 08F301 (2006).

[4] G. Bertotti, I. Mayergoyz, and C. Serpico, *Nonlinear Magnetization Dynamics in Nanosystems*, Elsevier (2009).

[5] G. Bertotti, C. Serpico, Z. Liu, A. Lee, and I. Mayergoyz, "Spin Torque in the Framework of Random Magnetization Dynamics Driven by a Jump-Noise Process," *Physica B* 435, 8-10 (2014).

[6] G. Bertotti, C. Serpico, I.D. Mayergoyz, R. Bonin, and M. d'Aquino, "Current-Induced Magnetization Dynamics in Nanomagnets," *J. Magn. Magn. Mater.* 316, 285-290 (2007).

[7] W.F. Brown Jr, "Thermal Fluctuations of a Single-Domain Particle," *Phys. Rev.* 130, 1677-1686 (1963).

[8] E.M. Chudnovsky and L. Gunther, "Quantum Theory of Nucleation in Ferromagnets," *Phys. Rev. B* 37, 9455 (1988)

[9] D.R. Fredkin, "Brownian Motion on Manifolds, with Application to Thermal Magnetization Reversal," *Physica B* 306, 26 (2001).

[10] D.A. Garanin, "Fokker-Planck and Landau-Lifshitz-Bloch Equations for Classical Ferromagnets," *Phys. Rev. B* 55, 3050 (1997)

[11] C.W. Gardiner, *Handbook of Stochastic Methods for Physics, Chemistry and the Natural Sciences*, Springer-Verlag (1985)

[12] I.I. Gihman and A.V. Skorohod, *Stochastic Differential Equations*, Springer-Verlag (1972).

[13] T.L. Gilbert, "A Lagrangian Formulation of the Gyromagnetic Equation of the Magnetic Field," *Phys. Rev.* 100, 1243 (1955).

[14] T.L. Gilbert, "A Phenomenological Theory of Damping in Ferromagnetic Materials," *IEEE Trans. Magn.* 40, 3443 (2004).

[15] D. Kannan, *An Introduction to Stochastic Processes*, North-Holland (1979).

[16] C.E. Korman and I.D. Mayergoyz, "Semiconductor Noise in the Framework of Semiclassical Transport," *Phys. Rev. B* 54, 17620 (1996).

[17] H.A. Kramers, "Brownian Motion in a Field of Force and Diffusion Model of Chemical Reactions," *Physica* 7, 284 (1940)

[18] R. Kubo, *Statistical Mechanics*, North-Holland (1990)

[19] L.D. Landau and E.M. Lifshitz, "Theory of the Dispersion of Magnetic Permeability in Ferromagnetic Bodies," *Physik. Zeits. Sowjetunion* 8, 153-169(1935).

[20] A. Lee, Z. Liu, C. Serpico, G. Bertotti, and I. Mayergoyz, "Monte Carlo Simulations of Landau-Lifshitz Dynamics Driven by a Jump-Noise Process," *J. Appl. Phys.* 111, 07D115 (2012).

[21] A. Lee, Z. Liu, G. Bertotti, C. Serpico, and I. Mayergoyz, "Analysis of Random Magnetization Switching using Monte Carlo Simulations," *Physica B* 435, 100-104 (2014).

[22] A. Lee, G. Bertotti, C. Serpico, I. Mayergoyz, "On Random Switching of Magnetization," *IEEE Trans. Magn.* 50, 1300904 (2014)

[23] A. Lee, G. Bertotti, C. Serpico, I. Mayergoyz, "Averaging Technique for Random Magnetization Dynamics Driven by a Jump-Noise Process," *IEEE Trans. Magn.* Vol. 50, No. 11, 1300804 (2014)

[24] Z. Liu, A. Lee, G. Bertotti, C. Serpico, and I. Mayergoyz, "Jump-Noise Process-Driven Magnetization Dynamics and Random Switching of Magnetization," *J. Appl. Phys.* 111, 07D108 (2012).

[25] Z. Liu, A. Lee, P. McAvoy, G. Bertotti, C. Serpico, and I. Mayergoyz, "Monte Carlo Simulations of Random Magnetization Dynamics Driven by a Jump-Noise Process on General Purpose Graphics Processing Units (GPUs)," *IEEE Trans. Magn.* 49, 3133 (2013).

[26] M. Lundstrom, *Fundamentals of Carrier Transport*, Addison-Wesley (1990).

[27] I. Mayergoyz, G. Bertotti, and C. Serpico, "Magnetization Dynamics Driven by a Jump-Noise Process," *Phys. Rev. B* 83. 020402 (2011).

[28] I. Mayergoyz, G. Bertotti, and C. Serpico, "Landau-Lifshitz Magnetization Dynamics Driven by a Random Jump-Noise Process," *J. Appl. Phys.* 109, 07D312 (2011).

[29] I. Mayergoyz, G. Bertotti, and C. Serpico, "Generalized H-Theorems for Magnetization Dynamics Driven by a Jump-Noise Process," *J. Appl. Phys.* 109, 07D327 (2011).

[30] I. Mayergoyz, A. Lee, C. Serpico, G. Bertotti, "Numerical Modeling of Random Magnetization Dynamics," *IEEE Trans. Magn.* Vol. 51, No. 3, 7200604 (2015)

[31] C. Serpico, I. Mayergoyz, and G. Bertotti, "Numerical Technique for Integration of the Landau-Lifshitz Equation," *J. Appl. Phys.* 89, 6991 (2001).

[32] C. Serpico, M. d'Aquino, G. Bertotti, and I. Mayergoyz, "Analytical Approach to Current-Driven Self-Oscillations in Landau-Lifshitz-Gilbert Dynamics," *J. Magn. Magn. Mater.* 290-291, 502-505 (2005).

[33] C. Serpico, G. Bertotti, I. Mayergoyz, M. d'Aquino, R. Bonin, "Thermal Stability in Spin-Torque-Driven Magnetization Dynamics," *J. Appl. Phys.* 99, 08G505 (2006).

[34] C. Serpico, I. Mayergoyz, G. Bertotti, M. d'Aquino, R. Bonin, "Generalized Landau-Lifshitz-Gilbert Equation for Uniformly Magnetized Bodies," *Physica B* 403, 282-285 (2008).

[35] J.C. Slonczewski, "Current-Driven Excitation of Magnetic Multilayers," *J. Magn. Magn. Mater.* 159, L1-L7 (1996).

[36] J. Tejada, X.X. Zhang, and E. M. Chudnovsky, "Quantum Relaxation in Random Magnets," *Phys. Rev. B* 47, 14977 (1993)

[37] J. Tejada, X.X. Zhang, and L. Balcells, "Nonthermal Viscosity in Magnets: Quantum Tunneling of the Magnetization," *J. Apl. Phys.* 73, 6709 (1993)

[38] L. Thomas, F. Lionti, R. Ballou, D. Gatteschi, R. Sessoli, and B. Barbara, "Macroscopic Quantum Tunnelling of Magnetization in a Single Crystal of Nanomagnets," *Nature* 383, 145 (1996)

[39] W. Wernsdorfer, E.B. Orozco, K. Hasselbach, A. Benoit, D. Mailly, O. Bubo, H. Nakano, and B. Barbara, "Macroscopic Quantum Tunneling of Magnetization of Single Ferromagnetic Nanoparticles of Barium Ferrite," *Phys. Rev. Lett.* 79, 4014 (1997)

[40] Z. Zhang and I.D. Mayergoyz, "The Use of Plasmon Resonance in Thermally Assisted Magnetic Recording," *J. Appl. Phys.* 103, 07F510 (2008).

[41] Y. Zhou, "Effect of the Field-Like Spin Torque on the Switching Current and Switching Speed of Magnetic Tunnel Junction with Perpendicularly Magnetized Free Layers," *J. Appl. Phys.* 109, 023916 (2011)